ABSTRACT

Title of Dissertation / Thesis: THE JOINT EFFECTS OF CLIMATE CHANGE AND URBANIZATION ON THE DISTRIBUTION OF STREAMFLOW MAGNITUDES IN THE MARYLAND PIEDMONT REGION

Mohamad Issa Hejazi, Master of Science, 2004

Dissertation / Thesis Directed By: **Associate Professor, Glenn E. Moglen,**

Department of Civil and Environmental

Engineering

This thesis examines the effect of climate and land use change on streamflow distributions in six urbanizing watersheds in the Maryland Piedmont region, and produces future predictions under three proposed scenarios of future climate and land use varying individually and then jointly. Future climate is modeled using precipitation and temperature predictions from the CCC and Hadley models. Two approaches are used to predict future streamflows: a regression model approach, and a continuous streamflow model approach. Trend tests at a 5% level of significance are used to statistically quantify emerging trends in the simulated climate and streamflow time series. Precipitation is the dominant factor and generally controls the directionality of trends in streamflows. Temperature has less influence on low flows and no apparent effect on peak flows. Land

use change has caused low flows to be slightly smaller and peak flows slightly larger, but no significant trends were detected.

THE JOINT EFFECTS OF CLIMATE CHANGE AND URBANIZATION ON THE DISTRIBUTION OF STREAMFLOW MAGNITUDES IN THE MARYLAND PIEDMONT REGION

By

Mohamad Issa Hejazi

Thesis submitted to the Faculty of the Graduate School of the
University of Maryland, College Park, in partial fulfillment
of the requirements for the degree of
Master of Science
2004

Advisory Committee:

Associate Professor Glenn E. Moglen, Chair
Associate Professor Kaye Brubaker
Professor Richard H. McCuen

ACKNOWLEDGEMENTS

I would like to pay my sincerest appreciation to Dr. Glenn Moglen for his constant support and direction. The completion of this thesis would not have been possible without his continuous assistance and inspiring encouragement. I would also like to thank Dr. Richard McCuen for his guidance on several technical aspects of this research.

This project was funded by the U.S. Environmental Protection Agency. Their support is greatly acknowledged.

TABLE OF CONTENTS

LIST OF TABLES

LIST OF FIGURES

CHAPTER ONE

INTRODUCTION

1.1 Background

We live in an urbanizing world with more pervious surfaces being covered with pavements and with larger industries and more automobiles emitting greenhouse gases. The former has a direct impact on hydrology through reduced infiltration of precipitation while the latter may also have an impact through the temperature and precipitation changes associated with climate change. These influences are critical and may lead to permanent changes in the hydrology of streams. Some past studies have shown the outcome of climate change and urbanization as two drivers in reducing base flows during the low flow season and making peak flows much greater during storm events (e.g., Klein, 1979; Barringer et al., 1994; Paul and Meyer, 2001).

The purpose of this research is to investigate the joint effects of both land use and climate change on the distribution of streamflows. Both a regression approach and a continuous streamflow modeling approach will be used to better understand the actual consequences of these two phenomena on streams in the Maryland Piedmont region.

1.2 Problem statement

Climate change and urbanization are generally two man-made phenomena that have induced both direct and indirect negative consequences to our natural system. Past studies (Wilby et al., 1994; Querrner et al., 1997) suggest that under the condition of climate change and an urbanized watershed, flows in rivers will exhibit larger peaks during storms and smaller base flows during drought seasons. Thus their studies are

important to better understand the consequences caused by each phenomenon. Understanding the consequences of climate change and urbanization can provide policymakers and legislators with better guidelines when developing policy on zoning the landscape or the allowable amount of carbon dioxide to be emitted by our vehicles and industry.

Precipitation and evaporation are other important drivers that can greatly affect streamflow distributions. Many studies have shown climate warming as a strong likelihood (e.g., I.P.C.C., 2001). Thus the effects of higher average temperatures and more extreme rainfall events on streamflow distribution need to be investigated in order to anticipate how streamflow might change with climate and adapt to any negative consequences on the conditions of our streams. Extreme rainfall events and longer durations between rainfall events will introduce greater peaks and drier base flows with longer drought events. Warming temperatures entail a bigger proportion of the budget for evaporated water back to the atmosphere. This would likely come at the expense of subsurface flow and groundwater flow. Thus it might be hypothesized that enhanced evaporation has the same effects on low flows as urbanization.

The amount of water that infiltrates the land surface, recharges groundwater storage, and appears later in a stream is certainly important to both the hydrology and the ecology of the stream. Additionally, more surface runoff implies less water to infiltrate as subsurface flow or groundwater flow. Water flowing through the ground takes a much longer time to reach the stream than surface water that travels freely. The longer time lags associated with groundwater contributions to the stream makes groundwater the main discharge source between storms and during dry seasons. Preventing the recharge of

groundwater implies less water reaching the stream when there is a drought or a lack of rainfall. Introducing longer drought durations in the streamflow can cause the death of all living organisms in the stream and the scarcity of water resources during times of low flow.

Thus far, some possible consequences of climate and land use changes on the streamflow distribution have been identified. Anticipating such changes based solely on qualitative physical reasoning is not sufficient and quantitative analyses and modeling must be preformed. The use of a regression model approach or a continuous streamflow model to carry out such an investigation effort is widely utilized. In this research, both approaches will be used as separate tools, and the possibility of using them in a complementary fashion will be investigated. The regression model is based on observed data and can only convey what is imbedded in the these data. Thus having poor data, a poor functional form, or missing one important predictor that is not presented in the data can lead to poor results. The continuous streamflow model, on the other hand, is a conceptually-based modeling approach and provides greater insight into the functioning of the entire hydrologic system than the regression approach. However this approach is subjective where every modeller can end up with a different answer. Thus, we anticipate that the combination of both approaches might provide greater insight than either approach alone.

Past research (Simmons and Reynolds, 1982; Liebscher, 1983; Warner, 1984; Arnell,1989; Ferguson and Suckling, 1990; Wilby et al., 1994; Querrner et al., 1997; Paul and Meyer, 2001) have utilized statistical approaches and hydrologic modeling to identify long-term trends in the streamflow distribution under either climate change or land use

change. Land use is usually dealt with as a static property of the watershed just like the area of the watershed. But in reality, land use varies temporally and should not be considered as a constant predictor especially if the watershed has undergone considerable development over the duration of the study period. One of the strengths of this research effort is the fact that land use is allowed to vary on an annual basis. The study will also investigate the capability of using regression models imbedded into the later selected continuous streamflow model to reduce the number of predictors for which subjective calibration is required. This will allow for less tuning by researchers; thus, reducing the subjectivity and bias of the continuous streamflow model approach.

1.3 Objectives

The objective of this research is to investigate the joint effects of land use and climate change on the distribution of streamflows. A regression model approach and a conceptually-based model approach are pursued to best achieve the objectives of this research. The following objectives will be pursued:

1. The first objective is to illustrate the individual and joint effects of climate change and land use change on the distributions of streamflows by simulating three distinct scenarios: holding land use constant while varying climate, holding climate constant while varying land use, and lastly varying both land use and climate simultaneously. Considering all three scenarios are expected to provide answers to several crucial questions concerning the expected distribution of streamflow (low and peak flows) as a function of differing future land use scenarios and climate model inputs. First, do both climate and land use change contribute the same effects on low flows and peak flows? Do both climate and

land use drivers impose the same level of influence, or does either one dominate with a stronger influence on the magnitude of streamflows? Answering these questions will possibly lead to better planning tools for developing future climate and land use policies.

2. The second objective is to select the most physically rational and practically attainable predictors when calibrating a regression model to predict low flows. Selecting the most representative predictors will allow us to effectively model the observed historical streamflow data. The calibrated model will provide the capability to predict the magnitude of low flow under the effects of both climate and land use change. Since low flows are the result of a lack of precipitation for a long duration, it is anticipated that physical predictors with some measure of long-term antecedent precipitation and temperature to be meaningful in predicting low flows.
3. The third objective is to employ a continuous streamflow model to perform the same analyses as described in the second objective. This will allow the computation of the distribution of streamflows using a numerical model in which the input variables need to be calibrated. In an effort to eliminate the subjectivity associated with calibrating hydrologic models, the continuous streamflow model will be embedded in to a numerical optimization program, NUMOPT, to provide the best match between predicted and observed streamflow. The level of acceptance of goodness-of-fit will rely on statistical measures. One of the advantages of using a continuous streamflow modeling approach over the

regression approach is that the continuous streamflow model provides information on the statistical distribution of daily streamflows in a year.

The continuous streamflow model to be used in this study is a conceptually-based hydrologic model modified somewhat from McCuen (1986) that takes as input a time series of precipitation and temperature and produces an output time series of streamflow. This model follows the same basic structure of the Stanford watershed model (Crawford and Linsley 1966) now called HSPF (Bicknell et al., 1997). We use this model because it is more readily modified than HSPF and will allow us greater flexibility in first calibrating streamflow response and ultimately in modifying the model to accept an input time series of land use. The fact that the continuous streamflow model will deal with imperviousness as a dynamic rather than static input, is one of the strengths of this work over past studies, which generally treat land use as a static quantity.

The continuous streamflow model will be modified to accept an input time series of land use (e.g., imperviousness). This version of the model will then be used to produce simulations that illustrate the model's ability to reproduce historical streamflow in the study watersheds. The consequences of future land use change on streamflow will then be simulated using the results from the scenarios mentioned in Objective 1.

4. The fourth objective of this thesis is to determine the primary sources of uncertainty in the regression and conceptual models, so future research can be directed to allocate greater weight to the most important sources of uncertainty in the model. The sources of uncertainty include the uncertainty of the structure of

the regression model, the uncertainty in the calibrated coefficients in the selected model form, the uncertainty in selecting the appropriate predictor variables for the regression model, and the uncertainty in the predicted streamflow values by the regression model and the continuous streamflow model. This analysis should address how much belief should be placed on the results of Objective 1 because the level of uncertainty might be sufficiently large to overwhelm any observed trend in magnitude of streamflows.

1.4 Summary

By calibrating both the regression and continuous streamflow models that predict stream discharges, this study will produce a better understanding of the consequences of climate change and urbanization on streams. Engineers need to calculate how the magnitude of streamflows will vary under the potential future scenarios when any hydrologic design is at stake. The ability to anticipate future streamflow distributions is valuable information to engineers to adequately manage and plan our water resources. Scientists can use the future predictions of streamflow distribution to study the effects of urbanization and climate change on the ecology and morphology of streams. Regional planners and policy makers can use the results of this study to aid in decision-making with regards to land use planning. Specifically, planners and policy makers could use these results to estimate potential changes in streamflow magnitudes that would result from different climate and land use scenarios. Finally, the outcome of the research can be a starting point for future research on similar or more sophisticated studies of the effects of climate change and urbanization on streamflow.

CHAPTER TWO

LITERATURE REVIEW

2.1 Introduction

Understanding the statistical distribution of streamflows of a watershed, especially extreme events of low and peak flows, is important to hydrologists, ecologists, and engineers. Researchers generally look at available historical data to make inferences about future predictions of streamflows, especially extreme events. With suggested climate warming and the rapid and continuous urbanization which would have apparent influence on the hydrology of streams, it is important to investigate their effect on streamflow distributions. It is of great interest to many to learn the possible effects that climate and land use change can bring upon the distribution of streamflows.

2.2 Regression models to predict low flows

Hydrologists are interested in low flows because they represent the extreme opposite of the flood response of the watershed. The low flow response of the watershed is indicative of the state of the underlying groundwater conditions, and reflects both the urbanization and the geology in the region. Low flows may be used by ecologists as an index of the ecological health of the stream system. Low flows stress the survival of species dependant on certain flow characteristics within the stream. Understanding and predicting low flows is a concern of engineers involved in water resources management to account for the availability of water-supply, the quality and quantity of water for human use, recreation, or irrigation purposes.

2.2.1 The effects of climate and land use change on low flows

Low flows are generally estimated from streamflow time series using methods such as flow duration curves, frequency analysis of extreme low flow events, continuous low flow intervals, deficit volumes, base flow separation, and characterization of streamflow recessions (Smakhtin, 2000). These techniques are used when low flows are estimated for gauged sites and inferences are only made about the particular watershed from which the gauge streamflow time series are obtained. In the case when continuous streamflow time series are used in a regional sense to make inferences about ungauged sites, the regional regression approach is perhaps the most widely used approach (e.g. Tasker, 1972; Ludwig and Tasker, 1993). This is generally accomplished by initially delineating a hydrologically homogeneous region with similar climate, geology, topography, vegetation and soils (Smakhtin, 2000). A regression model is then constructed by forming a relationship between dependant low flow characteristics and independent watershed and climatic predictors. This is generally accomplished by a multiple regression analysis. This process includes the selection of the form of the regression model, determination of the regression model parameters and the assessment of estimation errors.

Stepwise regression is typically the common procedure to decide on the needed predictor variables in the regression model. Some of the predictors that are most commonly related to streamflows include: watershed area, mean annual precipitation, channel and/or watershed slope, stream frequency and/or density, percentage of lakes or forested areas, various soil and geological indices, length of the main stream, watershed shape, watershed perimeter, and mean watershed elevation (Smakhtin, 2000). Tasker

(1972) concluded that drainage area and the average groundwater available from wells in some southeastern Massachusetts basins produce adequate regression models to predict the 7-day low flow at the 2-year and 10-year recurrence intervals (Tasker, 1972)

To assess the accuracy of the model, understanding the level of uncertainty can be an important part of the process of forming a regression model. Uncertainty can be measured quantitatively by using a Monte Carlo simulation technique. The Monte Carlo simulation technique is generally utilized in an effort to mimic the variability of a natural system, a hydrological system in this case, through many simulation runs (Ayyub and McCuen, 2003). Tasker (1987) used a Monte Carlo technique to compare four methods for estimating the 7-day low flow for a 10-year and 20-year recurrence intervals.

Additionally, many have used regression models to predict streamflows and to assess the effect of climate and land use on the magnitude of streamflows. As examples, Duell (1992) calibrated seasonal regression models; and Revelle and Waggoner (1983), and Duell (1994) calibrated annual regression models to study the sensitivity of streamflows to climate change. Duell (1994) concluded that precipitation has a greater effect on streamflows than temperature.

Low flows are generally influenced by natural factors, such as climate, topography, geology, and soil, as well as man-induced effects, such as urbanization and upstream water use (Smakhtin, 2000). Climate change, due to the increase in green-house gases, and land use change, due to the continuous urbanization trend, are two commonly studied factors to investigate the extent of their influence on streamflows and low flows in particular. Liebscher (1983) claimed that a climatic change is capable of exerting a change in the duration and volume of low flows as well as high flows and

suggested the additional use of long term temperature time series to better predict low flows. However, Arnell (1989) examined possible low flow trends in 89 catchments in western and northern Europe and observed a statistically significant increasing trend in annual number of low flows in only 7 of the basins attributable to climate warming.

Ferguson and Suckling (1990) studied an urbanizing watershed in Atlanta, Georgia, USA, and concluded through a regression approach that urbanization reduces low flows in dry years and increases low flows in wet years. Paul (2001) found that urbanizing watersheds exhibit a larger volume of the received precipitation as surface runoff and less as groundwater flow. The result is the observation of lower base flows in urbanizing watersheds. Simmons and Reynolds (1982), Warner (1984), and Ferguson and Suckling (1990) concluded that low flows in urbanized watersheds have a tendency to decrease due to the effects of the impervious surface, limiting infiltration and enhancing evaporation.

Wilby et al., (1994) studied the effects of both urbanization and climatic changes on low flows, and concluded that land use has a greater influence than climatic change. Querrner et al., (1997) also studied the effects of groundwater abstractions in addition to both urbanization and climatic change, on low flow trends in five small European catchments using physically-based models: BILAN (Kasparek and Krejcova, 1994), HBVMOR (Tallaksen and Erichsen, 1994), MODFLOW (McDonald and Harbaugh, 1988), and MOGROW (Querner, 1997). Their study illustrated that both temperature and precipitation are factors that influence low flows. An increase of 2 ^{o}C led to a deficit volume of up to 20 percent. For thorough details about low flows, many reviews have

been presented, include Riggs (1972), McMahon (1976), Beran and Gustard (1977), and a more recent review by Smakhtin (2000).

2.3 Continuous streamflow models to predict low and peak flows

Continuous streamflow models are generally used to better understand the hydrology of the watershed at stake and investigate the most effective indices that reflect the streamflow response in a watershed. Vogel and Kroll (1992) used a conceptual watershed model to identify the most representative indices to estimate low flows. They concluded that low flows are highly correlated with watershed area, average basin slope, and base flow recession constant. They also concluded that the use of a conceptually-based model could suggest the predictor variables and the functional form of the regional regression equations.

Continuous streamflow models are generally used as a tool to provide the best fit to the observed streamflow time series. Such models are driven by weather data time series, such as: precipitation, temperature, soil moisture, etc. They are also generally calibrated to achieve the optimum agreement between simulated and observed flows for some selected hydrologic inputs values that in essence describe the hydrologic characteristics of the watershed. Then inputs that are considered to represent the effect of climate and land use change are then forced to vary under new simulations to study their effect on streamflows. The availability of future climatic time series is only a very recent capability with the global circulation models, such as the Canadian Climate Centre, CCC (Boer et al., 1992; Flato et al., 2000) and Hadley (Fang and Tung, 1999). Further, land use within the watershed is generally treated as a static quantity due to the lack of most

continuous streamflow models to accept land use time series as an input. Also land use data are seldom available on an annual basis to the modeler.

The study of the effect of climate change on streamflows is, therefore, a more recent trend in the literature with the growing concerns about global warming in the research community. Flaschka et al., (1987), Gleick (1987), and McCabe and Ayers (1989) used applied water-balance models to study the effects of climate change on streamflows. Puacko (1993) investigated the effect of climate change on streamflows based on the analysis of historical records.

There are numerous continuous streamflow models available, some very simplistic and others more complex. We will utilize a continuous streamflow model developed by McCuen (1986), in which rainfall is disaggregated into three different storages: surface, unsaturated zone (near surface) and groundwater. Each storage contributes to a total runoff produced by the model. Losses from the system, in the form of evaporation, are also possible. The model inputs include specification of storage volumes for each of the three storage "buckets", as well as inputs that control flux rates between buckets.

The continuous streamflow model takes as driver data input time series of temperature and precipitation. Additionally, we allowed two model inputs that quantify urbanization effects to be varied so that we could examine singly and jointly, varying climate and urbanization at two different scales. However, one essential step prior to using any continuous streamflow model in a predictive sense is the calibration process of the model for some parameter values that describe the historical background of the watershed. This generally leads to a source of subjectivity which is a shortcoming of the

approach. The calibration process is generally considered complete based on some visual fit or goodness-of-fit measures set by the modeler. With the availability of numerical optimization packages, it may be more appropriate to allow a numerical optimization program to produce the optimum calibration based on some criterion variables set by the modeler. This will grant the elimination of subjectivity. This, as will be discussed in Chapter 4, has inspired the incorporation of a numerical optimization program, NUMOPT (McCuen, 1993), to calibrate our continuous streamflow model.

The details of how this study was performed and an analysis of the study results will be presented in the following chapters. Although this model is somewhat simpler compared to the more complicated hydrologic models that are available, this model is conceptually consistent with the more well-known Stanford Watershed Model (Crawford and Linsley, 1966), now commonly used as HSPF (Bicknell et al., 1997). Another conceptually similar continuous streamflow model is SWMM (Huber and Dickinson 1988, Roesner et al., 1988, Donigan and Huber 1991).

2.4 Expansion from past research

This research effort is an expansion on previous work with regression and continuous streamflow models. Some new tools and capabilities that were not available in the past will be utilized in this study to assess the effects of climate and land use change on streamflows with greater sophistication. In addition to a rich database of daily observed streamflow, daily precipitation, and daily temperature time series, a historical annual imperviousness time series for various watersheds that had experienced urbanization will allow us to more effectively incorporate the effect of land use in our work. The ability to utilize the imperviousness time series as a hydrologic input in a

continuous streamflow model will eliminate the need to make the commonly used assumption of static land use conditions. Furthermore, the use of two global circulations models, CCC and Hadley, will provide future climate time series of daily precipitation and daily temperature based on the geographic location of our study watersheds. The inclusion of these capabilities will allow us, with greater sophistication, to quantitatively examine the effects of climate and land use on the distribution of streamflows.

CHAPTER THREE

A REGRESSION MODELING APPROACH: TO ANALYZE THE EFFECTS OF CLIMATE CHANGE AND URBANIZATION ON STREAMFLOW DISTRIBUTIONS

3.1 Introduction

This chapter discusses the regression modeling approach as the means of quantifying the effects of urbanization and climate change on the distribution of streamflows. The study will concentrate on six single-watershed regression models, and then a more generalized regional model for the Maryland Piedmont will be calibrated. Each of the six single-watershed regression models as well as the regional regression model will be discussed at the conceptualization stage, the calibration stage, and the assessment stage for both goodness-of-fit and applicability.

The chapter will then investigate the significance of increasing or decreasing trends in streamflow distributions under three proposed future scenarios. The streamflow distribution is divided into peak flows, median flows, and base flows. The chapter will briefly discuss the effects of urbanization and climate change with respect to the annual peak flows and the annual median flows. However, this chapter will concentrate on the effects of urbanization and climate change on the modelling of the annual 7-day low flow in particular. It will then quantitatively examine the effects of urbanization and climate on low flows. Available observed daily flows will then be used to develop regression equations predicting low flows as a function of urbanization and climate. These equations will then be used to make inferences about possible future trends of minimum annual low flows under scenarios of continued urbanization and climate change.

Three future scenarios will be investigated to best understand the separate and joint effects of urbanization and climate change on low flows in particular. Some brief discussion will be directed to peaks and median flows and why their analyses were not carried out. Toward the end of the chapter, the outcome of the regression approach will be discussed and then summarized.

3.2 Advantages of regression modeling

The main advantage of calibrating regression models is to attain the capability of predicting the distribution of streamflows with simple regression models. Most previous researchers have presented the effects of ***urbanization or climate change acting alone over the distribution of streamflows (Simmons and Reynolds, 1982; Revelle and Waggoner, 1983; Warner, 1984; Ferguson and Suckling, 1990; Duell, 1992; Lowell and Duell, 1994).*** This chapter will explore further their effects by studying the joint effect of both land use and climate change simultaneously. Investigating whether urbanization and climatic changes contribute complementary or contradictory effects can provide a better understanding of changes in streamflows under such future scenarios. Moreover, past research has dealt with climate and land use variables as stationary variables while, in reality, they change temporally. Thus, the addition of annual land use (percentage of imperviousness) as a predictor in the calibrated regression model may be capable of adding better goodness-of-fit to the outcome of the regression model.

3.2.1 The study of low flows

Understanding the low-flow characteristics of a watershed is important to hydrologists, ecologists, and engineers. Hydrologists are interested in low flows because

they represent the extreme opposite of the flood response of the watershed. The low-flow response of the watershed is indicative of the state of the underlying groundwater and may be used by ecologists as an index of the health of the ecological stream system. Low flows stress the survival of species dependant on certain flow characteristics within the stream. Understanding and predicting low flows is a concern of engineers involved in water resources management to account for the availability of water supply, the quality and quantity of water for human use, recreation, or irrigation purposes.

3.2.2 The study of median flows

Peak flows and base flows tell about the extremes but lack any information about the distribution of streamflows. The median flow is the 50^{th} percentile streamflow event and thus conveys information about the center of the distribution of the streamflows. It can be representative of the smaller magnitude peak-flows or the larger magnitude base-flows. Thus its significance to convey how climate change and urbanization affect streamflows is somewhat unclear at this stage.

3.2.3 The study of peak flows

Peak flows are generally studied by hydrologists and engineers to better comprehend their impacts on the hydrology of watersheds and to adequately draw up plans for hydrologic designs such as culverts, inlets, and spillways. The literature shows that peaks have been of more concern to researchers. This is probably because peaks (floods) are considered natural disasters that can lead to loss of lives and property. Peak flows are - as will be shown in this study - another telling indicator of the reaction of streams to climate and land use change. Klein (1979), Barringer et al., (1994), and Paul

and Meyer (2001) have concluded that climate change and urbanization lead to larger peak flows.

3.3 Emphasis on the effects of climate change and urbanization on the magnitude of low flows

The warmer temperatures associated with climate change lead to enhanced evapotransporation. This change alone would be expected to have the impact of reduced ground water storages and thus reduced base flow levels in streams. When the increased impervious areas associated with continued urbanization are superimposed on the changing climate signal, the expected result is even more diminished recharge to ground water storages. The changes in precipitation magnitudes and temporal distribution also associated with climate change serve to further complicate the picture of how low base flows are expected to respond to climate and or land use change in the future.

3.4 Our selected study area

Six watersheds of varying drainage areas and varying urbanization levels in Montgomery County, Maryland, are selected to be studied as representatives of Maryland Piedmont region. The areas of the watershed ranged from 3.7 square miles to 101.0 square miles. Seneca Creek, Rock Creek, Hawlings, and Little Falls watersheds had undergone minor changes in land use with increases of imperviousness of (12.6% to 15.2%), (11.0% to 13.1%), (8.5% to 9.4%), and (35.2% to 36.6%) respectively. On the other hand, the Northwest Branch and Watts Branch watersheds have experienced much larger changes of imperviousness of (5.8% to 20.5%) and (16.1% to 28.9%), respectively. A more detailed description of each of the six watersheds is summarized below.

3.4.1 Northwest Branch watershed

The Northwest Branch (NWB) watershed of the Anacostia river has a drainage area of 54.7 km^2 (21.1 mi^2). The watershed outlet is the site of the USGS streamflow gage (01650500). The NWB watershed has undergone a large increase in imperviousness from 5.8% to 20.5% over a 40 year period. Figure 3-1 below shows the location of the NWB watershed approximately 6.2 kilometers (3.8 miles) north of Washington, DC, in Maryland.

3.4.2 Watts Branch watershed

The Watts Branch Branch watershed of the Potomac river has a drainage area of 9.6 km^2 (3.7 mi^2). The watershed outlet is the site of the USGS streamflow gage (01645200). The Watts Branch Branch watershed has undergone a large increase in imperviousness from 16.1% to 28.9% over a 29 year period. Figure 3-1 below shows the location of the Watts Branch watershed approximately 15.4 kilometers (9.6 miles) north of Washington, DC, in Maryland.

3.4.3 Seneca Creek watershed

The Seneca Creek Creek watershed of the Potomac river has a drainage area of 261.6 km^2 (101.0 mi^2). The watershed outlet is the site of the USGS streamflow gage (01645000). The Seneca Creek watershed has urbanized to some extent with an increase in imperviousnessfrom 12.6% to 15.2% over a 50 year period. Figure 3-1 below shows the location of the Seneca Creek watershed approximately 29.4 kilometers (18.3 miles) north of Washington, DC, in Maryland.

3.4.4 Rock Creek watershed

The Rock Creek watershed of the Potomac river has a drainage area of 25.1 km^2 (9.7 mi^2). The watershed outlet is the site of the USGS streamflow gage (01647720). The Rock Creek watershed has urbanized somewhat with an increase in imperviousness from 11.0% to 13.1% over a 10 year period. Figure 3-1 below shows the location of the Rock Creek watershed approximately 14.6 kilometers (9.1 miles) north of Washington, DC, in Maryland.

3.4.5 Hawlings watershed

The Hawlings watershed of the Anacostia river has a drainage area of 69.9 km^2 (27.0 mi^2). The watershed outlet is the site of the USGS streamflow gage (01591700). The Hawlings watershed has urbanized slightly with an increase in imperviousness from 8.5% to 9.4% over a 22 year period. Figure 3-1 below shows the location of the Hawlings watershed approximately 20.3 kilometers (12.6 miles) north of Washington, DC, in Maryland.

3.4.6 Little Falls watershed

The Little Falls watershed of the Potomac river has a drainage area of 10.6 km^2 (4.1 mi^2). The watershed outlet is the site of the USGS streamflow gage (01646550). The Little Falls watershed has urbanized very slightly with an increase in imperviousness from 35.2% to 36.6% over a 25 year period. Figure 3-1 below shows the Little Falls watershed to lie in both Washington, DC, and in Maryland, adjacent to the northwest border of Washington, DC.

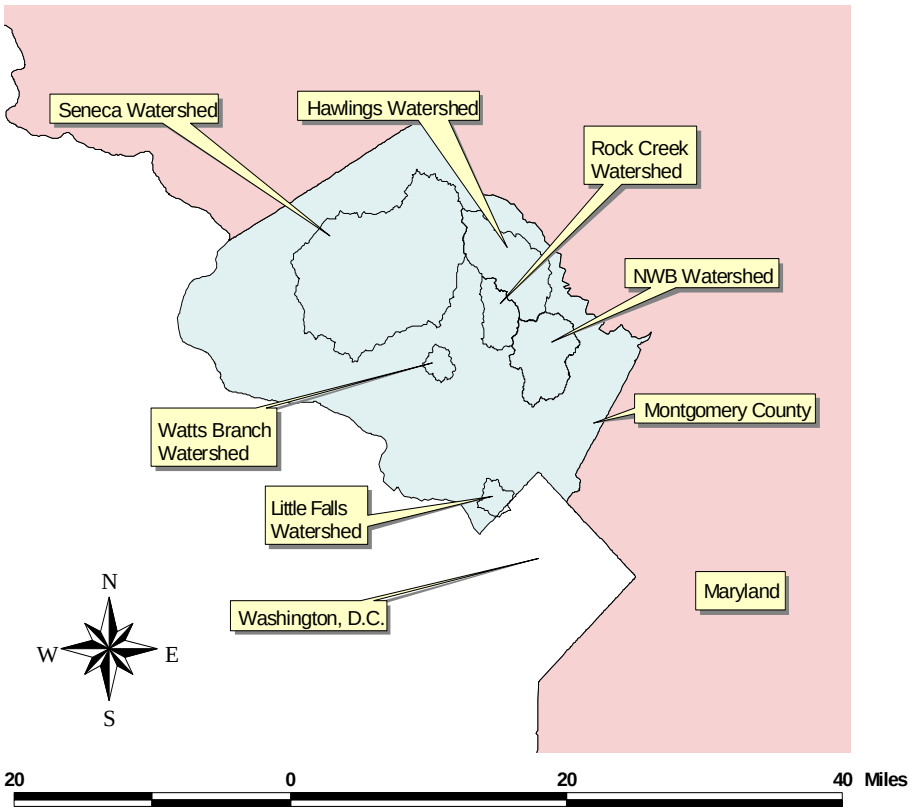

Figure 3 -1. Location map of our study area s in Montgomery C ounty, Maryland.

3.5 Collecting historical data

The first step of constructing a regression model to predict streamflow data under the effects of urbanization and climate change is to collect land use and climate time series to be utilized as predictors . These times series are usually collected and archived by professionals hired by certain agencies and they placed on the World -Wide -Web for potential users. A historical database of available time series for daily streamflow , daily precipitation, daily te mperature, drainage area of the watershed, and annual percentage of imperviousness of the watershed were obtained and manipulated to produce the needed regression models.

3.5.1 Historical streamflow time series

Each of the later calibrated regression models is used to predict the magnitude of streamflow based on physical indices that best describe the reaction of the watershed to urbanization and climate change. The daily observed runoff at each of the studied watersheds was obtained from the United States Geological Survey (USGS) website. It provided the daily runoff record at the six locations of our gages in Montgomery County, Maryland. The daily observed flows are then grouped on annual basis to produce the annual flow distribution of the particular stream or watershed.

3.5.1.1 Selection of the streamflow gages

The daily streamflow data at the outlet of each of the six watersheds were obtained by downloading the data from the USGS website online for each of the streamflow gages that define our watersheds. A list of the gage names, their USGS gage numbers, and their associated watershed names are summarized in Table 3-1. All available data were collected to be later matched with available temperature, precipitation, and imperviousness records for each of the watersheds. Missing data were estimated based on averaging streamflow values for each day of the year over the duration of available streamflow gage records.

Table 3-1. List of streamflow gages used to define the outlets of the six watersheds.

USGS Gage #	Name of USGS Gages	Watershed Name Abbrev.	# of Years
1650500	NW Branch Anacostia River Near Colesville	NWB	40
1591700	Hawlings River Near Sandy Spring	Hawlings	22
1646550	Little Falls Branch Near Bethesda	Little Falls	25
1647720	North Branch Rock Creek Near Norbeck	Rock Creek	10
1645000	Seneca Creek Creek at Dawsonville	Seneca Creek	50
1645200	Watts Branch Branch at Rockville	Watts Branch	29

3.5.2 Historical climatic time series

The daily precipitation and daily (maximum, minimum, and average) temperature time series were collected from nine local weather stations. The stations were assumed to be the most representative since they were the nearest to our selected watersheds. Figure 3-2 below shows the location of these stations. The precipitation and temperature time series were obtained electronically from National Climatic Data Center (NCDC, 2003). Precipitation and temperature are sufficient indices to represent the effects of climate change over the span of available historical record.

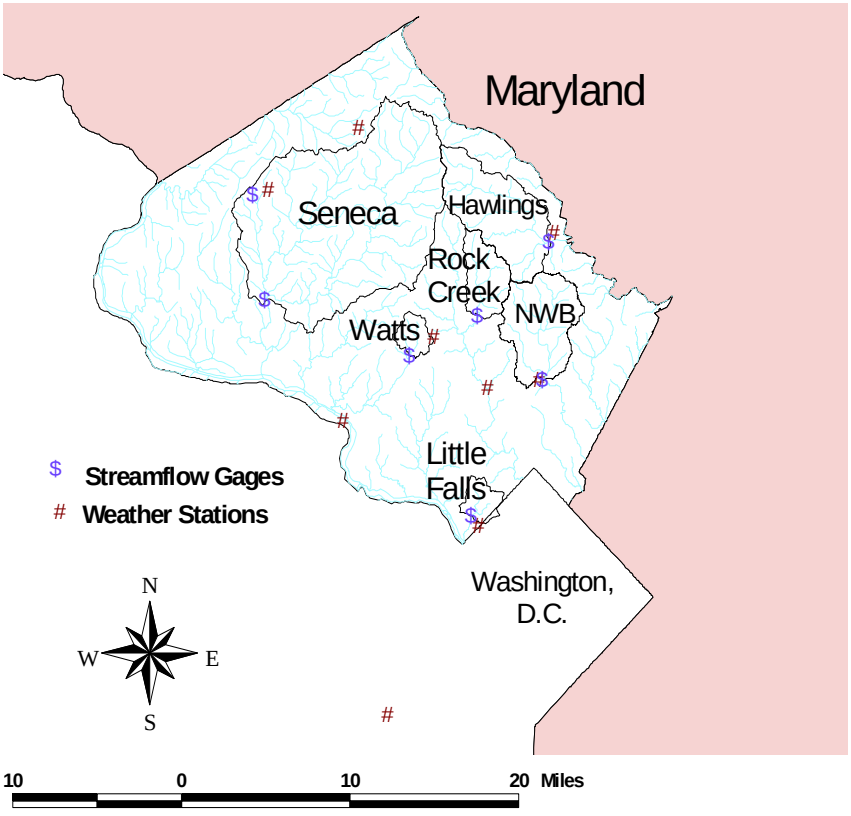

Figure 3-2. Locations of the weather stations in Montgomery, Maryland.

3.5.2.1 Rules in selecting the weather stations

The first challenge in manipulating the database is to set fixed rules on dealing with missing data and on associating a particular weather station to a particular watershed. Table 3-2 below summarizes the available weather stations that are closest to our selected watersheds and their period of record for precipitation and temperature. Time series of precipitation and temperature were formed using these nine stations.

Table 3-2. List of stations used to compile climate time series.

	Weather Station	NCDC ID#	Precipitation available data		Temperature available data	
			start date	End date	start date	end date
1	Boyds	181032	01/02/1953	28/01/1991	01/02/1953	28/02/1991
2	Brighton	181125	01/08/1948	28/02/1991	01/12/1948	31/12/1954
3	Brookdale	181170	01/08/1948	30/11/1973	N/A	N/A
4	Damascus1	182335	01/09/1973	31/01/1992	01/09/1973	31/01/1992
5	Damascus2	182336	01/04/1993	28/02/2003	01/04/1993	28/02/2003
6	Reagan	448906	01/07/1945	28/02/2003	01/07/1945	28/02/2003
7	Rockville	187705	01/08/1948	28/02/2003	01/08/1948	28/02/2003
8	Wheaton	189502	01/06/1961	31/12/1977	01/06/1961	31/12/1977
9	Potomac	187272	01/01/1993	28/02/2003	N/A	N/A

3.5.2.2 Dealing with missing data

Precipitation and temperature time series were created by compiling data from the multiple weather stations available to make a complete set. The goal was to produce continuous daily precipitation and temperature time series for the same durations of available daily runoff data for each of the six watersheds. For each of the six watersheds, the nine weather stations were put in ascending order in terms of physical distance from each of the watersheds. So data were obtained from the closest station with available data. This approach produced complete time series with no missing data for each of the six watersheds.

3.5.2.2.1 Missing daily precipitation data

Table 3-3 lists the order of weather stations in which they were used as sources of daily precipitation data for each of the six watersheds of our study. Station 1 is considered the primary source of daily precipitation data, and if precipitation information is missing for any particular date, the subsequent stations are used. This procedure was repeated for the compilation of daily precipitation time series for each of the watersheds. As a result, a complete precipitation time series was compiled for the same period of available daily streamflow data for each of the six watersheds from the list of nine weather stations.

Table 3-3. Order of stations in which they were used to compile daily precipitation time series for each of the watersheds.

Watershed	Hawlings	Little Falls	NWB	Rockville	Seneca Creek	Watts Branch
Station 1	Brighton	Brookdale	Wheaton	Rockville	Boyds	Rockville
Station 2	Rockville	Reagan	Rockville	Brighton	Damascus1	Wheaton
Station 3	Wheaton	Wheaton	Brighton	Wheaton	Damascus2	Brighton
Station 4	Damascus1	Rockville	Brookdale	Damascus1	Rockville	Boyds
Station 5	Damascus2	Brighton	Damascus1	Damascus2	Brighton	Damascus1
Station 6	Boyds	Boyds	Damascus2	Boyds	Wheaton	Damascus2
Station 7	Brookdale	Damascus1	Boyds	Brookdale	Brookdale	Brookdale
Station 8	Reagan	Damascus2	Reagan	Reagan	Reagan	Reagan
Station 9	Potomac	Potomac	Potomac	Potomac	Potomac	Potomac

3.5.2.2.2 Missing daily temperature data

In similarity to the construction of the precipitation time series, the temperature time series were compiled based on the selection of the closest weather station with available data as the preferred source. Hence, Table 3-4 below, which lists the priority of order of the weather stations, is almost identical to Table 3-3 except that Brookdale and Potomac weather stations lack the availability of temperature data and thus are eliminated as possible sources.

Table 3-4. Order of stations in which they were used to compile daily temperature time series for each of the watersheds.

Watershed	Hawlings	Little Falls	NWB	Rockville	Seneca Creek	Watts Branch
Station 1	Brighton	Reagan	Rockville	Rockville	Boyds	Rockville
Station 2	Rockville	Wheaton	Wheaton	Brighton	Damascus 1	Wheaton
Station 3	Wheaton	Rockville	Brighton	Wheaton	Damascus 2	Brighton
Station 4	Damascus 1	Brighton	Boyds	Damascus 1	Rockville	Boyds
Station 5	Damascus 2	Boyds	Damascus 1	Damascus 2	Brighton	Damascus 1
Station 6	Boyds	Damascus 1	Damascus 2	Boyds	Wheaton	Damascus 2
Station 7	Reagan	Damascus 2	Reagan	Reagan	Reagan	Reagan

3.5.3 Historical land use time series

Historical land use data were obtained by first obtaining aerial maps of our six watersheds at different time frames. The maps were, then, imported into the GIS. Once the maps were electronically recognized by the GIS interface, each of the watersheds was digitized manually into polygons of three categories: residential, forest, and agriculture. Current land use coverage is available through the generalized land use data provided by the Maryland Department of Planning. Knowing the distribution of land use coverage at some preliminary stage and the current stage allowed us to obtain annual imperviousness values for each of the watersheds. The detailed procedure of obtaining the annual land use values is presented by Moglen and Beighley (2002).

3.6 Selection of the most meaningful indices

Regression models may be calibrated to estimate any element of the flow distribution over the periods of available observed runoff data in each of the six watersheds. These periods of study are dictated by the concurrent availability of stream gage, rain gage, and land use data. This chapter will focus on the calibration of regression models to predict the annual minimum 7-day low flow under the effects of

climate and land use changes. The climatic factor is captured in the temperature and precipitation time series. Similarly, the imperviousness time series represents the effects of land use change.

3.6.1 Precipitation

Precipitation is considered as the first potential predictor for the calibration of a low-flow regression model. Hence, precipitation is, in essence, the main predictor because it simply dictates how much water has entered into the system. The magnitude and sequential occurrence of rainfall events can greatly influence the magnitude and timing of low flows. Thus for each minimum low-flow event, the total antecedent precipitation from the time of the low flow event back to 30, 60, 90, …, 330, 360 days prior to the event were recorded. A statistical analysis was performed to investigate the most meaningful antecedent precipitation event that showed the strongest correlation to the annual 1-day, 2-day, 3-day, and 7-day low-flow events.

Table 3-5. List of correlation values (R) between each of the four low flow events and their antecedent precipitation of 12 various durations to select the optimum precipitation index in the NWB watershed (Largest correlation values are shown in bold).

	min. 1-day runoff	min. 2-day runoff	min. 3-day runoff	min. 7-day runoff
prec-30	0.2011	0.2420	0.1500	0.1708
prec-60	0.4751	0.2797	0.4094	0.2343
prec-90	0.6175	0.3869	0.4925	0.5502
prec-120	0.6658	0.5718	0.5410	0.6513
prec-150	0.6887	0.5879	0.5795	0.6373
prec-180	0.6864	0.5784	0.5417	0.6461
prec-210	0.6691	0.6419	0.6048	0.6738
prec-240	0.7073	**0.6918**	0.6341	0.7268
prec-270	0.7161	0.6844	**0.6685**	0.7698
prec-300	0.7173	0.6835	0.6543	**0.7769**
prec-330	**0.7195**	0.6598	0.6454	0.7536
prec-360	0.6918	0.6160	0.6057	0.7565

Calculating the correlation coefficients between each of the 1, 2, 3 and 7-day low flow historical time series for the NWB watershed and the various antecedent precipitation periods, shows that an approximate duration of 8 to 11 months probably best explains the low-flow event. Regression models were calibrated for each of the 240, 270, 300, and 330-day antecedent precipitation durations to find the most telling duration to the low flow event. Three different model forms, which will be discussed later in this chapter, were calibrated for using each of the four antecedent precipitation durations. The nine months of antecedent precipitation was found to attain the optimum correlation coefficient value. This finding is in accordance with a past study that was performed by Ferguson and Suckling (1990). The 270 days time window has some physical basis. Base flows in the Maryland Piedmont region are generally lowest around the end of the summer period after having gone through relatively hot and dry summer season dominated by intense thunderstorm activity and before the cooler, frontally driven winter season starts. So low flows are the results of rainfall events that happened over the period of nine months (January to September) in which groundwater flow and subsurface flow are more likely to exceed recharge rates.

3.6.2 Temperature

Temperature time series were also obtained on a daily basis from the National Climatic Data and were also considered as a second potential predictor of the low flow regression model. A summary of the correlation coefficient between the historical low flow events in the NWB watershed and various ranges of average antecedent temperature records is listed in Table 3-6 for the purpose of selecting the most appropriate duration of antecedent temperature.

Table 3-6. List of correlation values (R) between each of the four low-flow events in the NWB watershed and their antecedent temperature of 12 various durations to select the optimum temperature index (Largest correlation values are shown in bold, and significant correlation (R) values for a 1% level of significance and a sample size of 35 are shown in *italic*)

Min.	Annual low flow events (NWB)			
Temp.	Q1	Q2	Q3	Q7
1	-0.319	*-0.502*	*-0.604*	*-0.441*
7	-0.351	*-0.554*	*-0.524*	*-0.510*
14	*-0.407*	*-0.606*	*-0.569*	*-0.560*
30	*-0.476*	*-0.619*	*-0.605*	*-0.558*
60	***-0.567***	***-0.681***	***-0.700***	***-0.612***
90	*-0.564*	*-0.559*	*-0.628*	*-0.526*
120	*-0.421*	-0.290	*-0.400*	-0.329
150	-0.241	-0.019	-0.136	-0.123
180	-0.115	0.138	0.046	0.024
210	-0.029	0.233	0.147	0.123
230	0.044	0.290	0.214	0.189
270	0.077	0.303	0.242	0.220
Max.	Annual low flow events (NWB)			
Temp	Q1	Q2	Q3	Q7
1	*-0.399*	*-0.564*	*-0.651*	*-0.559*
7	*-0.473*	*-0.626*	*-0.616*	*-0.579*
14	*-0.503*	*-0.651*	*-0.621*	***-0.621***
30	*-0.533*	*-0.645*	*-0.637*	*-0.592*
60	*-0.601*	***-0.668***	***-0.700***	*-0.615*
90	***-0.640***	*-0.607*	*-0.676*	*-0.573*
120	*-0.534*	*-0.409*	*-0.504*	*-0.400*
150	-0.296	-0.025	-0.164	-0.151
180	-0.155	0.155	0.045	0.005
210	-0.061	0.256	0.155	0.111
230	0.036	0.345	0.254	0.199
270	0.087	0.382	0.307	0.251
Avg	Annual low flow events (NWB)			
Temp.	Q1	Q2	Q3	Q7
1	-0.368	*-0.549*	*-0.650*	*-0.511*
7	*-0.422*	*-0.604*	*-0.587*	*-0.555*
14	*-0.469*	*-0.645*	*-0.611*	*-0.605*
30	*-0.521*	*-0.650*	*-0.636*	*-0.591*
60	*-0.611*	***-0.699***	***-0.724***	***-0.633***
90	***-0.639***	*-0.617*	*-0.686*	*-0.573*
120	*-0.506*	-0.367	*-0.476*	-0.377
150	-0.281	-0.023	-0.157	-0.142
180	-0.140	0.153	0.047	0.015
210	-0.047	0.254	0.157	0.121
230	0.042	0.330	0.243	0.202
270	0.088	0.360	0.288	0.247

Minimum, maximum, and average daily temperatures were initially considered as possible temperature indices. The average temperature was found to be the most representative quantity with the highest correlation for the 1, 2, 3, and 7-day low-flow magnitudes. Moreover, daily average temperature records over various durations from the time of the low flow event propagating back to 30, 60, 90, …, 330, 360 days prior to the event were collected and averaged as potential predictors. The average temperature over the antecedent two-months prior to the low flow event showed the highest correlation value. The fact that evapotranspiration is most active during the summer period, which is capable of reducing the magnitude of groundwater flows and as a result base flow, is a plausible explanation for the 60-day time window.

3.6.3 Imperviousness

Annual imperviousness time series were constructed based on methods developed by Moglen and Bieghley (2002). Imperviousness is the predictor intended to capture the effect of urbanization on low flows. It is anticipated that the higher the percentage of impervious area, the less groundwater recharge rates and thus the smaller base flows.

3.6.4 Watershed area

The area of a watershed is anticipated to strongly correlate to the magnitude of streamflow. Thus area is expected to be a very important predictor when generalizing this study to multiple watersheds of varying size. This predictor will be ignored when calibrating the six single-watershed regression models, but it will be used when calibrating the regional regression model.

3.7 Calibration of the optimum regression model form using "NUMOPT"

Regression models can only convey what is embedded in our data sets and thus understanding the trends in each of the time series for each of the watersheds can help in producing the most representative model form. This might require the selection of a model form that does not necessarily produce the minimum standard error or relative bias. At this point, we will use "NUMOPT", a numerical optimization package developed by McCuen (1993), to optimize each of the six regression models to give the lowest relative standard error, S_e/S_y, and the lowest relative bias, $\sum(\text{bias/Q})$. Later in the chapter, the selection of the most appropriate model form and how much belief should be placed on the calibrated models will be discussed.

3.8 Comparison among the various models forms

Selection of most representative model structure is an essential step in regression modeling and selecting the incorrect form can lead to irrational predictions and biased models. Three model structures were considered as candidates to reproduce historical annual low flow events: a linear model, a power model, and a linear model with a sinusoidal component.

3.8.1 A linear model

$$Q_7(t) = C_1 + C_2 \cdot P_x + C_3 \cdot T_y + C_4 \cdot I(t) \qquad (3\text{-}1)$$

where Q_7 is the annual minimum 7-day low flow in year t in ft^3/s, P_x is the x-day antecedent precipitation volume in mm, T_y is the y-day antecedent average temperature in

$^{\circ}C$, *I(t)* is the imperviousness in the watershed as a percentage in year *t*, and $C_1,\ldots, C_4$ are coefficients determined by numerical optimization.

3.8.2 A power model

$$Q_7(t) = C_1 \cdot P_x^{C_2} \cdot T_y^{C_3} \cdot I^{C_4}(t) \tag{3-2}$$

where Q_7 is also the annual minimum 7-day low flow in year *t* in ft^3/s, P_x is the x-day antecedent precipitation volume in mm, T_y is the y-day antecedent average temperature in $^{\circ}C$, *I(t)* is the imperviousness in the watershed as a percentage in year *t*, and $C_1,\ldots, C_4$ are coefficients determined by numerical optimization.

3.8.3 A linear model with a sinusoidal component

$$Q_7(t) = C_0 + C_1 \cdot Sin\left(\frac{2\pi \cdot i}{365.25} + \phi\right) + C_2 \cdot P_x + C_3 \cdot T_y + C_4 \cdot I(t) \tag{3-3}$$

where i is the Julian day in which the low flow event took place and ϕ is a phase shift to be determined by the optimization. Hence, the linear model form with a sinusoidal component considers the day of occurrence in the year, *t*, as a fourth predictor.

3.9 Criteria for selecting the most representative model structure

The process of selecting the most appropriate model form for the six single-watershed regression models was based solely on the NWB watershed data sets. A regression model was calibrated for each of Equations 3-1, 3-2, and 3-3, for each of the durations of low-flow events, for each of the durations of the antecedent precipitation time series, and for each of the durations of antecedent temperature time series for the NWB watershed. A summary of the time series data for the criterion and the predictors is

listed in Table A-4. The values of the calibrated coefficients and the goodness-of-fit measures are all summarized in Table A-3. As previously concluded the 270-day antecedent precipitation always produced higher correlation (R) values when predicting the 1, 2, 3 and 7-day low flows. Similarly the 7-day low flow showed the highest correlation coefficient (R) of 0.876 for the power model form (Equation 3-2), which is later selected as optimum model form due to rationality. Using correlation coefficients and rationality as the main measures of the accuracy of the models' predictions, Equation 3-2 with 270-day antecedent precipitation and the 60-day antecedent average temperature was selected as the best model. This model emerged as the only rational model of the three forms, yielding no estimated flows below zero (Figure 3-3). Further it produced roughly the same goodness-of-fit as quantified by the correlation coefficient as the other two linear models (Equations 3-1 and 3-3). Note, in 1966 and 1999 the lowest seven-day low flow was zero, the power model (Equation 3-2) lacks the ability to produce low flows of zero. This is a shortcoming of Equation 3-2, but was considered preferable to the negative flows that Equations 3-1 and 3-3 can possibly predict.

Fitting a regression model for the NWB watershed with the form of Equation 3-2, produced the following best-fit regression model:

$$Q_7(t) = 0.294 \cdot P_{270}^{2.122} \cdot T_{60}^{-0.325} \cdot I(t)^{-0.719} \quad (3\text{-}4)$$

Equation 3-4 has a 0.89 correlation coefficient between the predicted values and observed 7-day low flow values, a relative accuracy (S_e/S_y) of 0.46, and a relative bias of 1.2%. These quantities constituted the primary criteria of the selection of the most representative model form. They will be discussed in further detail below. The equivalent of Equation 3-4 will be calibrated for each of the remaining five watersheds.

3.9.1 Minimum relative standard error (Se/Sy)

One of the strengths of using NUMOPT over using the multiple regression calibration approach is that the former optimizes the standard error in term of Q_7 while the latter optimizes the standard error in terms of the logarithm of Q_7. Thus the absolute optimum S_e is achieved through using NUMOPT. Table 3-7 shows that all three models provide moderately accurate predictions with the lowest standard relative error of 0.458 associated with the power model (Model 2). However, it is important to state the lowest will not necessarily constitute the best model form and thus other statistical measures will have to be considered. The correlation coefficients for all three models are practically the same and, thus, can not be used as a measure to differentiate the best model form.

Table 3-7. Goodness-of-fit statistics for each of the three calibrated model forms (Sample size is 35).

Goodness-of-fit	MODEL 1	MODEL 2	MODEL 3
Corr. Coef. (R)	0.891	0.893	0.890
Bias (cfs)	-3.525	12.062	-1.278
Avg. Bias (cfs)	-0.101	0.345	-0.037
Avg. Q7 (cfs)	28.346	28.346	28.346
Rel. Bias (%)	-0.355	1.216	-0.129
Se (cfs)	10.520	10.445	10.538
Sy (cfs)	22.805	22.805	22.805
Se/Sy	0.461	0.458	0.462
C1	33.4623	0.2943	6.3502
C2	1.8552	2.1221	1.8776
C3	-1.8907	-0.3254	-1.4203
C4	-1.5711	-0.7186	-1.5244
C0			27.2984

Bias: The sum of errors
Avg. Bias: The average magnitude of errors
Avg. Q7: The average annual 7-day low flow
Rel. Bias: The ratio of average magnitude of errors to the average annual 7-day low flow
Se: The standard error of estimate
Se/Sy: The relative standard error of estimate

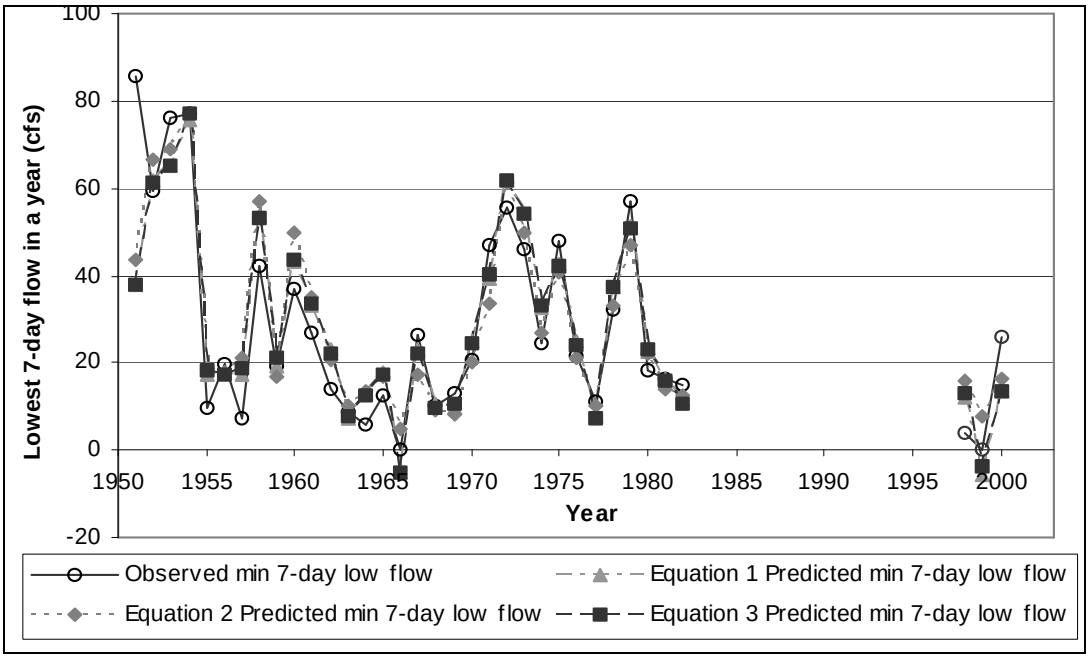

Figure 3-3. A plot of the predicted 7-day low flow events for the NWB watershed for each of the three proposed model forms.

3.9.2 Minimum relative bias

Although all three model forms produce low relative biases with the lowest being associated with the linear model with a sinusoidal component, there is no real difference among the three relative bias values. The two linear models (Equations 3-1 and 3-3) show a tendency to under predict the 7-day low flow whereas the power model (Equation 3-2) shows a tendency to over predict. Thus far, both the standard error and average relative biases have shown no real distinction among the three proposed models. Other measures will have to distinguish the best regression model form.

3.9.3 Residuals analyses

The study of the magnitude of residuals and their distributions can provide inferences on the selection of the proper model structure. The residuals are calculated by subtracting the observed 7-day low flow from the predicted value. If the difference is a positive quantity the model over predicts for that particular date, and if it is a negative

quantity then it under predicts. The mean bias for all three models is close to zero and all three histograms of the residual distributions show normal distributions. Thus all three models seem adequate. Additionally, none of the three models show any existence of local biases where the model would tend to under-predict or over-predict for certain range of values.

3.9.4 Sensitivity analyses

The intercorrelation matrix (Table A-5) shows that the precipitation time series is the most correlated predictor to the criterion variable of 7-day low flow. Temperature is the second most correlated, followed by the imperviousness. This is not completely in agreement with the magnitude of the calibrated coefficients for each of the three models (Table 3-7). This is probably due to the moderate intercorrelation existing between the temperature predictor and both the precipitation and imperviousness predictors. However, the signs of the calibrated coefficients are all rational and in agreement with the physical relationship between the predictors and the quantity of the 7-day low flow event. Precipitation is positively correlated to the 7-day low flow and the calibrated coefficient associated with the precipitation predictor for each of the three models is a positive quantity. Temperature and imperviousness are both negatively correlated to the 7-day low flow and the calibrated coefficients associated with them for each of the three models are negative quantities.

3.9.5 Rationality

The model form must not only give the most accurate prediction but also rational results. The two linear models show a possibility of producing negative flows which is

physically impossible and thus irrational. This makes the power model the only rational form and thus the only appropriate model form. Rationality becomes the most important criterion in making the final selection of the best model form.

3.10 Necessity of a regional regression model

The calibrated power model is based on the NWB watershed and thus its outcome should only be applicable to predictions associated with the NWB. A regional model will be calibrated to expand the applicability of our regression model to a larger scale. The NWB watershed and five additional watersheds, all in the Maryland Piedmont region, were analyzed separately and then combined to best understand the usefulness of the regional model. The addition of the other five watersheds, Seneca Creek, Hawlings, Watts Branch, Rock Creek, and Little Falls, is to eliminate any idiosyncratic characteristics of the NWB watershed that are captured by the selected predictors. All of the selected watersheds are all in Montgomery County, Maryland, of varying drainage area, and exhibit different urbanization levels. The regional model will be calibrated based on four indices: 270-day antecedent precipitation, 60-day average antecedent temperature, annual percentage of imperviousness, and watershed area. The regional model is then to be used in a predictive sense to simulate the effects of two phenomena: the effect of climate change and urbanization on the distribution of streamflows. Although the regional model was calibrated by using the data from all six watersheds combined, calibrating a regression model for each of the six watersheds individually and then a regional model will allow to us compare how the calibrated coefficient values vary and what final coefficients should be believed to be most representative.

3.10.1 Calibration of a regional model of low flows

The decision of expanding the scale of this work to a regional regression model will require the analysis of selecting the most appropriate model structure to be applied to the combined data of all six watersheds. Four model structures were investigated to determine the best form. The power model form was determined to be the optimum model form to predict the NWB 7-day low flow data, but now historical 7-day low flow data from five additional watersheds were added. The model forms to be tested for are: a linear model, a power model, a linear model with a sinusoidal component, and a power model with a sinusoidal component. These models are similar to Equations 3-1, 3-2, and 3-3 with the addition of a watershed area component, where area is in squared miles.

3.10.1.1 A linear model

The linear model form was calibrated using the multiple regression approach (MRA). The model form is as shown in Equation 3-5:

$$Q_7(t) = C_1 + C_2 \cdot P_x + C_3 \cdot T_y + C_4 \cdot I(t) + C_5 \cdot A \qquad (3\text{-}5)$$

The calibrated values for the coefficients C_1, C_2, C_3, C_4, and C_5, are summarized in Table 3-8. The coefficient associated with the imperviousness predictor, $I(t)$, is irrational because it carries a positive sign whereas $I(t)$ is inversely correlated to the 7-day low flow quantity.

3.10.1.2 A power model

The power model form was calibrated using two approaches: using Stepwise regression and using a numerical optimization method (NUMOPT). As will be noted later, NUMOPT will deliver the more accurate calibrated coefficients because it produces the lower standard error. The model form is shown in Equation 3-6:

$$Q_7(t) = C_1 \cdot P_x^{C_2} \cdot T_y^{C_3} \cdot I(t)^{C_4} \cdot A_y^{C_5} \quad (3\text{-}6)$$

The values of the calibrated coefficients based on both approaches are listed in Table 3-8 below. Note, the values of the calibrated coefficients are different for each of the two approaches, but none of the values are irrational in terms of magnitude or sign.

3.10.1.3 A linear model with a sinusoidal component

The sinusoidal component is used to possibly capture the seasonal trend of low flows based on the occurrence time in the year. However, as was the case with the model form associated with the NWB data set, this model form proves inadequate due to irrationality. The model form is as shown in Equation 3-7. The calibrated coefficients are listed in Table 3-8. The calibrated coefficient associated with imperviousness is irrational in sign.

$$Q_7(t) = C_0 + C_1 \cdot Sin\left(\frac{2\pi \cdot i}{365.25} + \phi\right) + C_2 \cdot P_x + C_3 \cdot T_y + C_4 \cdot I(t) + C_5 \cdot A \quad (3\text{-}7)$$

3.10.1.4 A power model with a sinusoidal component

Since the power model has shown to perform well in the prediction of 7-day low flows, calibrating a power model with a sinusoidal component seems like it might produce good results. It will allow us to test for the necessity of the addition of the sinusoidal component to capture any seasonal trends in the unexplained variance experienced in Equation 3-6. The model form is as shown in Equation 3-8. The calibrated coefficients are summarized in Table 3-8. All calibrated values of coefficients are rational.

$$Q_7(t) = C_0 + C_1 \cdot Sin\left(\frac{2\pi \cdot i}{365.25} + \phi\right) + C_6 \cdot P_x^{C_2} \cdot T_y^{C_3} \cdot I(t)^{C_4} \cdot A_y^{C_5} \quad (3\text{-}8)$$

Table 3-8. List of calibrated coefficient values for the regional model proposed forms.

Calibrated Coefficients	Model				
	Linear Mult. Reg. (Equ. 3-5)	Power Stepwise (Equ. 3-6)	Power NUMOPT (Equ. 3-6)	Linear + Sin NUMOPT (Equ. 3-7)	Power + Sin NUMOPT (Equ. 3-8)
Ø				-0.9078	-0.0797
C_0				189.68	19.5193
C_1	124.79	7.6393	0.1390	29.9224	28.6371
C_2	3.6277	2.2963	1.9332	3.8956	0.1000
C_3	-3.4030	-2.1123	-1.0066	-4.3430	1.9173
C_4	0.2412	-0.4147	-0.1310	0.4400	-0.9148
C_5	1.9381	1.1347	1.1438	1.9437	-0.0143
C_6					1.0811

3.10.2 Comparison among the proposed regional model structures

A comparison of the goodness-of-fit statistics among the five calibrated models in Table 3-9 shows that the NUMOPT power model and the power model with a sinusoidal component are superior. The relative standard error, S_e/S_y, for the power models is lower than the ones based on the other forms. Similarly, the explained variance based on the power model form is higher than the others. A further comparison between models 3-6 and 3-8, shows that a slight improvement in accuracy was gained by adding the sinusoidal component. However, this does not necessarily recommend the addition of the sinusoidal component, because the addition of three extra coefficients is probably the main element in producing a better fit. Generally, the more coefficients are calibrated, the better fit that can be achieved. But additional coefficients add complexity to the model form. In this case, the additional accuracy achieved was judged not to be worth the added complexity. Therefore, the power model, Equation 3-6, was determined to be the best model structure to predict the 7-day low flow in the Maryland Piedmont region. This is in

agreement with the conclusion that was reached based on the NWB watershed data solely.

Table 3-9. Goodness-of-fit statistics for each of the proposed regional model forms.

Goodness-of-fit Statistics	Linear Mult. Reg. (Equ. 3-5)	Power Stepwise (Equ. 3-6)	Power NUMOPT (Equ. 3-6)	Linear + Sin NUMOPT (Equ. 3-7)	Power + Sin NUMOPT (Equ. 3-8)
Bias (cfs)	N/A	-7.5571	0.6070	-0.0001	0.0000
S_e (cfs)	48.6835	53.0771	30.3459	47.3481	29.6534
S_y (cfs)	97.8579	97.8579	97.8579	97.8579	97.8579
S_e/S_y	0.4975	0.5424	0.3101	0.4838	0.3030
R	0.8707	0.8441	0.9519	0.8797	0.9549
R^2	0.7582	0.7125	0.9060	0.7739	0.9118

The goodness-of-fit statistics of the power model, Equation 3-6, shows a substantial difference between the outcomes of stepwise regression and NUMOPT. This illustrates that NUMOPT is a more accurate approach when calibrating for a power model form. NUMOPT optimizes to the lowest possible standard error value, Se, which is generally, but not necessarily always, the best form. Stepwise Regression, on the other hand, is based on an incremental F test or the analysis of variance on R. It illustrates the significance of the addition of each of the proposed predictors to the accuracy of the model; it will be later used as a tool to investigate the necessity of the incorporation of the four predictors.

3.10.3 Residuals analyses

The goodness-of-fit statistics have concluded that Equation 3-9 is the best option from the pre-selected model structures:

$$Q_7(t) = 0.1390 \cdot P_x^{1.9332} \cdot T_y^{-1.0066} \cdot I(t)^{-0.1310} \cdot A_y^{1.1438} \qquad (3\text{-}9)$$

The residuals need to be examined to test for the normality of residuals and to identify any local biases among the six selected watersheds. The study of errors will probably prove the adequacy of using the model form of Equation 3-9.

3.10.3.1 Normality of the residuals

The distribution of residuals of the regional model form in Equation 3-9, are plotted below in Figure 3-4. The figure indicates that the residuals follow a normal distribution. This supports the power model form selected to reproduce the low flow data events for all six watersheds.

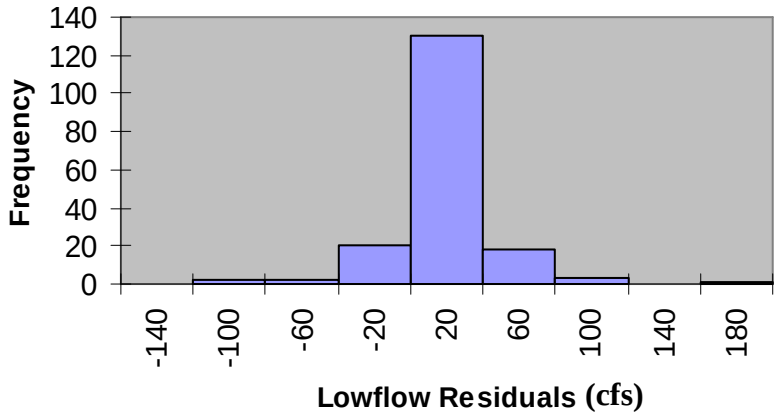

Figure 3-4. Distribution of residuals of the regional power model form.

3.10.3.2 Existence of local biases among the six selected watersheds

The existence of local biases in the residuals suggests that the selected model form is inadequate to predict the 7-day low flow in our study area. Even though normality was shown above, it is important that the model does not consistently over or under predict for certain low flow ranges. Figure 3-5 below supports the claim of

normality of the residuals since fewer points exist as we move to larger low flow events. However, some shift of the level of variation is apparent, which might be associated with the variation in the range of magnitudes for each of the six watersheds. Thus it is probably more meaningful to look at the relative errors instead.

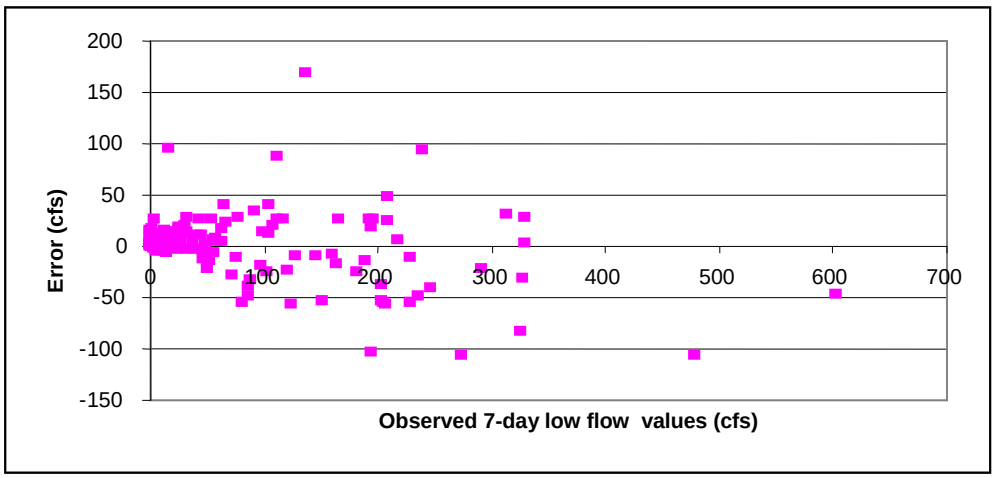

Figure 3-5. Distribution of residuals of the regional power model form (Equation 3-9).

In Figure 3-6, it is shown that the regional power model produces larger magnitudes of relative errors for the smaller magnitudes of low flow events. This might be an indication of the poor performance of the model for the smaller watersheds. However, it might be that the larger relative errors are associated with perhaps only one or two of the six watersheds.

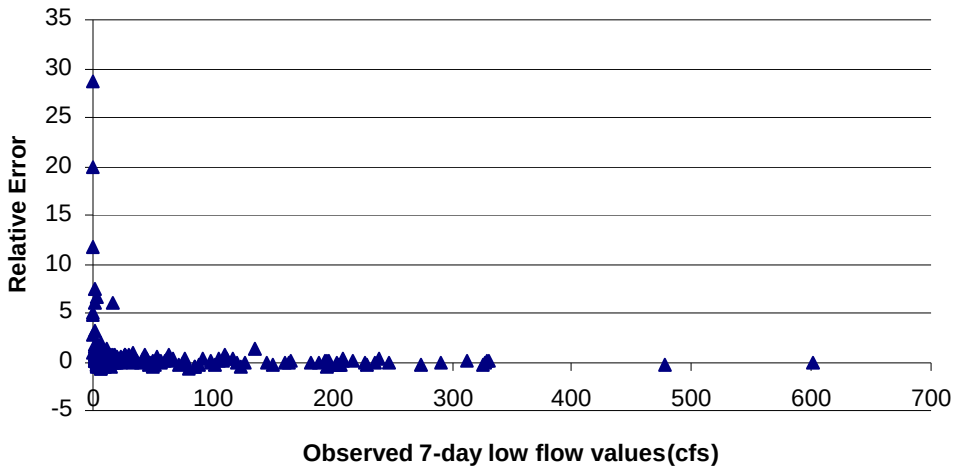

Figure 3-6. Distribution of relative residuals of the regional power model form (Equation 3-9).

Thus, plotting errors separately for each of the watersheds will provide a better understanding of the reasons contributing to the existence of local biases and if they affect the adequacy of the calibrated regional model form. A set of plots that indicate the residuals of the regional power model associated with each of the six watersheds are shown below in Figure 3-7.

The plot associated with Little Falls (Figure 3-7) shows a strong signal of local biases. It also suggests that the power model is an inadequate model structure to predict low flow values associated with Little Falls watershed. This can explain the poor performance of the regional power model to predict some of the lower low flow values observed previously in Figure 3-5. The surprising results for Little Falls watershed will be later related to the fact that the low flow data of Little Falls watershed exhibit an irrational correlation with urbanization, where low flows increase with an increase in urbanization. The residuals associated with the other five watersheds show no clear trends of local biases. Yet there seems to exist a slight tendency to under predict higher low flow magnitudes and over predict lower low flow magnitudes.

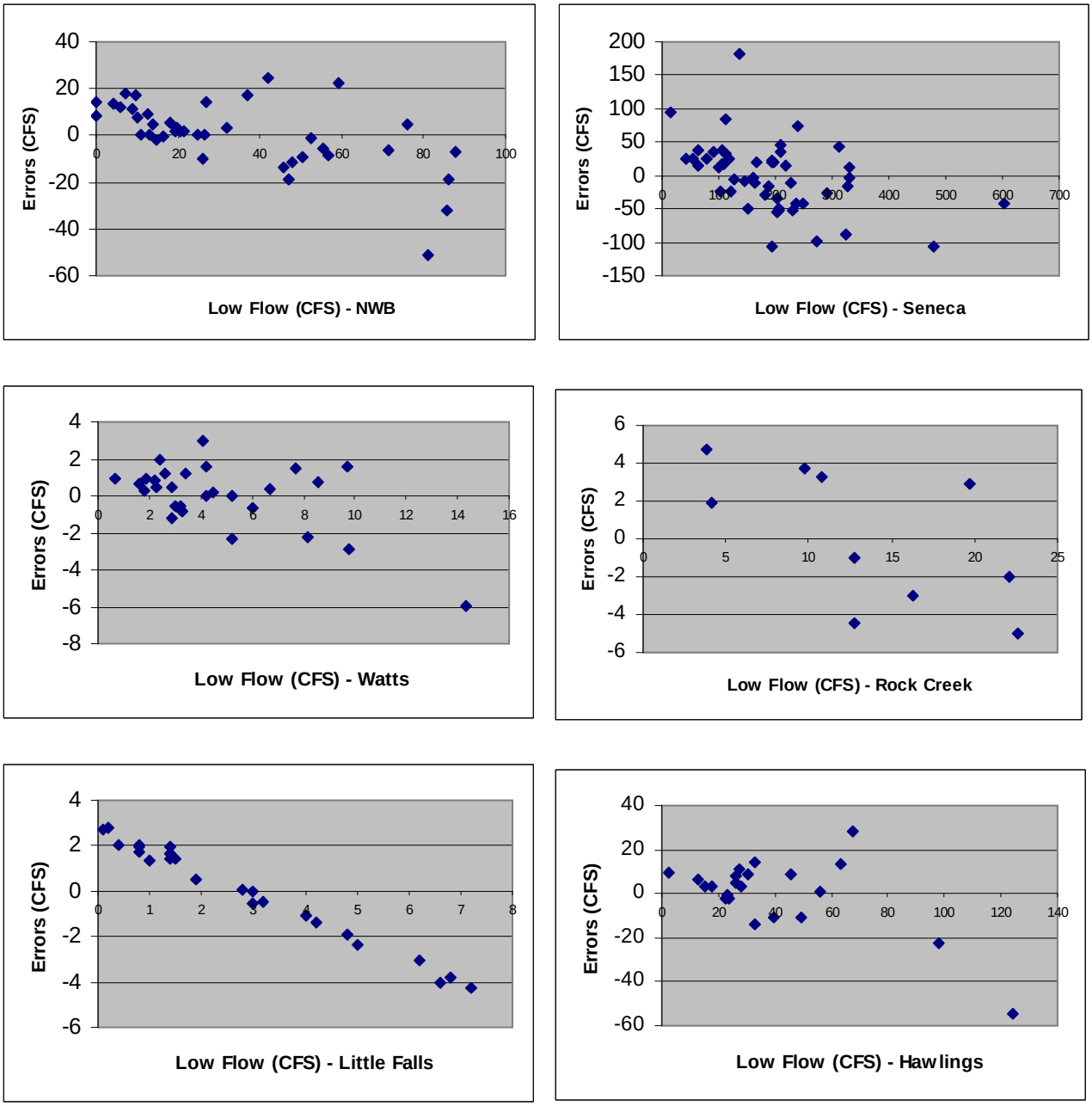

Figure 3-7. Distribution of residuals of each of the individual watersheds based on the predictions of the regional power model form.

3.10.4 Sensitivity analyses

The relative sensitivity of the predictors is captured by the relative magnitudes of the calibrated coefficient associated with each of the predictors. So the predictor with the largest exponent is the most sensitive predictor. Obtaining the regional model form is achieved by substituting the calibrated values of the coefficients in equation 3-6.
The calibrated coefficients in Equation 3-9, show that antecedent precipitation is the most sensitive variable, then follows area of the watershed, and antecedent temperature, respectively. Imperviousness is the least sensitive predictor with a value that is close to zero. This prompts us to question the necessity of using imperviousness as a potential predictor to make inferences about 7-day low flow events. A thorough analysis will be discussed later in the chapter to statistically justify the necessity of each of the four predictors.

Constructing a one-dimensional response surface of relative standard error and relative bias can also convey the relative sensitivity of the predictors. The one-dimensional response surfaces convey the same results as learned from the relative magnitude of the exponents. Precipitation is the most sensitive variable and a change in its coefficient value can cause the largest change in the accuracy of the model. So a 5% change in the value of the calibrated coefficient associated with the precipitation predictor leads to the largest shift in the values of the relative standard error, Se/Sy, and the relative bias of the regional model form. This is also apparent in Figures 3-8 and 3-9 since the precipitation predictor's response surface forms the steepest curve.

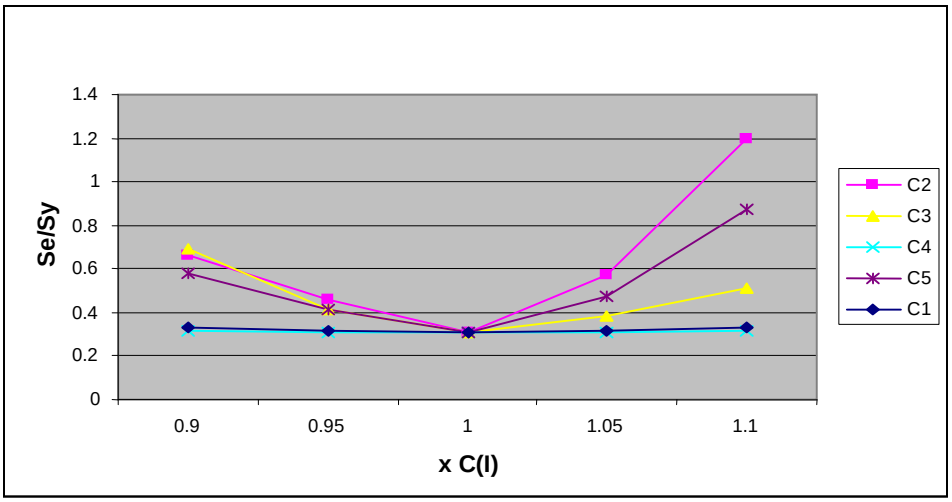

Figure 3-8. One-dimensional response surface based on the relative error (Se/Sy) criterion, which compares the relative sensitivity of the calibrated exponents of the regional regression model.

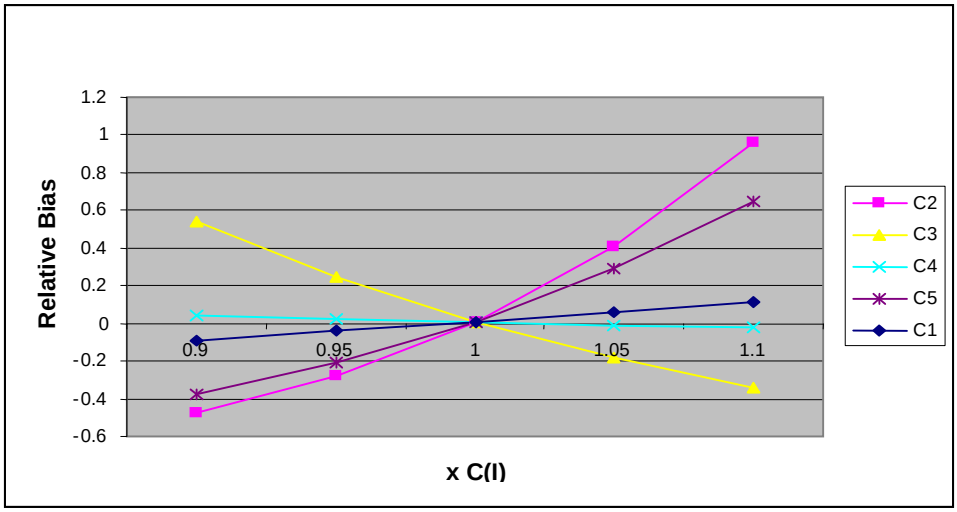

Figure 3-9. One-dimensional response surface based on the relative bias criterion, which compares the relative sensitivity of the calibrated exponents of the regional regression model.

3.10.5 Rationality

Rationality is another important measure of the adequacy of the model structure. Irrationality of the linear model forms was sufficient to eliminate them as possible structures. The power model form, on the other hand, has rational coefficients' signs and magnitudes. Precipitation was anticipated to have the largest influence on low flows and

has produced the largest exponent. The exponent of the area predictor is a positive value that is close to one. Temperature and imperviousness have inverse relationships with low flows and thus should attain negative quantities for their exponents.

3.10.6 Comparing the regional model to each of the six single-watershed calibrated models

A power model of the form of Equation 3-2, was calibrated for each of the six watersheds including the NWB watershed. NUMOPT was used to determine the values of the coefficients. A summary of the goodness-of-fit statistics and the values of the calibrated coefficients is listed in Table 3-10 below.

Table 3-10. Summary of goodness-of-fit statistics and calibrated coefficients for each of the single-watershed calibrated model forms (Calibrated coefficients with irrational signs are shown in bold).

Goodness-of-Fit Statistics	NWB	Seneca Creek	Little Falls	Hawlings	Rock Creek	Watts Branch
Mean of observed Q7 (cfs)	35.5243	190.9521	2.8170	39.5870	13.6056	4.6932
Mean of Predicted Q7 (cfs)	35.9587	189.8160	2.7960	39.2727	13.4900	4.6828
Standard Error of Estim., Se (cfs)	15.5056	54.0013	2.3482	17.6375	4.4350	1.8328
Standard Deviation of y, Sy (cfs)	26.1328	107.9954	2.2289	28.5435	6.7131	3.0926
Se/Sy	0.5933	0.5000	1.0535	0.6179	0.6607	0.5926
Correlation Coefficient, R	0.8015	0.8574	0.1776	0.7832	0.7597	0.7999
Explained Variance, R^2	0.6423	0.7351	0.0316	0.6134	0.5771	0.6399
Bias, sum of residuals (cfs)	0.4343	-0.6012	0.0145	0.2772	0.1293	-0.0007
Mean Bias (cfs)	0.4343	-0.6012	0.0145	0.2772	0.1293	-0.0007
Standard Deviation of Bias (cfs)	14.8390	52.3185	2.1965	16.3267	3.6186	1.7318
Relative Bias	0.0122	-0.0031	0.0052	0.0070	0.0095	-0.0001
C_1	3.1568	7.1615	0.0164	1.5441	0.0046	1.0386
C_2 (prec. In.)	1.9954	1.9223	**-0.3677**	2.7504	1.3921	2.0148
C_3 (temp. F)	-0.5682	-0.9610	-0.1900	-2.4075	**0.4897**	-0.8466
C_4 (imperv. %)	-0.8790	**0.3209**	**2.0005**	**1.8467**	**0.4274**	-0.5528

The relative magnitudes of the average 7-day low flows and standard errors are consistent with the size of the watersheds. Thus in order to compare the statistics of the six watersheds, it is more meaningful to concentrate on the values of the explained

variances, the relative bias, and the relative standard errors. The power model seems to fit the data for all the watersheds except the Little Falls watershed which exhibits an extremely low explained variance of 3.2%. So the model form can only explain 3.2% of the scatter of the data and the rest is considered random fluctuations. The relative standard error values are in agreement with the correlation coefficients values. All watersheds show a substantial reduction in standard error with the power model form except the Little Falls watershed which has a higher standard error than standard deviation of the criterion variable. Relative bias values are small for all six watersheds, and they do not suggest any inadequacy with the power model form.

When analyzing the rationality of the calibrated coefficients, only the NWB watershed and Watts Branch produce all rational coefficient values. Little Falls being the poorest, produces a negative coefficient value for the precipitation predictor and a positive coefficient value for the imperviousness predictor. This says that the historical record of Little Falls conveys smaller low flow events with larger antecedent precipitation magnitudes and smaller impervious areas. This is irrational and is probably better explained by the dominance of the much larger magnitude of the imperviousness coefficient, which in essence is capable to cause irrationality in the other less dominant predictors. The calibrated coefficients of the imperviousness predictor show irrationality in the case of Seneca Creek, Little Falls, Hawlings, and Rock Creek watersheds. This is mainly due to the modest changes of urbanization levels over their periods of record.

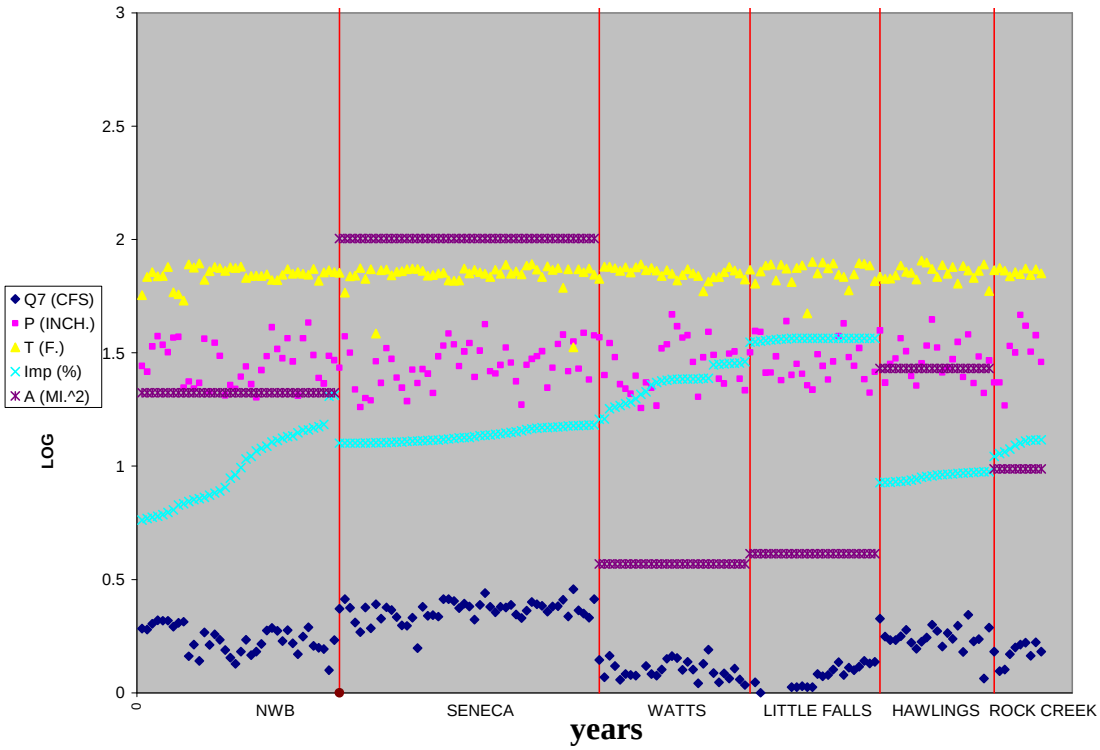

Figure 3-10. Log-log plot of the historical time series for all four predictors as well as the 7-day low flow variable; plot separates time series by watershed.

Three questions arise and become important to answer to better assess the reliability of the regional power model structure. First, if in four out of six watersheds, the calibrated coefficients associated with imperviousness predictor are irrational, then is imperviousness really a statistically important predictor? Also acknowledging that the calibrated coefficients are random variables and that in the cases of Little Falls and Rock Creek some coefficients became irrational due to the dominance of other predictors, raises the question of how much we believe in these calibrated coefficients. This can be addressed by calculating confidence intervals on the exponent values. Last, the poor goodness-of-statistics and the irrationality of the calibrated coefficients associated with the Little Falls watershed question the credibility of the data for Little Falls. So should Little Falls be omitted?

3.11 Investigating the necessity of the four predictors statistically

This discussion will focus on the necessity of the imperviousness predictor in particular and to investigate if any significant trend in the historical data between the 7-day low flow and imperviousness exist. Three different approaches were performed to confirm the need to maintain the imperviousness predictor in the regional model.

3.11.1 Stepwise regression analysis

The stepwise regression approach has shown area to be the most sensitive variable. Antecedent precipitation and antecedent temperature are second and third, respectively, while imperviousness is the least sensitive variable. Table 3-11 below shows that the regional power model form is rational. Another observation is that the addition of the antecedent temperature predictor and then the imperviousness predictor have caused a large uncertainty in the accuracy of the coefficients. The signs of the calibrated coefficients are all rational and in agreement with the signs of the correlation coefficient, R, values. This adds to the reliability of the regional power model form with the selected four predictor variables.

Table 3-11. Summary of the outcome of stepwise regression goodness-of-fit statistics used in selecting the number of predictors that add significant accuracy to the regional power model form.

Variable	b	R	R^2	Se(bi)	Se(bi)/bi	Intercept (cfs)
A	1.2366	0.8053	0.6485	0.0802	0.0649	0.4999
A	1.2504	0.8053	0.6485	0.0623	0.0499	0.0001
P	2.4829	0.2572	0.0661	0.3561	0.1434	
A	1.2318	0.8053	0.6485	0.0602	0.0488	1.8653
P	2.3070	0.2572	0.0661	0.3472	0.1505	
T	-2.1207	-0.2400	0.0576	0.7404	0.3491	
A	1.1347	0.8053	0.6485	0.0724	0.0638	7.6393
P	2.2963	0.2572	0.0661	0.3390	0.1476	
T	-2.1123	-0.2400	0.0576	0.7229	0.3422	
I	-0.4147	-0.5470	0.2992	0.1806	0.4355	

Investigating further the goodness-of-fit statistics of the regional power model with the addition of each of the predictors can convey which of the predictors add significant improvement to the accuracy of the model and which don't. The Table 3-12 below summarizes the effects of the addition of each of the proposed predictors to all of the explained variance, R^2, the relative standard error, Se/Sy, and the relative bias quantities. The addition of the area predictor has explained 58% of the total variance and has improved the accuracy of the model by 35%; but it has a very large relative bias of 23%. The addition of the antecedent precipitation predictor improves the explained variance significantly by 24.6%, reduced the relative standard error and the relative bias significantly by 23 % and 10%, respectively. Unlike the first two predictors, the addition of antecedent temperature predictor reduces the explained variance by 23%, increases the relative standard error to approximately 64%. These are considered very significant losses to the accuracy of the model despite the reduction of relative error by 9%. Moreover, the addition of the imperviousness predictor, improves the accuracy of the model by increasing the explained variance by 11.6%, and reducing the relative standard error by 10%. Relative bias is worsened by 6.5%. The outcome of the stepwise regression does not only question the necessity of an imperviousness predictor but also it recommends the elimination of the antecedent temperature predictor as well, thus further studies should be done to confirm the necessity of the predictors.

Table 3-12. Summary of goodness-of-fit statistics of the regional power model after the addition of each of the four predictors (stepwise regression).

Variable	Δ R^2	R^2	R	Se (cfs)	Sy (cfs)	Se/Sy	Bias (cfs)	Relative bias
A	0.5812	0.5812	0.7624	63.5081	97.8579	0.6490	-15.7540	-0.2303
P	0.2455	0.8268	0.9093	40.9633	97.8579	0.4186	-9.1498	-0.1338
T	-0.2298	0.5970	0.7726	62.6634	97.8579	0.6404	-3.1478	-0.0460
I	0.1156	0.7125	0.8441	53.0771	97.8579	0.5424	-7.5571	-0.1105

3.11.2 Multiple part-correlation to eliminate the effects of more dominant predictors that tend to offset the effect of the least dominant predictors (imperviousness, temperature)

The coefficient of correlation between the criterion variable and a predictor variable does not actually represent the actual relationship between them when other more dominant predictors exist. This is the purpose of the multiple-part correlation method. This method is the analog of a modified correlation coefficient after eliminating the effects of the more dominant predictors that tend to obscure the effect of the least dominant predictors. In this case each of imperviousness and antecedent temperature values were tested for significant correlation to the 7-day low flow. The null hypothesis is that there is no significant relationship between *I* (or *T*) and *Q7*, and the alternative hypothesis is that there exists a significant relationship. This test was performed on the NWB and Watts Branch historical time series. A complete summary of the multiple-part correlation analysis is provided in Appendix A. The null hypothesis was rejected in both cases for the NWB and it showed that there exists strong relationships between base flow and both antecedent temperature and imperviousness. In the case of Watts Branch watershed, the null hypothesis was rejected at a significance level of 5% and 15% for the tests between base flow and imperviousness, and base flow and antecedent precipitation, respectively. The outcome of the multiple part-correlation statistical test indicates that there exists significant relationships between base flow and both of antecedent temperature and imperviousness, but they were undetected during the calibration process because of the effects of the more dominant predictors.

3.11.3 Plotting the residuals against the imperviousness time series to detect possible correlations

Another approach to study the effects of land use change on low flows in the NWB and Watts Branch watersheds was to calibrate a regression model based on the more dominant predictors- antecedent precipitation and antecedent temperature. Then, the imperviousness time series was plotted against the residuals time series obtained by the calibrated regression model based on two predictors. This allows us to first remove the influence of the first two predictors from the low flow time series; so a trend between urbanization (imperviousness) and low flow can emerge if it exists. This was done on both the NWB and Watts Branch time series. Summaries of the calibrated models and the residuals are listed in Tables A-15 and A-16, respectively. Figures 3-11 and 3-12 below, show an emerging relationship between the imperviousness time series and the residuals. The NWB produced a stronger signal between imperviousness and the residuals with a correlation coefficient of -0.5541 verses -0.3317 for the Watts Branch time series.

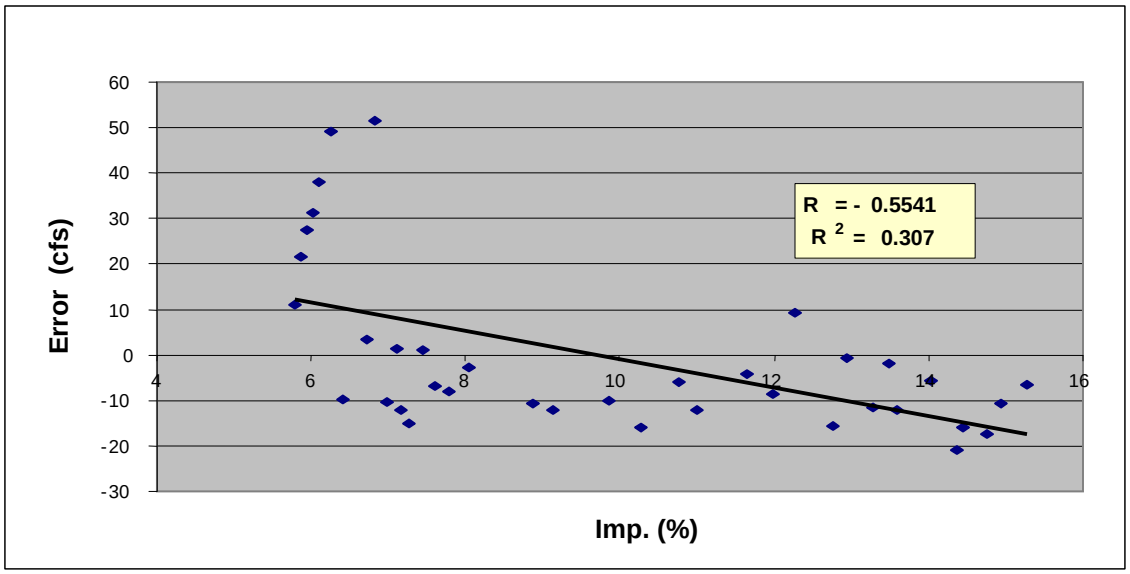

Figure 3-11. The emerging relationship between low flow time series and imperviousness time series after the removal of the effects of precipitation and temperature (NWB).

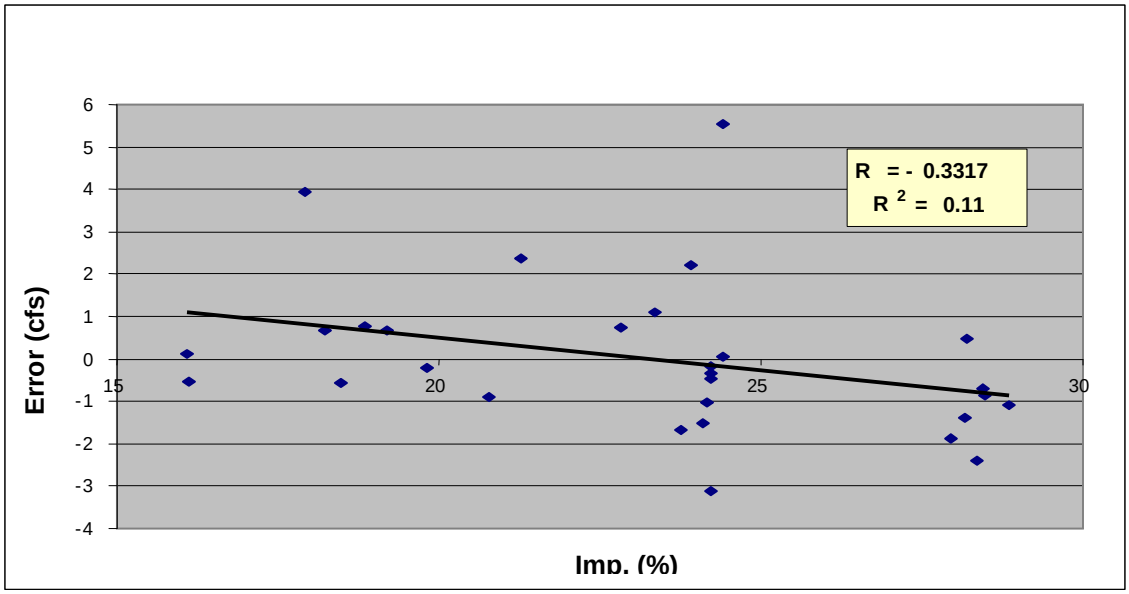

Figure 3-12. The emerging relationship between low flow time series and imperviousness time series after the removal of the effects of precipitation and temperature (Watts Branch).

3.11.4 Selecting subsets time series where some of the predictors are similar in magnitude so the effect of less dominant predictors can be observed

Knowing that in regression modeling the effect of one predictor can be obscured by the influence of a more dominant predictor necessitates further study of the data time series to verify the need for an imperviousness predictor. This scenario generally exists when predictors are highly intercorrelated. In our case, to verify the importance of imperviousness as a potential predictor to predict 7-day low flows, subsets of the NWB and Watts Branch watersheds were further studied. The selection of these two watersheds in particular is because they are the only two watersheds out of the six watersheds that have experienced a considerable change in imperviousness over their period of gage record. The subsets are formed based on the relative closeness of the antecedent precipitation and temperature predictors. In other words, events with relatively similar values of antecedent precipitation and relatively similar antecedent temperature values are grouped together. So the relationship between imperviousness and the 7-day low

flow can emerge if it exists. Six subsets from the NWB data and four subsets from the Watts Branch data, were formed with no fewer than four observations and an apparent inverse trend was noticeable as shown in Table A-20.

A regression model was calibrated for each of the sets. A summary of the predicted values as well as the residuals are listed in Tables A-21 and A-22. Furthermore, a summary of the goodness-of-fit statistics and the calibrated coefficient values are listed for the NWB and Watts Branch in Tables A-23 and A-24, respectively. All the sets except set 3 in the case of the NWB data, produced negative coefficient values for the imperviousness exponent. The four subsets of Watts Branch data did not show a pronounced influence of urbanization with only two of them producing negative exponents. The subsets were compiled based on collecting the low flow events associated with a close range of values for antecedent precipitation and evaporation predictors so the effect of urbanization on low flows could emerge. In another analyses, regression models were calibrated for the same subsets with the elimination of the precipitation and temperature predictors. This was done solely for the NWB data since it seemed to show a stronger urbanization effect on low flows. The calibrated coefficients and the correlation coefficients suggest the existence of the relationship between urbanization and low flow. Based on the results from this and earlier tests, it was decided to keep all four predictors (A, P, I, T) in our regional model form.

3.12 Recalibration of the regional model form

Since we concluded that imperviousness is a significant predictor based on analyses of the NWB and Watts Branch watersheds, it is more meaningful to recalibrate for the imperviousness predictor based on inferences from these two watersheds only.

The other four watersheds produced irrational coefficients for the imperviousness predictor; thus, it is reasonable to omit them when calibrating with the imperviousness predictor. The power models calibrated for the NWB and Watts Branch watersheds, produced imperviousness exponents of minus 0.88 and minus 0.55, respectively. Those would seem more realistic and are more indicative of the expected relationship between imperviousness and low flow. Another calibration to produce the equivalent of the regional model form was performed but with the use of only the NWB and Watts Branch data. This produced all rational coefficients with an imperviousness coefficient of minus 0.89. Thus, NUMOPT was used again to produce the equivalent of Equation 9 with the restriction of enforcing an exponent value for imperviousness. This was done for the values of minus 0.80, 0.85, and 0.90.

The equivalent of Table 3-10 is reproduced for each of the proposed imperviousness coefficients. They are summarized in Tables A-17 through A-19. The results show that fixing the imperviousness predictor value at 0.90 reduced the relative error by 1.0% but also reduced the relative bias by 3.3%. Thus, the optimum regional model form becomes as shown in Equation 3-10 below.

$$Q_7(t) = 0.2875 \cdot P_{270}^{2.0461} \cdot T_{60}^{-1.0366} \cdot I(t)^{-0.9000} .A^{1.3642} \qquad (3\text{-}10)$$

where Q_7 (t) is the annual minimum 7-day low flow in year t in ft^3/s, P_{270} is the 270-day antecedent precipitation volume in inches, T_{60} is the 60-day antecedent average temperature in $^{\circ}F$, $I(t)$ is the imperviousness in the watershed as a percentage in year t, and A is the area of the watershed in square miles.

3.13 Investigating the primary sources of uncertainty in the calibrated regional model

Having decided on the final regression model form, we should illustrate the primary sources of uncertainty in the regression model, so future research can be directed to give greater emphasis to the more important sources of uncertainty in the model. Uncertainty in the calibrated regional model is anticipated in the selection of the proper model structure, the calibration process of the coefficients and their confidence intervals, the formation process of the predictors' time series, and the lack of consideration of an important predictor that is not represented by the collected data.

3.13.1 Model structure

The decision on the best model structure is the first obvious source of uncertainty. Our analyses showed that the power model is the optimum form. However, it is possible that there exists another form that better predicts the annual 7-day low flows that was not considered. We only compared four model forms. So a power model form is not necessarily the absolute optimum relationship between low flows and each of the four predictors.

3.13.2 Calibrated coefficients (confidence intervals)

Constructing 90%, 95%, and 99% confidence intervals around the values of the calibrated coefficients can reveal more information about how much belief we should place on the calibrated values. Stepwise Regression was used to determine confidence intervals around each of the four calibrated coefficients. Table 3-13 below summarizes the results.

Table 3-13. Summary of 99%, 95%, and 90% confidence intervals around the exponents associated with the four predictors of the regional power regression model.

	Upper Limits				Lower Limits			
Var	b	at 99%	at 95%	at 90%	b	at 99%	at 95%	at 90%
P	1.84227	2.22585	2.13249	2.08544	1.84227	1.45869	1.55205	1.59910
T	-1.67633	-0.86415	-1.06182	-1.16144	-1.67633	-2.48851	-2.29084	-2.19122
I	-0.42810	-0.22475	-0.27424	-0.29918	-0.42810	-0.63144	-0.58195	-0.55701
A	1.13704	1.21832	1.19854	1.18857	1.13704	1.05576	1.07554	1.08551

Table 3-13 illustrates the ranges over which each of the coefficients is expected to vary. None of the coefficients switch signs, which is a notable indication of the reliability of our calibrated coefficients. This builds on our decision that all four predictors are significant in forming the regional regression model.

3.13.3 Determining the predictor variables (precipitation, temperature, imperviousness, and area)

There is a source of uncertainty in the process of collecting the time series of the four predictors. Initially, the fact that climate data are given at single points leads to uncertainty to take information from a single point to make inferences over an area. In some cases, the weather stations are not even located within our watersheds. In most, data had to be compiled from multiple stations to form a complete time series. This introduces the issue of intercorrelation among the various stations and biasedness of their data. Many factors actually contribute to the source of uncertainty in our climate time series. The same level of uncertainty is probably also expected in the imperviousness data. First, the step of scanning in aerial maps of our watersheds, transforming them into GIS data, geo-referencing them, and matching current coordinates, and then digitizing these watersheds into polygons of different land use, introduced a source of error and subjectivity by the digitizer. Besides, land use data are usually classified into many categories whereas in our case, we grouped them in only three categories which required

judgment calls on what constitutes each one of them. These all contribute to some source of error to be embedded in our urbanization data. Now, area is assumed to be a known value. Areas are precisely calculated by the GIS, and there is not a source of subjectivity in obtaining them.

3.13.4 Unexplained variation due to not accounting for predictors that have an influence on streamflows but are unknown, unavailable or not strong enough to show a signal.

As stated earlier, regression modeling can only convey what is embedded in our data sets. And it is often the case that we are not aware of all the contributing physical factors in a low flow event or we lack the ability to form a time series that physically represents each of the factors. In other cases, predictors are intercorrelated, which makes it far more complicated to predict low flows with a simple regression model; and the use of physical models become preferred. Besides there can be other contributing factors that can not be shown when their signals are lost in the noise of the random component of the data. These are all shortcomings of the regression modeling approach which add up to the uncertainty in a calibrated regression model.

3.14 Future simulations and future trends

The thrust of all the analyses in the previous part of this chapter was to produce a reliable and sufficiently accurate regional regression model that can be utilized in a predictive sense to predict the annual 7-day low flow under the effects of climate change and urbanization. The regional model form is given in Equation 3-10. Future analyses will be performed on the NWB time series only for the reason of reducing the scale of this work, and because we anticipate the same outcome to be learned had we selected any of the other five watersheds.

We will consider three future scenarios of base flows in the NWB watershed: base flows responding to future climate change with land use held constant at current conditions, base flows responding to future land use change with climate held constant at current conditions, and base flows responding to jointly changing climate and land use.

3.14.1 Collecting data to represent future scenarios

The ability to simulate low flows under the effects of future climate and land use change requires the availability of a future temperature, precipitation, and imperviousness time series. Ideally, future imperviousness in a watershed is projected based on the ultimate development anticipated for the watershed. For purposes of illustration in this study imperviousness is projected to increase by an estimated percentage. We will consider a 10% change in imperviousness that increases linearly over the span of the 99-year time series for the NWB watershed. Future daily precipitation and future daily average temperature time series were obtained for a 99-year period, 1994 to 2093, from two commonly used global climate models: the Canadian Climate Centre (CCC) (Boer et al., 1992; Flato et al., 2000), and Hadley (Fang and Tung, 1999). However, we need to initially investigate the selection of a grid point to represent our region of study and addressing the issue of correlations among the time series of the available grid points.

3.14.1.1 Correlations among grid points

The CCC and Hadley only provide climatic data at very specific locations and it was not possible to select one point that falls within the NWB watershed. Thus, future climate time series were compiled for four grid points which are closest to the NWB watershed. Tables A-26 and A-27 show that there exist strong correlations among the minimum and maximum temperature time series of the four selected grid points. This is

physically rationale because temperature is generally spatially persistent at a regional scale. Precipitation, on the other hand, can be much more variable especially for thunderstorms events. The precipitation time series associated with the four selected grid points, as shown in Table A-28, are uncorrelated, with a highest correlation coefficient of 0.0548. Table A-29 suggests that each of the four grids experiences approximately the same number of rainy events, and approximately 30 to 35 % of the days are rainy during the simulated 99 years of precipitation data. Yet the poor correlation would suggest independence between the series. So although they produce approximately the same number of rainy days in the 99 year time series as shown in Table A-29, their poor correlations would suggest that rainy events do not coincide among the four grid points. Thus, a simple experiment was performed to test whether an average precipitation time series based on the four time series would be representative. Only the rainy days at grid one was compared to each of the three neighboring grids during the same days. Table A-30 shows that only 30 to 36 % of those days were also rainy at the other grid points. In other words, if it rains at station one, it is likely that only one other grid point will have a rainy event.

This experiment was taken a further step by constructing a weighted average precipitation time series based on the relative distance of the NWB and Hawlings watersheds to each of the four grid points. The distances between the centers of the watersheds and each of the four grid points were measured using GIS capabilities. So the averaged daily precipitation value for the NWB, for example, is a weighted average based on the inverse distance squared to each of the four grids. So the furthest grid point would have the least weight contribution to the averaged time series. Table A-31

summarizes the results of the number of rainy events that are determined to be assigned to NWB and Hawlings watersheds based on their relative inverse distances squared from the four grid points. As concluded previously, the number of rainy days in the NWB and Hawlings are two to three times more frequent than at any of the grid points. This simple experiment confirms our claim and suggests that using a weighted average will lead to a precipitation time series with less extreme events and more rainy days. Thus it was concluded that any of the four points is as representative as any of the others, and the option of forming a weighted average time series based on all four grid points was omitted since it was proven inappropriate. The grid point we selected to represent the future daily time series of precipitation and temperature in our study is located at 38.8 N^o and 77.2 W^o and is closest to the NWB watershed. (NCAR, 2003).

3.14.2 Monte Carlo approach

The regression model developed earlier in Equation 3-10 allows us to simulate the effects of climate change and urbanization on low flows using the 99-year future time series of the four predictors, 270-day antecedent precipitation, 60-day average antecedent temperature, annual imperviousness, and the area of the watershed. However one essential component that the regression model lacks is the ability to predict the date when the low flow event is likely to occur. An analysis was performed on the historical time series to better understand what dictates the occurrence of low flow on a particular day of the year. We concluded that although both the 270-day antecedent rainfall and the 60-day antecedent temperature are excellent predictors of the magnitude of the low flow itself, they are not good predictors of the precise timing of the event. Generally the 7-day low flow event did not occur at the time of the absolute minimum of the 270-day

antecedent rainfall or maximum of the 60-day antecedent temperature.

Precipitation magnitude is not the only factor that influences the timing of the minimum annual 7-day low flow. The temporal distribution of precipitation over many months also plays a role. Further evapotransporation rates and their dependencies on temperature also affect the low flow event timing. We also recognize a limitation in our data. The raingages were not actually located within the boundaries of the watersheds. Moreover, since low flows generally occur in late summer when small-scale thunderstorms are the dominant precipitation form, the information reported at the raingages is much less representative of what occurs within each of the watersheds than during the frontal storm dominated cold season.

A Monte Carlo modeling approach was used to address the issue of selecting the day of the minimum flow event. Figure 3-13 below shows the frequency histogram of the month in which the 7-day low flow events occurred in the available years of historical data from all six watersheds. Both a normal and a triangular distribution were investigated as possible probability density functions that best capture the distribution of the timing of the observed low flow data. We found that a normal distribution of mean date of September 8 and a standard deviation of 35.8 days best approximated our observed data. A summary of the calculation of the optimum normal curve parameters and the test for normality are presented in Appendix D.

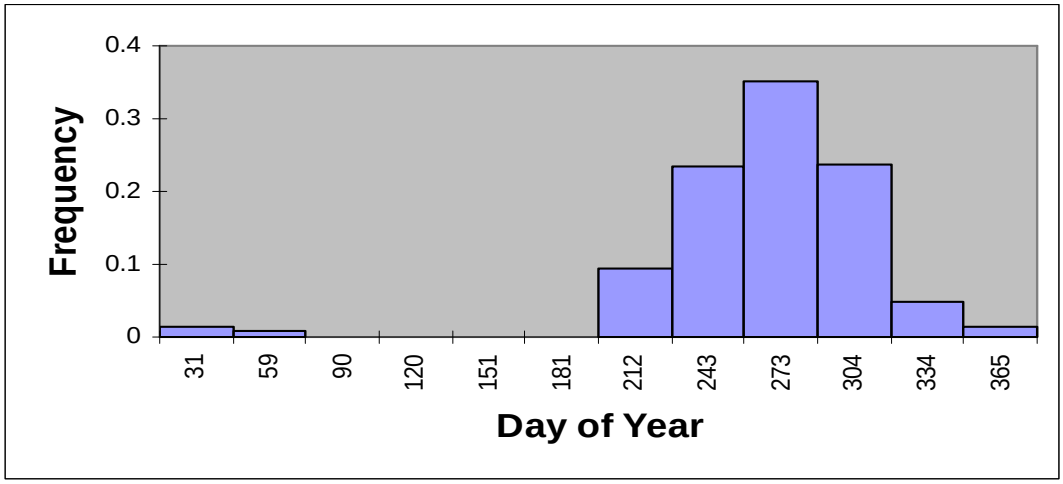

Figure 3-13. Frequency histogram of day of occurrence of minimum 7-day low flow (data of all six watersheds combined, sample size of 231 events).

To implement the Monte Carlo approach, we generated 100,000 random values per year assuming the normal distribution parameters determined above. These values determined the date of each trial's 7-day low flow. With the date determined, equation 3-10 was then used to determine the simulated low flow for that trial. The distribution of the simulated low flows is shown as a whisker box for each year. Five plots (Figures 3-18 through 3-22) were generated for the three previously proposed future scenarios using CCC and Hadley climate predictions.

3.14.3 The CCC and Hadley models

Both the CCC and the Hadley models assume a 1% annual rate of increase in the concentration of CO_2 in the atmosphere (Kittel et al., 2000; Kittel et al., 2003). Increased CO_2 concentrations lead to an increasing trend in the projected daily temperature time series for both models as shown in Figure 3-14. Unlike the Hadley precipitation time series, the CCC precipitation time series did not show a significant trend over the period studied (See Figure 3-15).

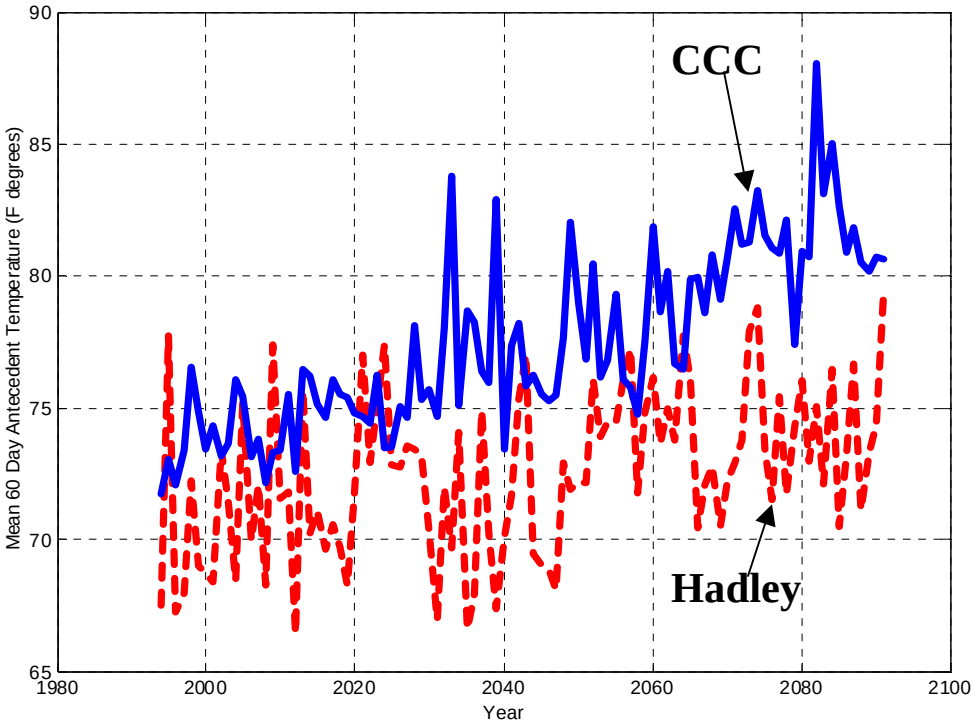

Figure 3-14. Projected average 60-day antecedent temperature

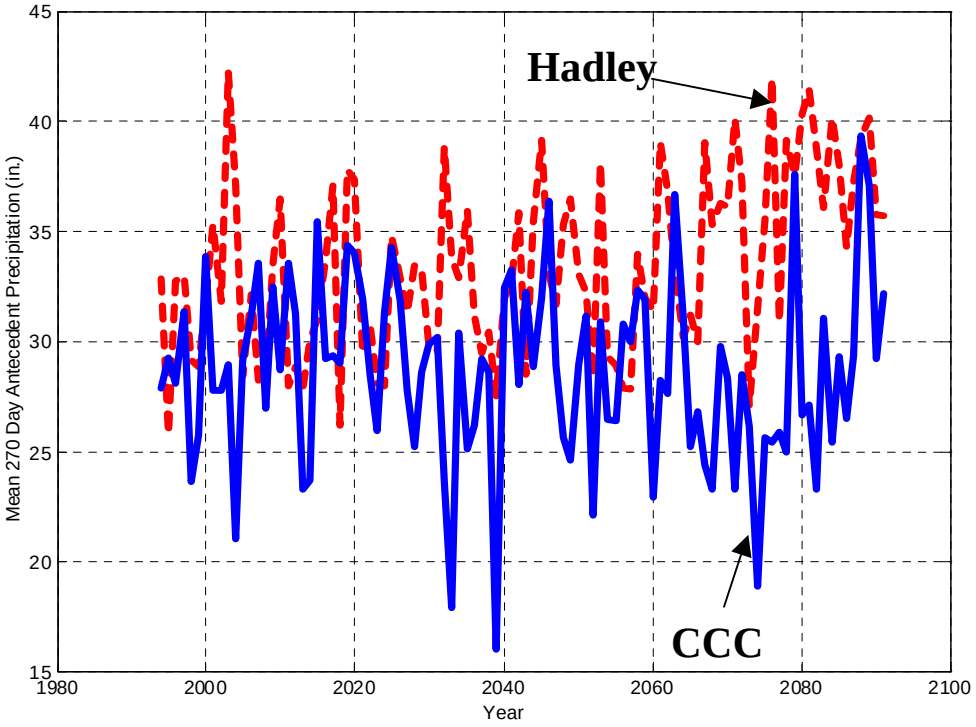

Figure 3-15. Projected average 270-day antecedent precipitation.

Therefore, it will be later shown in Table 3-15 that the CCC and Hadley temperature time series and the Hadley precipitation time series have significant increasing trends in the future 99 years of data. They were tested with the Cox-Stuart test (McCuen, 2003) for trend at a significance level of 5 percent. The Hadley predictions suggested a wetter and cooler period than did the CCC predictions.

3.14.4 Test the significance of simulated secular trends in streamflows

Table 3-14 summarizes the rejection probabilities for the Cox-Stuart trend test on the significance of observed trends in climate and streamflow time series. Tables 3-15 and 3-16 show the outcomes of the Cox-Stuart trend test at a 5 percent level of significance for each of the scenarios studied. Given the trends already detected in the precipitation and temperature time series and the low flow equation calibrated in Equation 3-10, the outcomes in Table 3-16 are not surprising. Figure 3-16 supports graphically the results shown in Table 3-16.

Table 3-14. Rejection probabilities for the Cox-Stuart trend test for the simulated precipitation, temperature, and the 7-day low flows under future predictions (significant trends at a 5 % level of significance are shown in bold).

T_{60} (^{o}F.) historical	T_{60} (^{o}F.) CCC	T_{60} (^{o}F.) Hadley	P_{270} (in.) historical	P_{270} (in.) CCC	P_{270} (in.) Hadley
(+) 7.62%	(+) **0.00%**	(+) **0.19%**	(+) 19.58%	(-) 38.77%	(+) **0.47%**
Q7 (in.) Scenario 1a	Q7 (in.) Scenario 1b	Q7 (in.) Scenario 2	Q7 (in.) Scenario 3a	Q7 (in.) Scenario 3b	
(-) 12.64%	(+) **1.06%**	(-) 12.64%	(-) **0.19%**	(-) 28.41%	

Table 3-15. Cox-Stuart test for trend at a 5 percent level of significance for both climatic inputs.

	Hadley	CCC	Historical
270-day Antecedent Precipitation Time Series	significant increase	no significant trend	no significant trend
60-day Antecedent Temperature Time Series	significant increase	significant increase	no significant trend

Table 3-16. Cox-Stuart test for trend at a 5 percent level of significance for low flows under the two proposed scenarios.

	Hadley	CCC
Climate Change Only	significant increase	no significant trend
Climate and Land Use Change	no significant trend	significant decrease
Landuse Change Only	no significant trend	

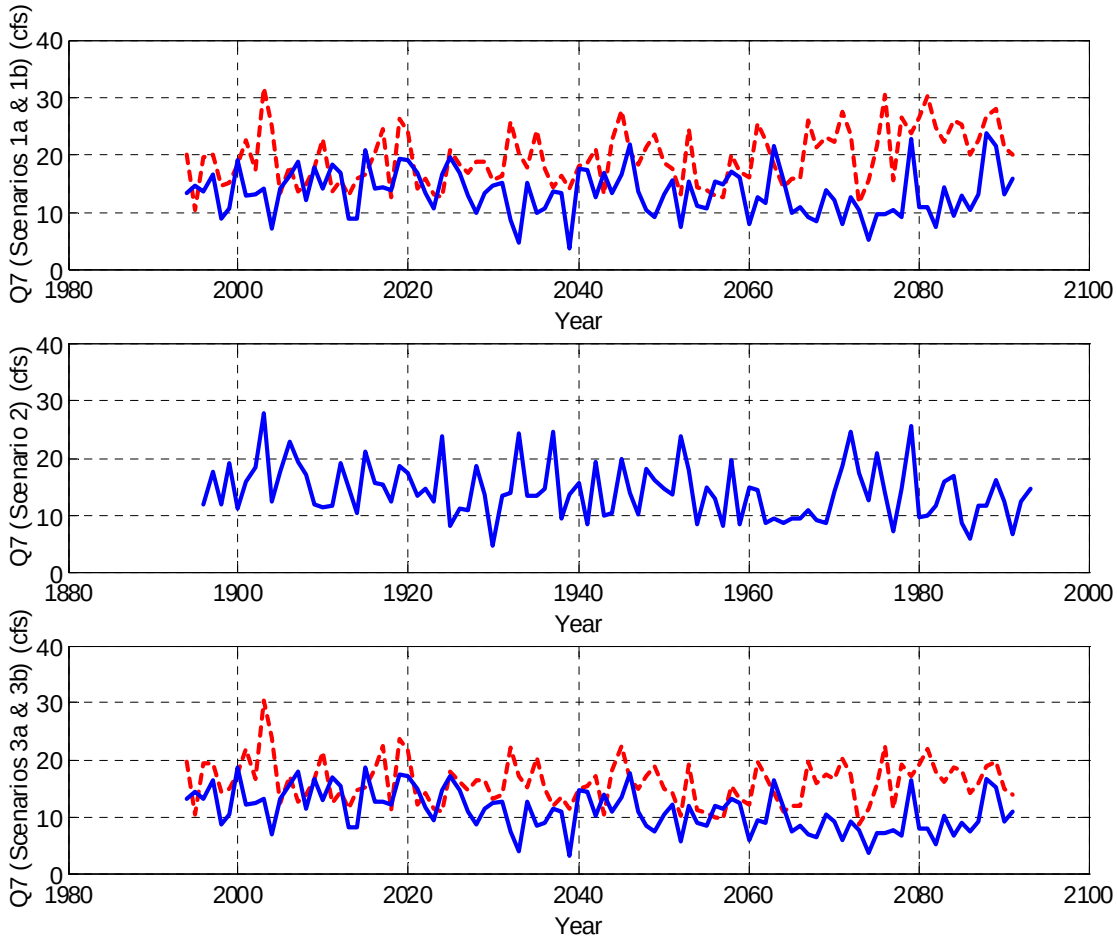

Figure 3-16. Simulated 7-day low flow events under all scenarios (the top plot is for scenario 1, the middle plot is for scenario 2, and the bottom plot is for scenario 3). CCC is shown in solid lines and Hadley is shown in dashed lines.

3.14.5 Simulations of three future scenarios

3.14.5.1 Scenario 1: hold annual imperviousness constant / vary precipitation and temperature

Let us first consider the low flow predictions under climate change and constant land use. The positive trends in temperature for both the CCC and Hadley predictions indicated in Table 3-15 would be expected to physically lead to increased evaporation and thus a reduction in low flows. Turning to Equation 3-10, the negative exponent on temperature is consistent with this interpretation. Now we must also consider the superposition of the precipitation predictions. Under the CCC predictions, no significant trend in low flows was observed. The absence of an increasing trend in precipitation and the presence of an increasing trend in temperature, even warmer than predicted by Hadley, did not lead to a decrease in predicted base flows, Figure 3-17. The strong increase in temperature was not sufficient to result in a decreasing trend in low flows because of the modest effect of temperature on low flows. Under the Hadley predictions, a positive trend in precipitation coupled with a positive exponent on the antecedent precipitation variable of equation 3-10 would be expected to lead to an increase in predicted base flows (See Figure 3-18). Hence, precipitation was capable of counteracting the effect of temperature on predicted base flows. This indicates that precipitation was sufficient not only to counteract the significant positive trend in temperature, but also to produce a positive trend in low flows under the Hadley climate predictions. This again indicates that low flows are more sensitive to precipitation than temperature. This finding is in agreement with the work of Duell (1994) which concluded that precipitation has a greater influence on streamflow than temperature.

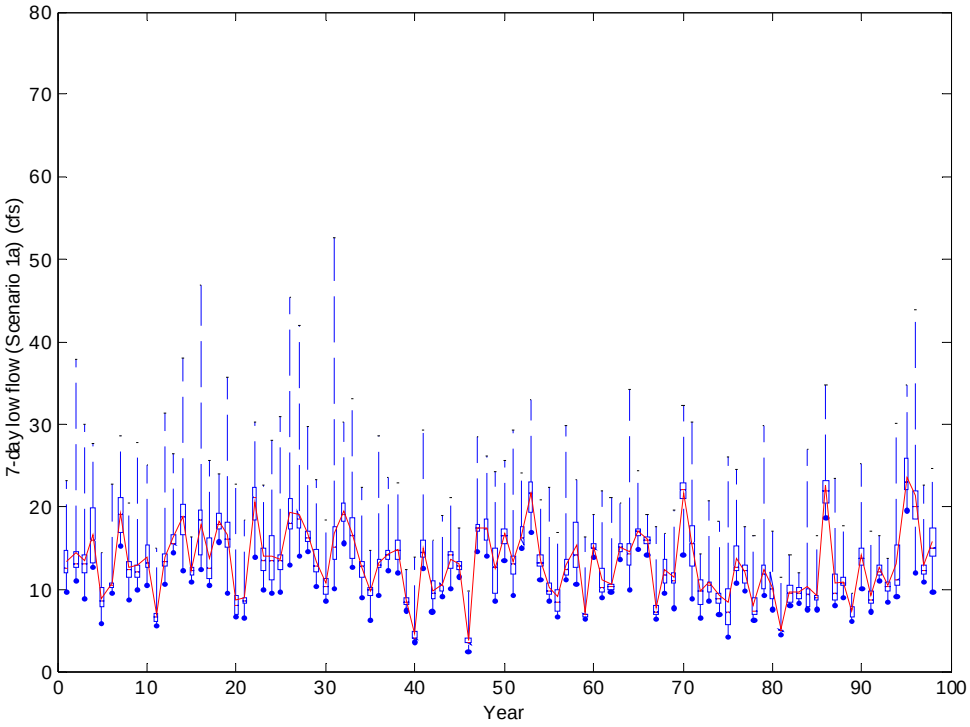

Figure 3-17. Simulated 7-day low flow events under climate change only (Scenario 1: CCC) - Indicate no significant trend at a 5% level of significance.

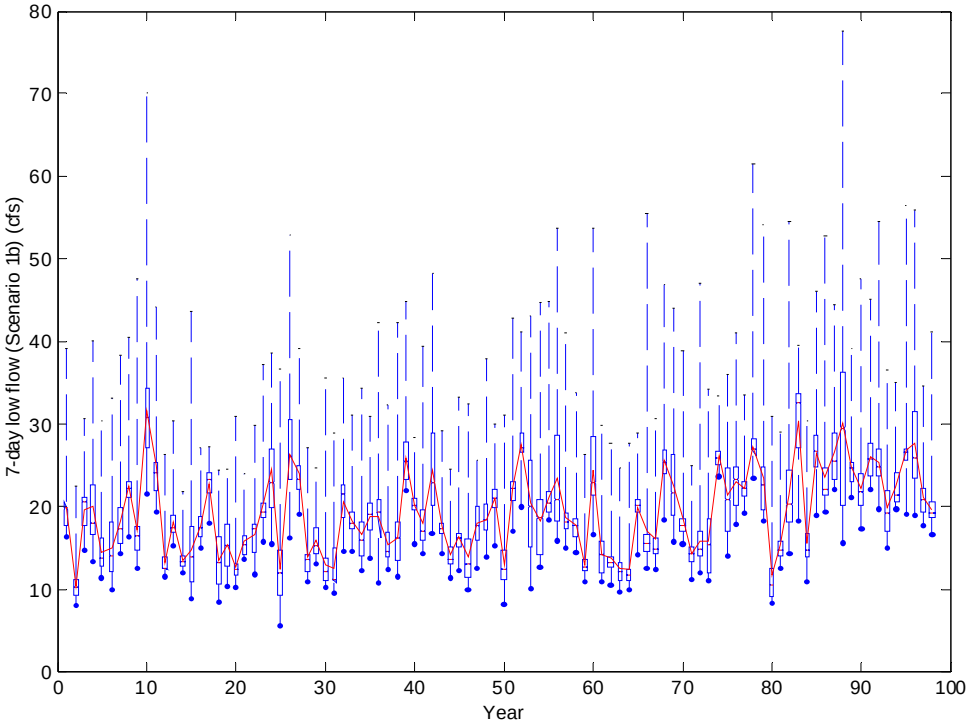

Figure 3-18. Simulated 7-day low flow events under climate change only (Scenario 1: Hadley) - Indicate significant positive trend at a 5% level of significance.

3.14.5.2 Scenario 2: vary annual imperviousness / hold precipitation and temperature constant

A constant climate condition was imposed by obtaining 99 years of historical data for the same grid point, 38.8 N^o and 77.2 W^o, used in predicting the future climate data. Table 3-15 indicates that the historical precipitation and temperature time series show no indication of an increasing trend over the 99-year historical record. Thus imperviousness is anticipated to be the main source of influence on low flows. To implement the urbanization effect, the current imperviousness of the NWB watershed was projected to increase linearly by 10 percent (from 20.5% to 30.5%) over a 99-year interval. Figure 3-19 below indicates that land use change alone was not sufficient at a 5% level of significance to show a decreasing trend in low flows under the constant climate conditions. This suggests that if the climate change effect is to be eliminated and the NWB watershed to urbanize by another 10%, low flows will not experience a significantly diminishing trend. It should be noted that a decreasing effect is apparent but is only considered significant at a confidence level of 12.6% or higher, Table 3-16.

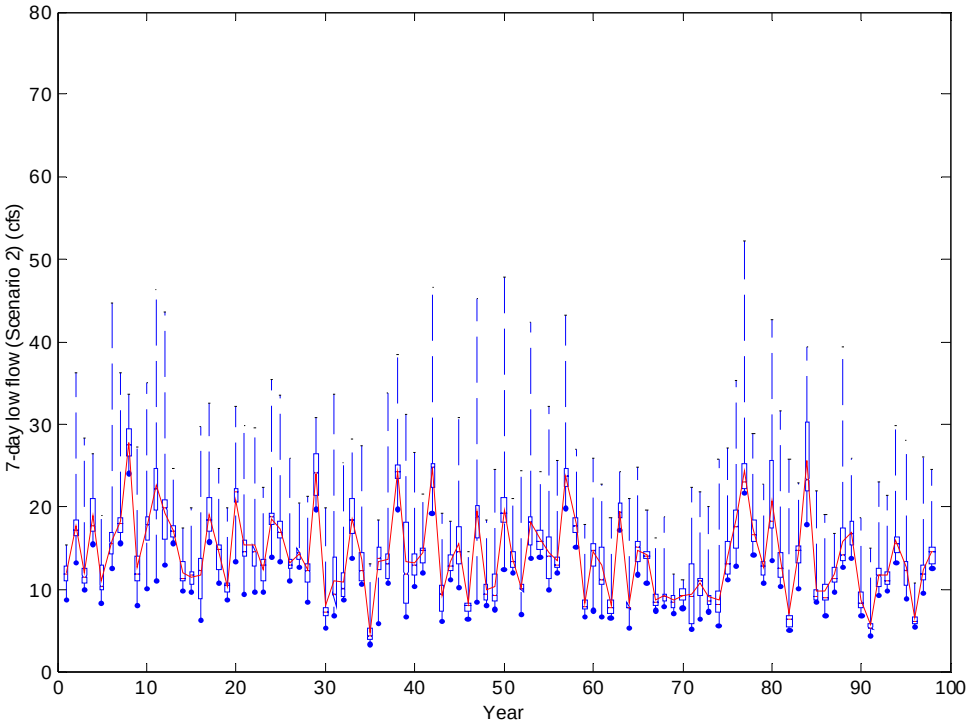

Figure 3-19. Simulated 7-day low flow events under land use change only (Scenario 2: based historical climate data).

3.14.5.3 Scenario 3: vary annual imperviousness / vary precipitation and temperature

In comparison to the outcomes of Scenario 1, the introduction of urbanization reduced the magnitude of the predicted low flows for both the CCC and Hadley scenarios. The drier and warmer predictions in the CCC scenarios coupled with a 10% increase in impervious area, led to a significant decrease at a 5% level of significance in the magnitude of low flows (See Figure 3-20). Under the Hadley predictions, the addition of land use change joined with an increasing trend in temperature, were capable of offsetting the effects of the predicted increasing trend in precipitation on low flows leading to no significant trends in the predicted low flows (See Figure 3-21). Further, Figure 3-20 shows that employing the 10 percent increase in urbanization in the NWB watershed reduced the magnitude and the variation around the mean annual 7-day low flow discharges. Note, however, both magnitude and variation are reduced by the same factor, that is urbanization. Thus, even though the addition of land use change leads to what seems to be a decreasing trend in variations around the mean 7-day low flow, the mean itself is also reduced by the same factor, urbanization, and the coefficient of variation is constant regardless of any change in land use.

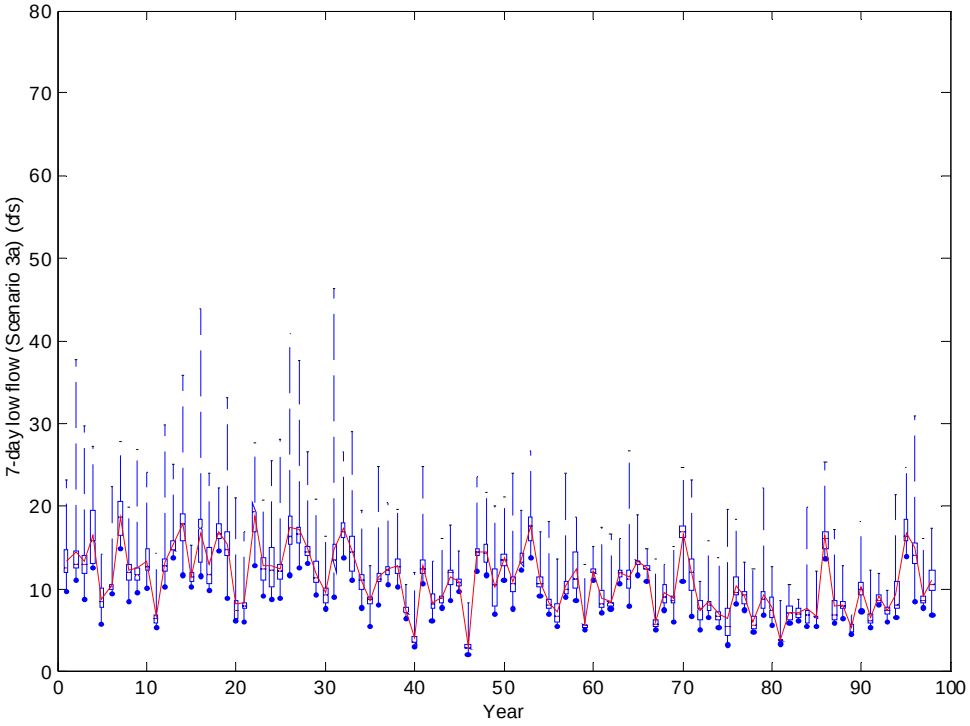

Figure 3-20. Simulated 7-day low flow events under the joint effect of climate and land use change (Scenario 3: CCC).

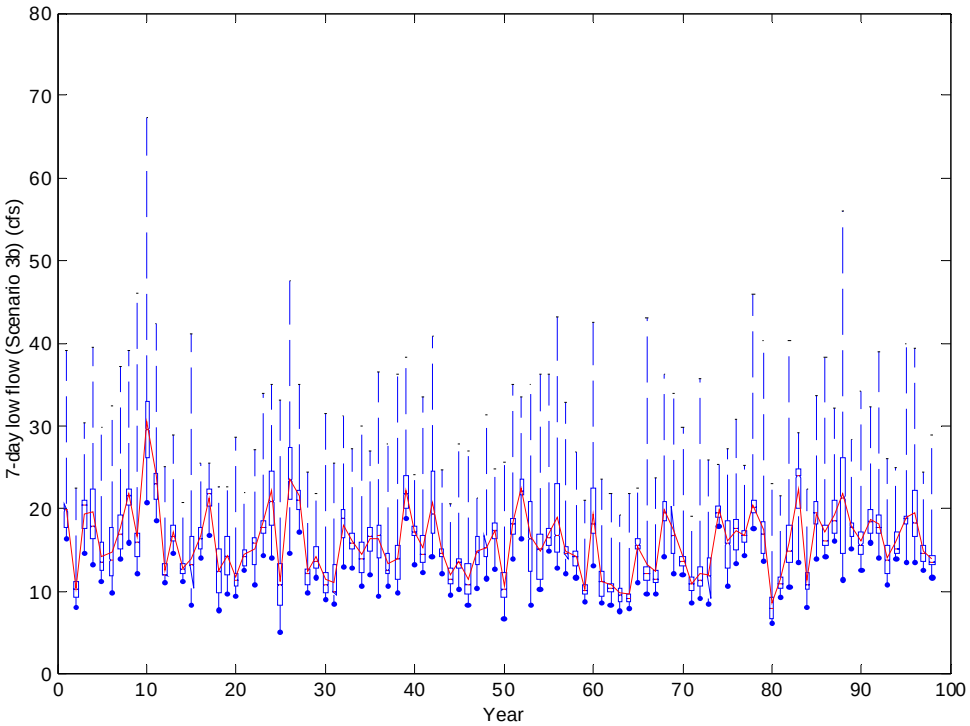

Figure 3-21. Simulated 7-day low flow events under the joint effect of climate and land use change (Scenario 3: Hadley).

3.15 Summary

The regression approach presented here predicts trends in low flows considering the effects of both climate change and urbanization by using daily time series of precipitation, temperature and imperviousness as predictors of the low flow discharge. A Monte Carlo approach was used to predict the low flow estimates for the proposed future scenarios. The Cox-Stuart trend test has indicated a significant decreasing trend in future low flows under the CCC climate predictions with both climate and land use change. On the other hand, a significant increasing trend in future low flows was observed using the Hadley climate predictions. Comparing the CCC and Hadley predictions of low flows under constant land use, shows that the climatic inputs of temperature and precipitation play contradicting effects on low flows. These findings are explained by two arguments. First, the CCC model predicted a drier and warmer climate than the Hadley model. Second, low flows have a stronger dependency on precipitation than on urbanization or temperature. This is in agreement with the magnitude and signs of the exponents of the calibrated model form Equation 3-10, where precipitation has an exponent that is approximately two times higher in magnitude than the exponents of the temperature predictor and the imperviousness predictor.

CHAPTER FOUR

USING A CONTINUOUS STREAMFLOW MODEL TO INVESTIGATE THE EFFECTS OF CLIMATE AND LAND USE CHANGE ON STREAMFLOW DISTRBUTIONS

4.1 Overview

To study the effects of climate and land use change on the distribution of the streamflows in the Maryland Piedmont region, a continuous streamflow model was applied at the same six watersheds that were utilized in the regression modeling approach. The continuous streamflow model takes as input time series of temperature and precipitation. Additionally, two model inputs that quantify urbanization effects were allowed to vary so that varying climate and urbanization could be individually and jointly examined. The details of how this study was performed and an analysis of the study results will be presented in this chapter.

4.2 The continuous streamflow model

The continuous flow model used in the analysis presented here is largely outlined in McCuen (1986). Although this model is somewhat simpler compared to the more complicated continuous streamflow models that are available, this model is conceptually similar with the more well-known Stanford Watershed Model (Crawford and Linsley, 1966), now commonly used as HSPF (Bicknell et al., 1997). Another conceptually similar continuous streamflow model is SWMM (Huber and Dickinson, 1988; Roesner et al., 1988; Donigan and Huber, 1991).

Some modifications have been made to the model structure presented in McCuen (1986). Specifically, the infiltration mechanism has been modified slightly to capture saturation behavior and evaporation has been generalized to make it functionally

dependant on daily temperature values. An extra input variable, PTHRESH, was created such that this is the maximum daily infiltration value possible. For daily precipitation volume (PREC) less than the ratio of the maximum daily infiltration value (PTHRESH) to the fraction of precipitation that infiltrates (PINF), infiltration originally takes place with the fraction, PINF * PREC infiltrating (INFILT), and the fraction (1-PINF) * PREC going to surface runoff (SRO) (Equation 4-1a). The difference is if PREC is greater than PTHRESH/PINF then the fraction PTHRESH infiltrates, and the remainder (PREC – PTHRESH) goes to surface runoff (Equation 4-1b). This modification produces more realistic storm runoff behavior for large magnitude storms.

$$PREC \le PTHRESH/PINF \Rightarrow \begin{matrix} INFILT = PINF \cdot PREC \\ SRO = (1 - PINF) \cdot PREC \end{matrix} \quad (4\text{-}1a)$$

$$PREC > PTHRESH/PINF \Rightarrow \begin{matrix} INFILT = PINF \cdot PTHRESH \\ SRO = (1 - PINF) \cdot PTHRESH + (PREC - PTHRESH) \end{matrix} \quad (4\text{-}1b)$$

The second modification is implemented in handling the available evaporation back to the atmosphere from the available water in subflow storage. Evaporation is modeled to be some fraction of the potential evaporation. Potential evaporation is determined using the Hamon (1963) equation:

$$PE(T_a, t) = 29.8 \cdot D(t) \cdot \frac{e_a^*(T_a)}{T_a + 273.2} \quad (4\text{-}2a)$$

where $PE(T_a, t)$ is the daily potential evaporation in millimeters/day, $D(t)$ is a number of daylight hours, $e_a^*(T_a)$ is the saturation vapor pressure in KPa, T_a is the mean daily temperature in degrees Celsius, and t is the day of year. Actual evaporation, E, is determined as the product of ETCO and the potential evaporation, PE, given by equation 4-

1a and a scaling input variable, PETAMP (Equation 4-2b). The variable, ETCO, is determined internally as a value between 0 and 1 that is non-linearly dependent on SUBFLO/SAT, which is the ratio of near sub-surface storage (SUBFLO) to a fitting input variable, SAT. SAT represents the maximum storage volume possible in the near sub-surface.

$$E = PE \cdot ETCO \cdot PETAMP \tag{4-2b}$$

4.2.1 Continuous streamflow model calibration

Calibration of any continuous streamflow model is necessary to capture the hydrologic characteristics of the watershed by trying to reproduce its observed streamflow time series. In this study, calibration of the model was performed using temperature and precipitation time series as input and the observed daily discharge at the six USGS streamgages as the observed time series that were to be matched. The continuous streamflow model also required the input of eleven hydrologic input variables in addition to the three mentioned before time series. The list of the eleven input variables and their physical interpretations are summarized in Table 4-1 below. Area is determined for each watershed and is a fixed input variable.

Table 4-1. Hydrologic input variables for the continuous streamflow model.

Variable	Physical interpretation of variable
AREA	Drainage area in square miles
GWS	Initial groundwater storage (inches)
SUBFLO	Initial sub-surface storage (inches)
PINF	Fraction of precipitation that infiltrates
PTHRESH	Maximum daily infiltration depth threshold (inches)
SROP	Input variable that controls unit hydrograph shape
GWSM	Maximum groundwater storage (inches)
BFPM	Input variable that controls groundwater flux to stream (inches/day)
SFP	Input variable that controls sub-surface flux to stream
PETAMP	Potential evaporation scaling factor
SAT	Input variable that quantifies saturation conditions (inches)

4.2.2 Criteria of an optimum calibration

Calibration is generally achieved by adjusting the input variables until the model is optimized to best reproduce the observed streamflow time series. However this approach is subjective and the "best" calibration is based on the modeler's judgment. The subjectivity is only eliminated by implementing a systematic procedure to reach the optimum calibration. This was achieved by the incorporation of the continuous streamflow model into NUMOPT. NUMOPT is a numerical optimization program that was used to produce the optimum regression model forms. It is again utilized as the tool to optimize the continuous streamflow model calibration. Instead of using NUMOPT to optimize a simple model form, it is used here to optimize a more complex model form that is the continuous streamflow model. This allows NUMOPT to handle the job of the modeler to modify the input variables until the optimum simulated streamflow times series is produced. NUMOPT optimizes based on an objective function that minimizes the summation of errors squared. This in essence would lead to minimizing the standard error value. However, this did not necessarily produce the best visual fit because by minimizing the errors, NUMOPT would minimize peak flow errors at the expense of larger errors on smaller flows. Thus, a weighted average of two different objectives was incorporated in the NUMOPT program.

While the visual assessment of a calibration is important, it is often necessary to quantitatively assert the quality of a given simulation in its approximation of observed streamflow. Better goodness-of-fit statistics between two hydrographs can generally be achieved by minimizing the summation of errors squared, minimizing the standard error, or maximizing the correlation coefficient. However, minimizing the summation of errors

squared or the standard errors tends to give higher emphasis to fitting the peaks since they are the largest contributors to the overall total sum of errors. The correlation coefficient is also not an appropriate measure of goodness-of-fit in this case since the data are serially correlated and because this measure lacks the ability to take into consideration the difference in water volume between the simulated and observed flows. Another measure of goodness-of-fit is the modified correlation coefficient, R_m, which is in essence equivalent to the correlation coefficient multiplied by a factor, a/b, that incorporates the water budget balance (McCuen and Snyder, 1975).

$$R_m = R \cdot a/b \tag{4-3}$$

$$a = \left[\frac{\sum Q_p^2 - \sum (Q_p)^2 / n}{n} \right]^{0.5} \tag{4-3a}$$

$$b = \left[\frac{\sum Q_{obs}^2 - \sum (Q_{obs})^2 / n}{n} \right]^{0.5} \tag{4-3b}$$

Q_p : Simulated streamflow in inches

Q_{obs}: Observed streamflow in inches

n : Sample size

However, optimizing on the modified correlation coefficient is not adequate either because NUMOPT would optimize the (a/b) ratio component at the cost of the correlation coefficient component. Thus, the idea of a weighted objective emerged with fixed weights given to different objective functions. The objective function used in optimizing the calibration of the continuous streamflow model was a weighted average of two criteria: summation of errors squared and the (a/b) ratio. The objective function was to minimize the quantity, S, which minimizes the summation of errors squared (and thus

minimizing the standard error Se), and maximizes the ratio of *a/b* (Equation 4-4). The variable *w*, which ranges between 0 and 1, indicates the weight given to each component of the criterion variable. After some experimentations with various values for *w*, calibrations were performed with a *w* of 0.2, which gave 80% weigh to minimizing the sum of errors squared and 20% to maximizing the (*a/b*) ratio:

$$S = w \cdot \sum (\hat{Q}_p - Q_{obs})^2 + (1-w) \cdot \left| 1 - \frac{a}{b} \right| \qquad (4\text{-}4)$$

4.2.3 Calibration of the continuous streamflow model based on historical data from six watersheds in the Maryland Piedmont region

After the successful merger between the continuous streamflow model and NUMOPT, the next step was to form the historical time series to carry out the calibration process of the continuous streamflow model. 174 watershed–year records of daily streamflow data on a daily basis with the corresponding daily precipitation and temperature data were available. The historical data consisted of data collected for six watersheds: the Northwest Branch (USGS streamflow gage # 01650500), Seneca (USGS streamflow gage # 01645000), Little Falls (USGS streamflow gage # 01646550), Rock Creek (USGS streamflow gage # 01647720), Hawlings (USGS streamflow gage # 01591700), and Watts Branch (USGS streamflow gage # 01645200). The 174 years of data were split into 47 distinct runs (33 time series with 4-year durations and 14 with 3-year durations). The calibration of 47 calibration runs will allow us to create an imperviousness time series and eventually to impose the land use change scenarios in the continuous streamflow model. Additionally, the use of a 3-year or 4-year duration for each calibration run instead of an annual duration was sought to eliminate the spin-up

effect on the calibration which tends to affect the goodness-of-fit of the calibration at the beginning few months of the hydrograph. Also, to minimize the effect of land use change during the duration of each run, time series were compiled with the consideration of grouping consecutive watershed-years of close annual imperviousness values. So an abrupt change in the annual imperviousness values for a particular watershed was considered as a suitable split point between two time series.

4.2.4 Selection of input variables to be calibrated

Prior to start looking at the performance of the 47 calibrations, an investigation of how the calibration runs will be utilized to later impose the climate and land use change conditions on the continuous streamflow model should be performed. First, it is anticipated that some of the calibrated input coefficients might vary with land use change, specifically changes in imperviousness. Thus, a modest study was undertaken to determine which input variables were dependent on land use and it was determined that PINF and SROP exhibited such a dependency. A cursory examination of the streamflow model formulation reinforces the view that these input variables vary with land use. Thus, the calibration process was allowed to calibrate for those two input variables. NUMOPT was also allowed to calibrate for GWS and SUBFLO which are initial condition input variables and have an influence solely on producing a better fit for the initial months of a calibration run reducing the spin-up effect. The spin-up effect generally occurs in the early simulation period in which the continuous streamflow model tries to come to a dynamic agreement with the initial water budget conditions of the watershed. Thus calibrating for GWS and SUBFLO lead to better goodness-of-fit statistics, yet they describe an initial condition of the watershed and have little hydrologic

value to our research context. The remaining six coefficients were fixed as constants and NUMOPT was used to calibrate for only four input variables: PINF, SROP, GWS, and SUBFLO.

To obtain the values of the other six input variables, the 47 historical runs were initially calibrated for all 10 input variables listed in Table 4-1. Then SAT and PETAMP were averaged across the six watersheds since they capture in a sense the temperature or the evaporation component in the continuous streamflow model that is assumed to be constant across a region. The calculated averages of SAT and PETAMP are 1.0315 inches and 1.2430, respectively. A value of "1" was substituted for both of SAT and PETAMP as shown in Table 4-2 below. Assigning a value of "1" to PETAMP suggests that the scaling factor to the potential evaporation rate is not necessary and the PETAMP component can be eliminated from equation 4-2b. Fixing the values of SAT and PETAMP led to a minor reduction in the accuracy of the model goodness-of-fit.

Table 4-2. Input variables used in the continuous streamflow model in calibrating the 47 historical runs.

	Hawlings	Little Falls	NWB	Rock Creek	Seneca	Watts Branch
PINF	$f_1[I(t)]$	$f_1[I(t)]$	$f_1[I(t)]$	$f_1[I(t)]$	$F_1[I(t)]$	$f_1[I(t)]$
SROP	$f_2[I(t)]$	$f_2[I(t)]$	$f_2[I(t)]$	$f_2[I(t)]$	$F_2[I(t)]$	$f_2[I(t)]$
PTHRESH	2.3446	2.9608	2.6554	2.1249	1.9487	2.6050
GWS	14.3553	12.3928	16.7970	14.0838	11.6097	23.8425
SUBFLO	4.0176	7.8050	3.0435	5.6971	3.7336	5.0669
GWSM	14.31	46.92	16.63	16.82	10.50	32.56
BFPM	0.000057	0.000161	0.000043	0.000094	0.000123	0.000078
SFP	0.0108	0.0035	0.0109	0.0084	0.0092	0.0098
PETAMP	1	1	1	1	1	1
SAT	1	1	1	1	1	1

In addition, average values of GWSM, BFPM, SFP, and PTHRESH were determined for each of the watersheds. These values are summarized in Table 4-2.

Having produced the values of six of the ten input variables, they were input into the NUMOPT program as constants and the optimization was performed by calibrating for the remaining four input variables: PINF, SROP, GWS, and SUBFLO. The values of GWS and SUBFLO that are listed in Table 4-2 above are the average values per watershed determined after optimizing the 47 historical runs. These values are later used as constant values under the future simulations. PINF and SROP are to be later used as the means through which land use change can be imposed in the future simulations.

4.2.5 Adjusting model input variables for imperviousness

The continuous streamflow model was calibrated for the 47 historical runs, and the results were used to investigate any significant dependency between imperviousness and each of PINF and SROP (Figures 4-1 and 4-2). Although results were noisy, the two input variables show a decline with increasing imperviousness, a result that is consistent with the physical interpretation of these input variables. Simple linear regression models relating PINF and SROP to imperviousness were developed:

$$PINF = -0.0017 \cdot I(t) + 0.8003 \quad \text{(4-5a)}$$

$$SROP = -0.0038 * I(t) + 0.3842 \quad \text{(4-5b)}$$

where *I(t)* is the percent imperviousness of the watershed at time, *t*. Equations 4-5a and 4-5b indicate that PINF and SROP decrease with increasing imperviousness. These indications are consistent with the physical interpretation of both of PINF and SROP: as imperviousness increases, less water would be expected to infiltrate into the ground, indicated by a smaller PINF value, and a faster surface runoff response would be expected,

indicated by a smaller value of SROP. The correlation coefficients, R^2=0.0596 and R^2=0.0261, for equations 4-5a and 4-5b, respectively were not significant at a 5% level of significance, but these equations are used here to illustrate how the modeling process proceed.

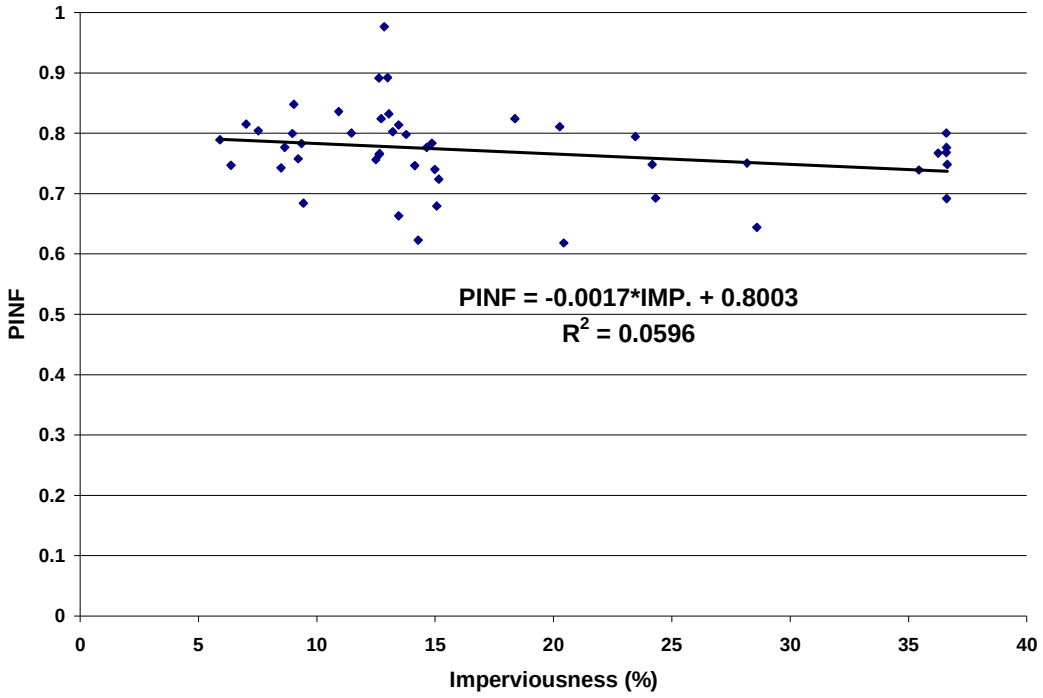

Figure 4-1. Dependency of infiltration input variable, PINF, on imperviousness based on a data set of 47 historical runs.

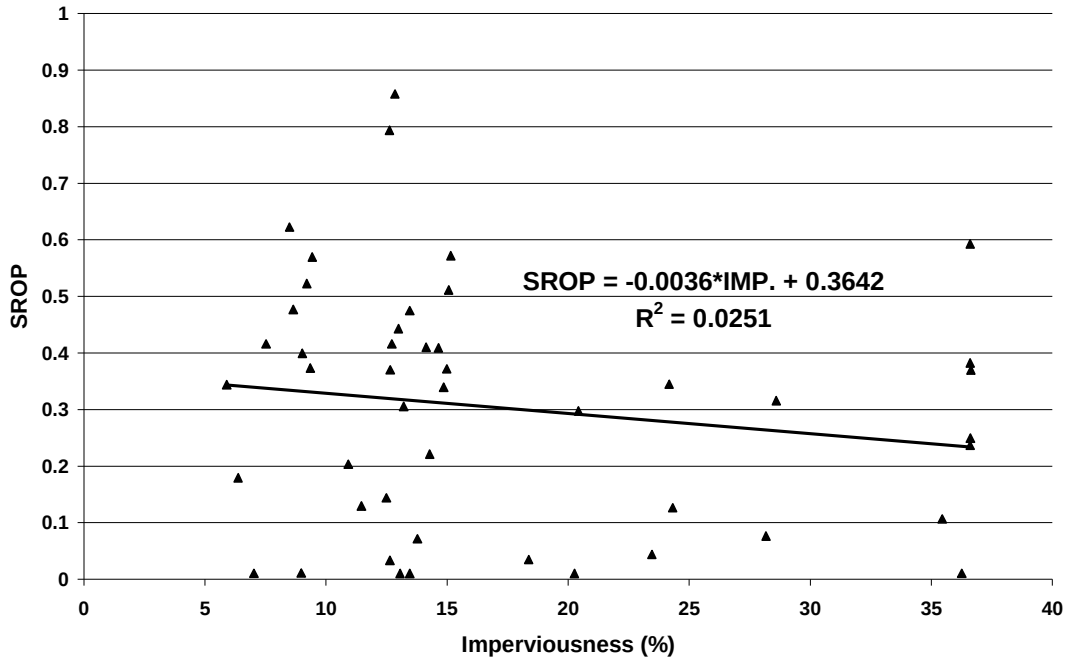

Figure 4-2. Dependency of hydrograph shape input variable, SROP, on imperviousness based on a data set of 47 historical runs.

Equations 4-5a and 4-5b will be used in simulations of future streamflow along with predictions of future land use to help account for the anticipated changes in streamflow as a function of land use change alone or in concert with changing climate. However, it is instructive to investigate the level of loss of accuracy by reapplying the future version of the continuous streamflow model on the historical runs. This can be thought of as the validation step because it does not involve calibration of any coefficient. PINF and SROP are determined based on the imperviousness value associated with each run and the remaining eight coefficients are used as input to the model as constants for each watershed. Note that each of the 47 historical runs is assigned an imperviousness value by taking the arithmetic average of the annual values comprising the duration of each run. Figures B-2 and B-3 show the loss of accuracy when using the continuous streamflow model in the predictive mode for the future scenario. They are presented in terms of loss in relative

standard error, Se/Sy, and bias. They provide a comparison between the calibration statistics for the continuous streamflow model and the validation statistics. The average reduction in magnitude of the relative standard error, Se/Sy, and bias were 8.19% and 0.29%, respectively. The reader should note that the goodness-of-fit statistics are superior in the calibration runs, as would be expected.

4.2.6 Visual goodness-of-fit of calibration runs

Figure 4-3 provides a snapshot of a 50-day stretch within the calibration period to illustrate model behavior in the Northwest Branch watershed versus observed flows across a range of hydrologic conditions. It shows a typical 50-day period indicating good overall match although the tendency to under-predict base flows and to over-predict discharge for smaller storm events seems to exist.

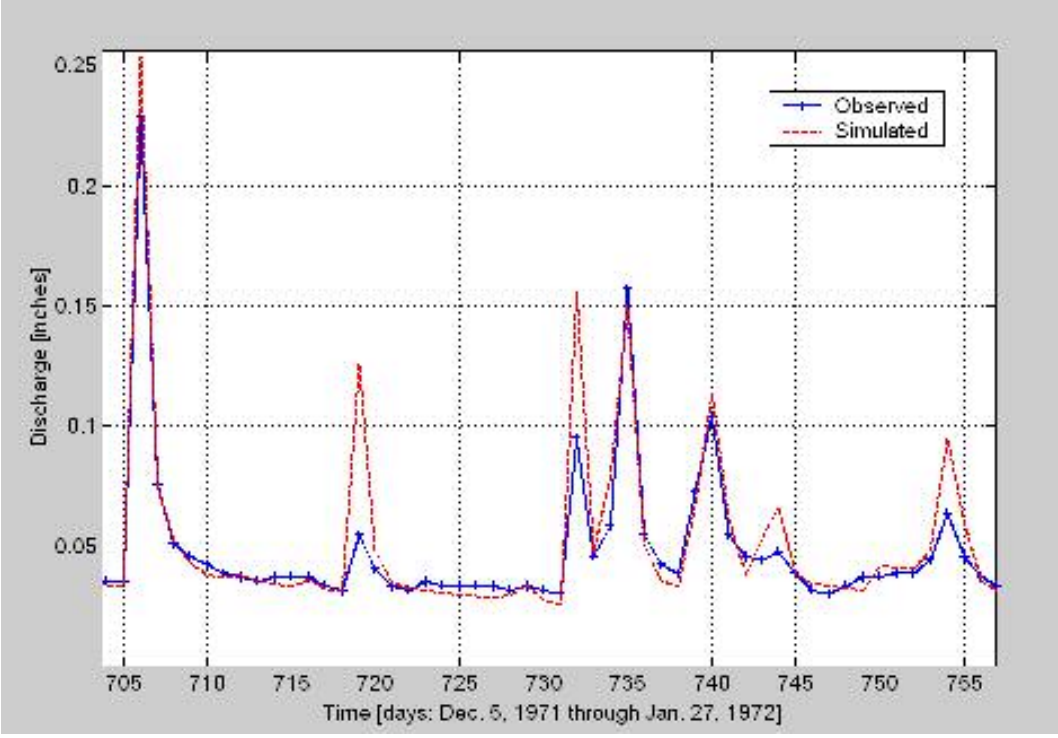

Figure 4-3. A 50-day stretch of calibrated streamflows that shows the performance of the continuous streamflow model at the NWB gage.

Figures 4-4 and 4-5 show visual goodness-of-fit of the calibrated model for the NWB for the period between January 1, 1970, through December 31, 1973. Figure 4-4 shows that the model reasonably predicts runoff from large magnitude storms. It particularly shows that on Day 904 which corresponds to the June 22, 1972, event (Hurricane Agnes). However, it also shows the lack of the model to perform as well when fitting base flows. This is evident in Figure 4-4, where base flows are generally under estimated. Yet, it is important to note that these values are plotted in logarithmic scale and base flow values are generally very small values. Thus, although the discrepancy in predicting low flows seems substantial, the error magnitudes are generally very small values. This is clearer when plotting the same calibration run in the arithmetic space (Figure 4-5).

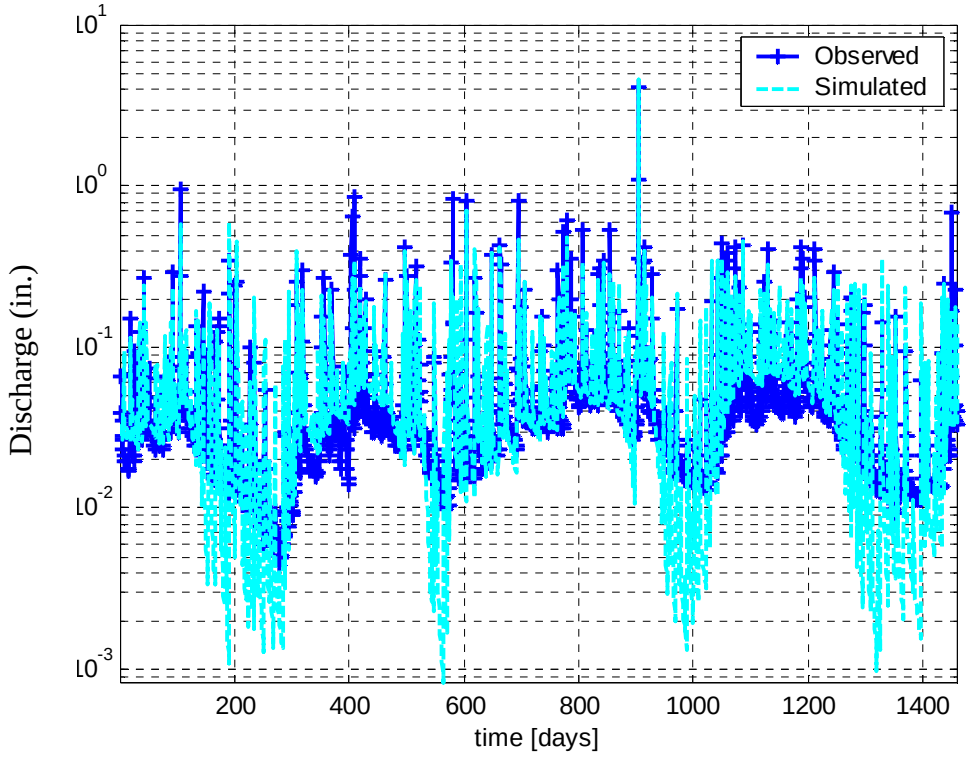

Figure 4-4. Visual representation of a calibration run of streamflows in logarithmic space for the years 1970 through 1973 at the NWB gage.

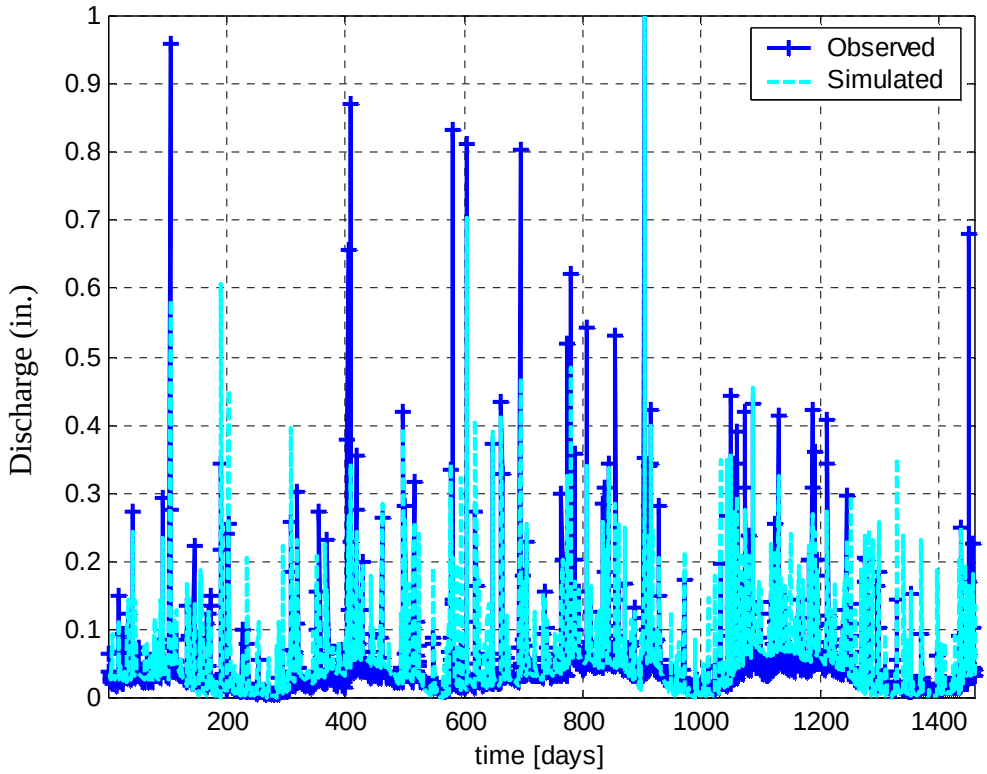

Figure 4-5. Visual representation of a calibration run of streamflows in units of inches for the years 1970 through 1973 at the NWB gage.

The continuous streamflow model seems to perform better in fitting the middle range of flows. And the goodness-of-fit statistics are generally indicative of an adequate fits. A summary of the coefficients values obtained in calibration and the goodness-of-fit statistics for each of the individual 47 historical calibration runs is provided in Table A-34.

4.3 Simulations performed

With the model calibrated for all watersheds and with relationships for PINF and SROP as a function of land use, it is now possible to perform a number of different simulations corresponding to different permutations of climate and land use conditions. Climate can either come from historical precipitation and temperature, or can come from

the future climate data as predicted by the Hadley and CCC models. Land use may correspond either to present (2000) land use or predicted future land use. Table 4-3 summarizes the scenarios that are considered.

Table 4-3. Scenarios of Land Use and Climate Change.

Scenario	Land Use	Climate	Purpose/Description
1a	Present (No change)	CCC	Land use reflective of 2000 conditions with climate (temperature and precipitation) obtained from CCC model.
1b	Present (No change)	Hadley	Land use reflective of 2000 conditions with climate (temperature and precipitation) obtained from Hadley model.
2	Future (Linear incr.)	historical	Land use is changed to reflect anticipated ultimate urbanization while historical climate data is used to reflect the "no climate change" condition.
3a	Future	CCC	Land use is changed to reflect anticipated future urbanization with climate obtained from CCC model.
3b	Future	Hadley	Land use is changed to reflect anticipated future urbanization with climate obtained from Hadley model.

Results from Scenarios 1a and 1b will represent the case of fixed land use but changing climate with the "a" and "b" runs illustrating the differences in the CCC and Hadley climate projections. Results from Scenario 2 represent the case of changing (additional urbanization) land use but fixed climate. Scenarios 3a and 3b will represent the case of jointly varying climate and land use. Collectively, these simulations will allow us to project hydrologic change due solely to changing climate, solely to increasing urbanization, or to jointly varying climate and increasing urbanization.

4.4 Discussion of results

The hydrologic output will be examined solely from the viewpoint of the flow distributions. The flow distribution is described in terms of the exceedence of x% of the streamflow over a period of time. For example, the Q1 is the daily average discharge that exceeds only 1% of the streamflow over a study period – a very small discharge, that may likely correspond to drought conditions. The Q99 is a very large discharge that exceeds 99% of all discharges over a study period and corresponds to flood conditions.

The flow distribution of a watershed is useful to quantify the flashiness of the watershed's response to a storm event. A high degree of flashiness would be indicated by large peak flows and low base flows. For instance, the larger the ratio of a watershed's Q90 to its Q50 (the median discharge) or the smaller the ratio of its Q10 to Q50 the more flashy the watershed would be said to be. It has been observed (Klein, 1979; Barringer et al., 1994; Paul and Meyer, 2001) that urbanization tends to lead to enhanced peak flows and reduced base flows. Given the larger storm volumes and fewer number of storms predicted by both the CCC and Hadley models we might expect that future climate would lead to increased flashiness of watershed behavior as well. Examining the flow distribution will help us test this hypothesis.

The future simulations are imposed on the NWB watershed as a representative example to show the effects of land use and climate change on the streamflow distributions. The Cox-Stuart trend test on the significance of observed trends in simulated streamflow time series will be presented later in the chapter to quantify the significance of the effects of land use and climate change on streamflows under each of the three proposed scenarios. The annual values for each of Q1, Q5, Q10, Q50, Q90, Q95, Q99 will be shown as thin

traces while heavier lines of the same line-type will correspond to the 9-year moving average of these same quantities.

4.4.1 Scenario 1

In Scenarios 1a and 1b, land use is kept constant at present (year 2000) conditions while climate is varied according to the predictions from both the CCC and Hadley models, respectively. In Scenario 1a peak flows remain essentially unchanged while low flows decrease noticeably. The median discharge, Q50, also seems unchanged relative to the historical periods. Figure 4-6 illustrates these observations. It also conveys that under the CCC climate change and while holding land use to current conditions, low flows tend to diminish to even lower values whereas no clear trends seem to emerge when comparing the higher flows, Q50, Q90, Q95 and Q99, to their historical counterpart values. Although Q50, Q90, Q95 and Q99 fall within the bounds of their historical counterpart values, one might argue that there exists, at least visually, a slightly decreasing trend for the median and the higher flows under the CCC climate condition.

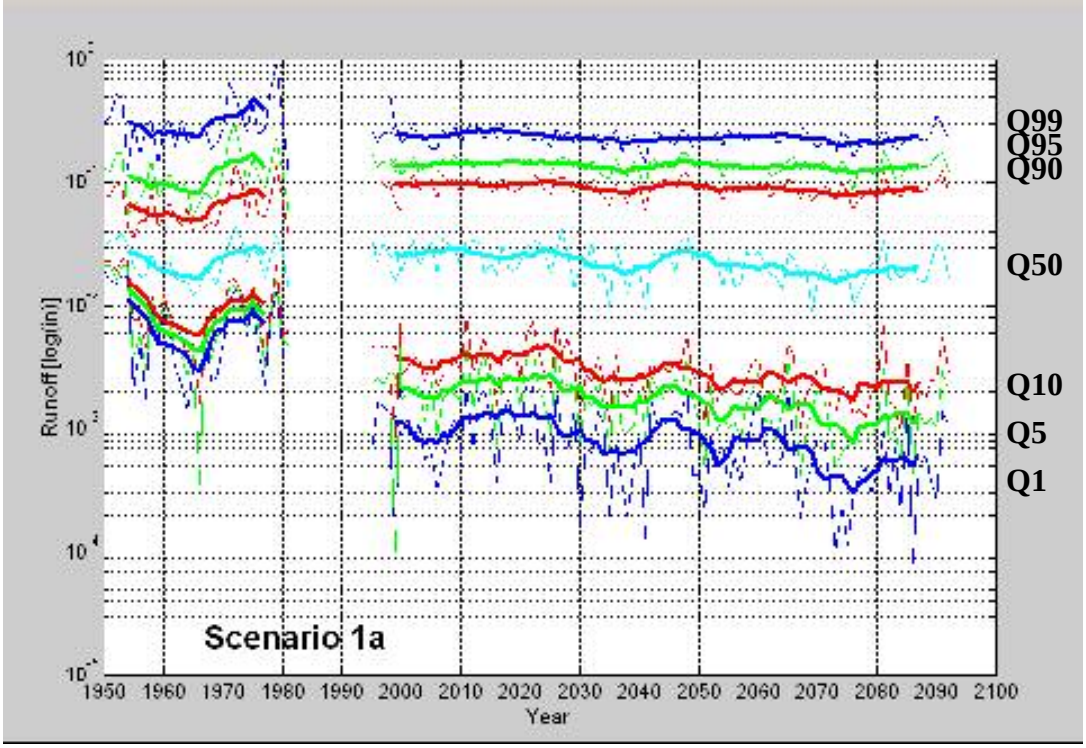

Figure 4-6. Future streamflow distribution based on the continuous streamflow model approach when imposing climate change only under the CCC climate conditions (Scenario 1a).

The flow distribution under Scenario 1b (Hadley climate) suggests a slight tendency towards enhancing the higher flows: peak flows as well as the median flows increase relative to the historical periods (Figure 4-7). The increase in peak flows and median flows is more profound for Q50, Q90 and Q95. The extreme peak flows (Q99) seems to vary within the range of the historical records. Low flows, on the other hand, are lower in magnitude than their historical counterpart values. Peak flows and median flows show a more apparent positive trend in flows than is observed for the low flows.

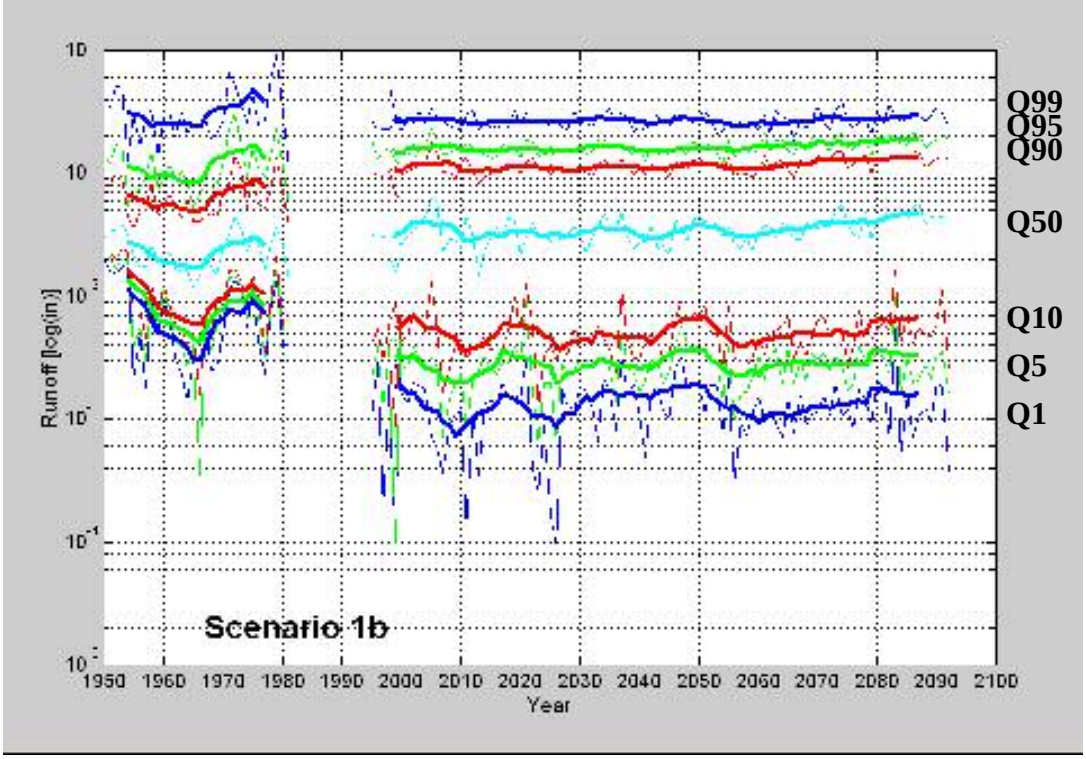

Figure 4-7. Future streamflow distribution based on the continuous streamflow model approach when imposing climate change only under the Hadley climate conditions (Scenario 1b).

The overall increasing trend in the distribution of flows under the Hadley climate condition is mainly due to the fact that Hadley predicts a much wetter future than observed historically or even predicted by the CCC climate model. So even though Hadley also predicts a warmer climate condition in the future, precipitation seems to be more dominant than evaporation on the outcome of the continuous streamflow model. The larger amount of precipitation volume was capable to offset any possible reduction in low flows due to the warmer temperatures, and thus more potential evaporation. Figure 4-8, compares between the CCC based future simulations and the Hadley based future simulation under which land use is assumed to be fixed at current conditions. Hadley predicts always larger flows than the CCC when looking at the simulated annual values for each of Q1, Q5, Q10, Q50, Q90, Q95, and Q99. This is mainly because Hadley predicts a wetter future scenario in which a

larger precipitation volume is driving into the continuous streamflow model than in the CCC climate conditions.

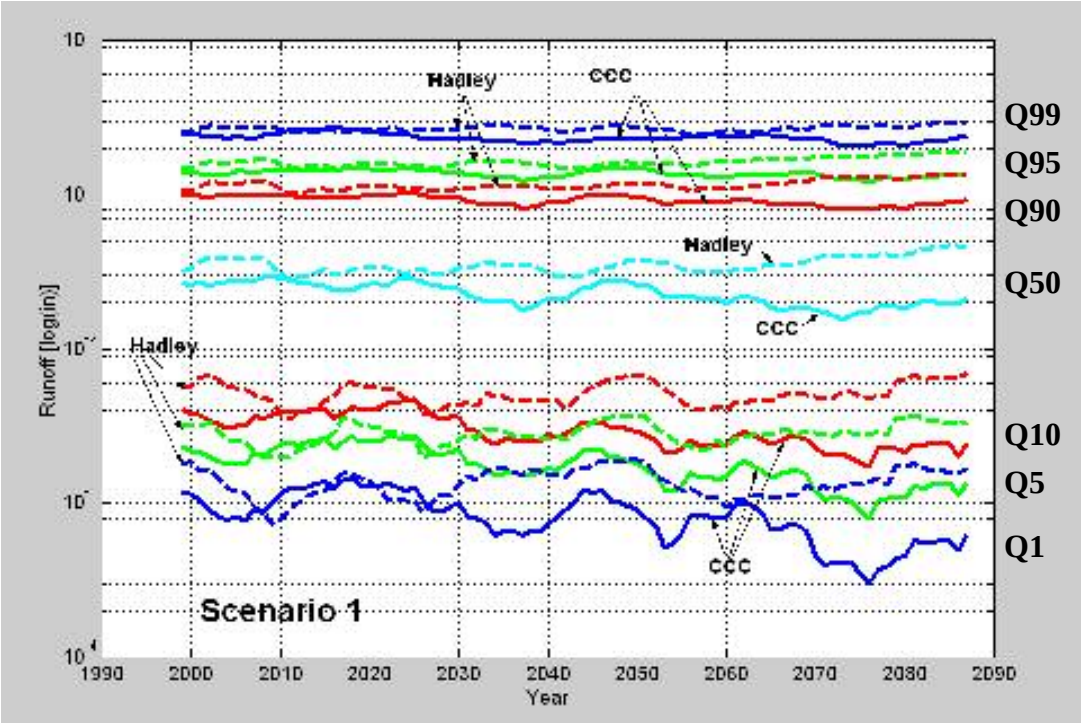

Figure 4-8. A comparison between the future streamflow distribution based on the continuous streamflow model approach when imposing climate change only under each of the CCC (Scenario 1a) and Hadley (Scenario 1b) climate conditions. The 9-day moving average is plotted here to convey the outcome of the simulations. CCC is shown in solid lines and Hadley is shown in dashed lines.

4.4.2 Scenario 2

In Scenario 2, land use is changed to reflect urbanization while historical climate time series are used to reflect the "no climate change" condition. The constant climate condition was imposed by obtaining 99 years of historical data for the same grid point, 38.8 N^o and 77.2 W^o, used in predicting the future climate data. Thus, this scenario considers the effects of continued urbanization only, in the absence of any change in climate. As previously indicated in Chapter 3, imperviousness will be assumed to increase linearly by

10% from the current condition of the NWB watershed (from 20.5 to 30.5%) over the course of 99 years. Imperviousness is modified on an annual basis.

Figure 4-9 shows a slight increase in both peak flows and median flow and a clear reduction in low flows from their historical counterpart values. The figure also shows a very slight increase in peak and median flows, and no apparent changes in low flows over the span of the 99-year future simulation with only degree of urbanization changing. Our expectation was to observe a tendency to a flashier condition: peak flows becoming larger and low flows becoming smaller. The reason for this expectation was straightforward. Increased imperviousness leads to less infiltration of precipitation during storm events. This increases peak flows during the storms themselves, and because less water infiltrates during these storm events, there is less available water to emerge as subsurface or groundwater flow at later times between storms. The result is a flashier flow distribution under conditions of greater urbanization. Thus, the results in Figure 4-9 are not consistent with our expectations nor with those reported elsewhere by others (Klein, 1979; Barringer et al., 1994; Paul and Meyer, 2001) for watersheds undergoing urbanization.

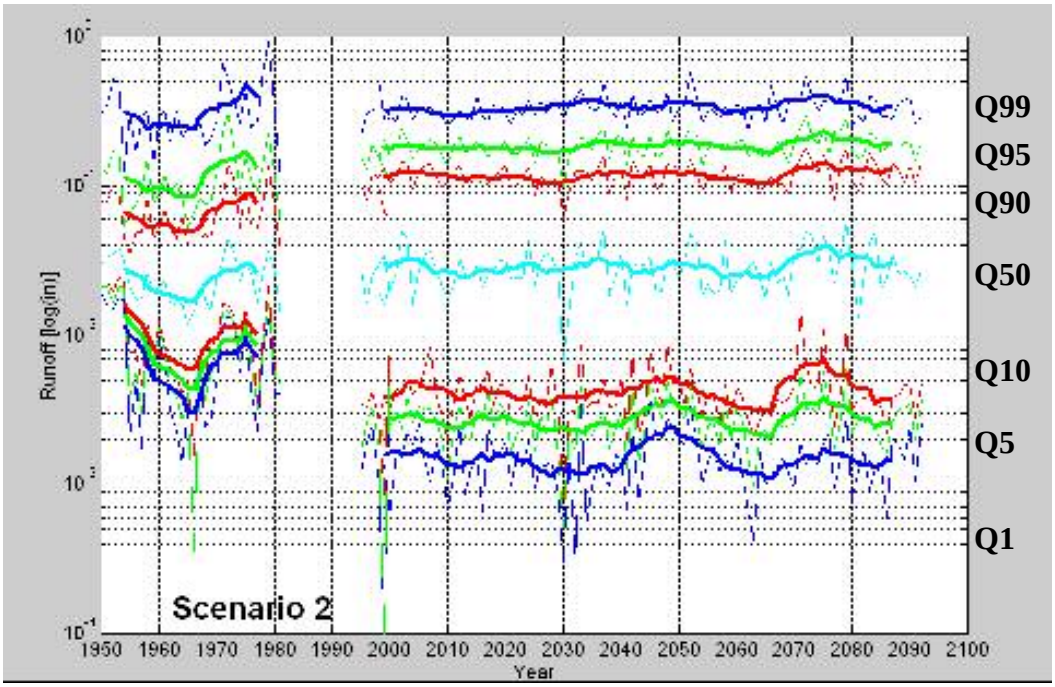

Figure 4-9. Future streamflow distribution based on the continuous streamflow model approach when imposing land use change only (Scenario 2).

4.4.3 Scenario 3

Scenario 3 concerns the effects of jointly changing land use and climate. Simulations start in 1994 to be consistent with the available climate data. This scenario is of value because it addresses the potentially synergistic effects of jointly changing land use and climate. In comparison between the results presented here against the corresponding results under Scenario 1, the differences (if any) will reflect the added effect of land use change (under Scenario 2) along with the climate change effect already contained in Scenario 1.

The results of the Scenario 3 simulations are not surprising. The figure shows that the addition of the effect of urbanization to the continuous streamflow model was able to make peak flows larger and the low flows smaller. Such results were anticipated even though Figure 4-9 in Scenario 2 could not conclude such an outcome when comparing the future simulations to the historical runs. The median flow also drops with the addition of

land use change component to the continuous streamflow model. Since both Scenarios 1a and 3a utilize the same future climate input time series to be used as input to the continuous streamflow model, the effect of climate change is common between them and thus any difference is solely due to urbanization. Furthermore, the same precipitation time series is used in both Scenario 1a and 3a; the water volume is conserved. In other words, if peak flows increase and low flows decrease then the median flow is expected to be lower if the increase in the peaks is larger (in total volume) than the reduction in low flows. This is the case illustrated in Figure 4-10 below. Streamflow values are plotted in logarithmic space and thus the gap observed between Q99 for Scenario 1 and Q99 for Scenario 3 is much larger than the reductions experienced by low flows (e.g. Q10 for Scenario 1 vs. Q10 for Scenario 3).

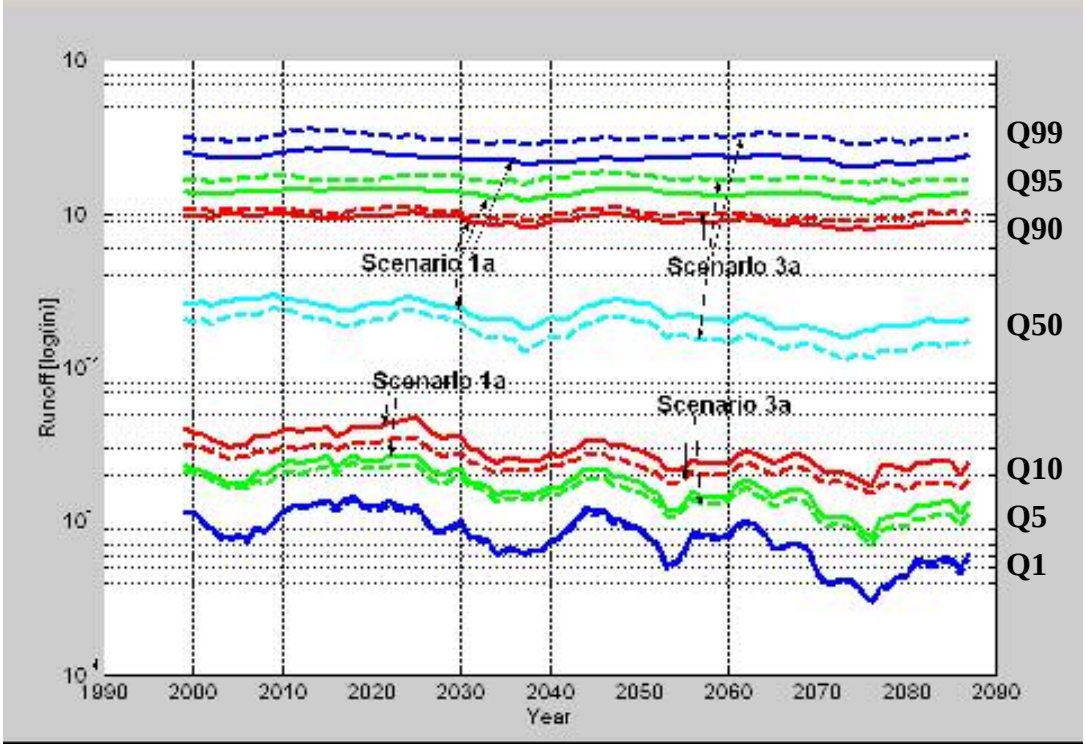

Figure 4-10. Comparison between Scenario 1a and Scenario 3a and the effect of the addition of land use change on the distribution of streamflows. The 9-day moving average is plotted here to smooth noise in annual variations and more clearly convey trends. Solid lines are scenario 1a, dashed lines are scenario 3a.

Comparing Figures 4-11 and 4-12 against Figures 4-6 and 4-7, reiterates on the conclusions drawn from Figure 4-10 by indicating the additional consequences of land use change on flow distribution beyond those already remarked upon due to climate change. These changes manifest themselves as increases in peak flows (e.g. Q90, Q95, Q99) for Scenario 3 versus Scenario 1, for both climate model sets. Changes to low flow (e.g. Q1, Q5, Q10) are small if at all observable. Overall, these flow distribution results suggest a flashier streamflow behavior in Scenario 3 (with land use and climate change acting together) than in Scenario 1 or 2 where only climate or land use change are modeled individually.

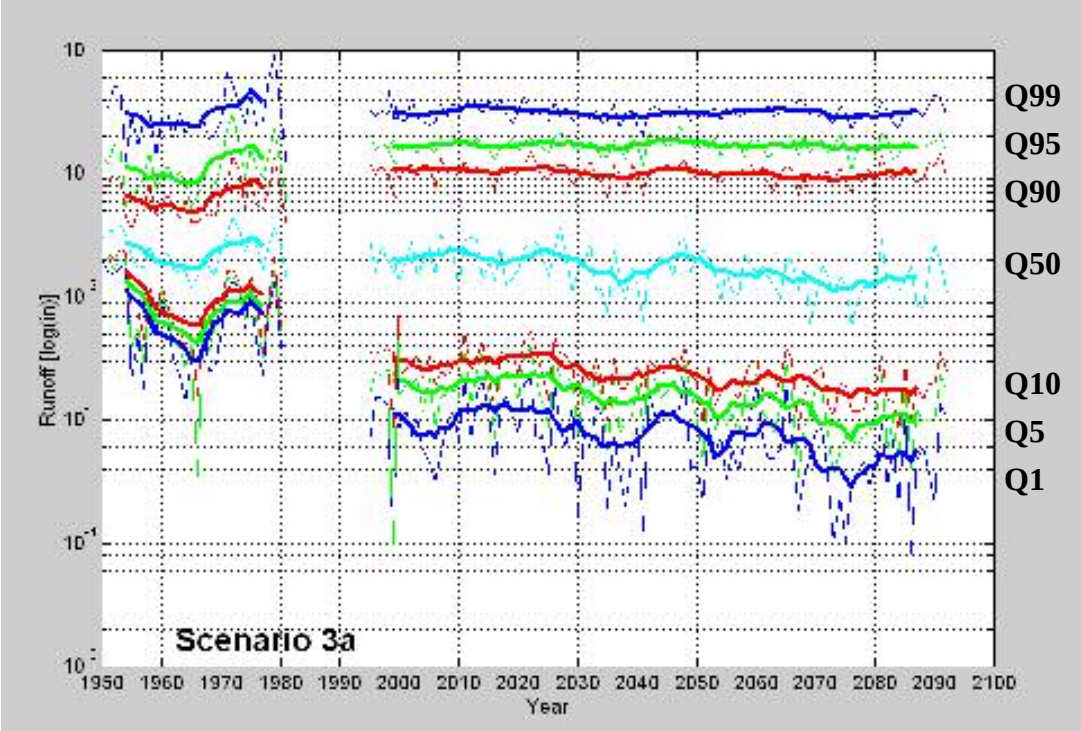

Figure 4-11. Future streamflow distribution based on the continuous streamflow model approach when imposing climate and land use change under the CCC climate conditions (Scenario 3a).

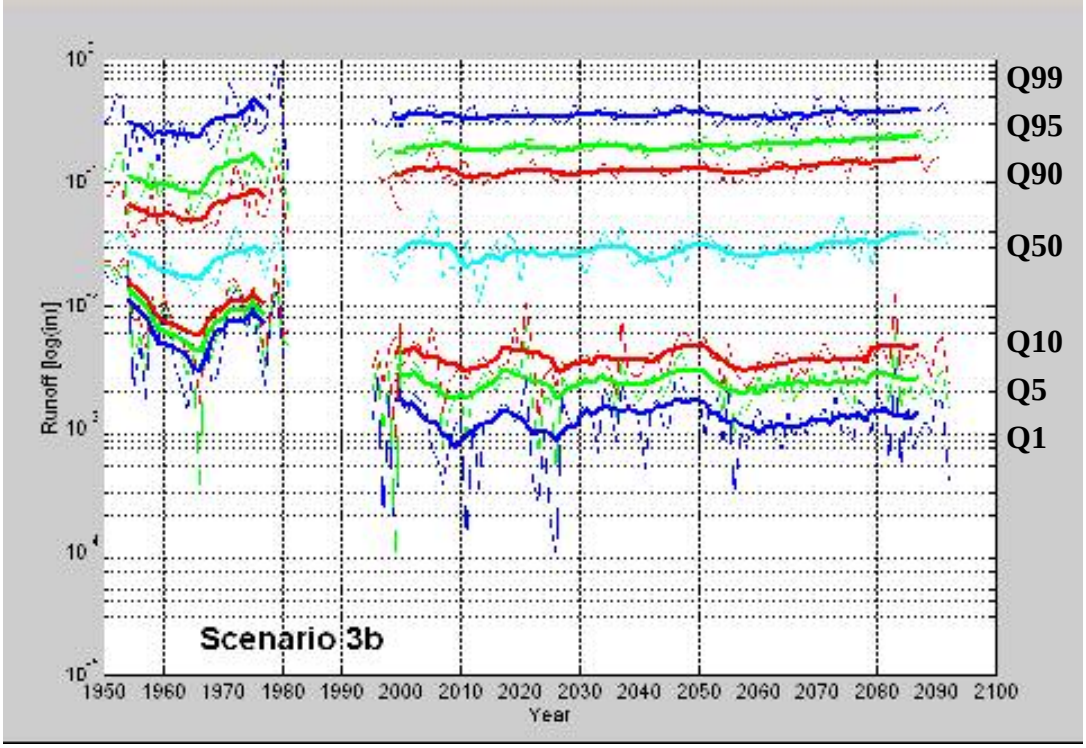

Figure 4-12. Future streamflow distribution based on the continuous streamflow model approach when imposing climate and land use change under the Hadley climate conditions (Scenario 3b).

The addition of the land use effect, however, in Scenario 3b was not sufficient to offset the trends initially observed under the sole climate change imposed in Scenario 1b. Scenario 3a, under the CCC climate predictions, shows a significant decreasing trend in low flows, and similarly the observed trends in Scenario 3b, under the Hadley climate predictions, are consistent with those that `emerged under Scenario 1b by showing a significant increasing trend in peak flows. This will be more apparent when discussing the rejection probabilities for the Cox-Stuart trend test for each of the flows under each scenario later in this chapter.

4.5 Test the significance of simulated secular trends in streamflows

Table 4-4 summarizes the rejection probabilities for the Cox-Stuart trend test on the significance of observed trends in streamflow time series. It shows the significant

trends in bold, at a 5 percent level of significance for each of the Q1, Q5, Q10, Q50, Q90, Q95, and Q99 time series under each of the scenarios studied. Given the trends previously detected in the precipitation and temperature time series under the CCC and Hadley climate predictions, the outcomes in Table 4-4 are not surprising.

Table 4-4. Rejection probabilities for the Cox-Stuart trend test for the different continuous streamflow quantiles studied and across each Scenario. (significant trends at a 5% level of significance are shown in bold).

%ile	Scenario 1a	Scenario 1b	Scenario 2	Scenario 3a	Scenario 3b
Q1	**(-) 1.06%**	(+)19.58%	(+)7.62%	**(-) 0.47%**	(+)50.00%
Q5	**(-) 0.01%**	(+)12.64%	(+)7.62%	**(-) 0.00%**	(+)19.58%
Q10	**(-) 0.00%**	(+)19.58%	(+)19.58%	**(-) 0.01%**	(+)19.58%
Q50	(-) 7.62%	**(+) 1.06%**	(+)38.77%	**(-) 1.06%**	**(+) 0.19%**
Q90	(-) 7.62%	**(+) 0.02%**	(+)28.41%	(-) 19.58%	**(+) 0.00%**
Q95	(-) 12.64%	**(+) 0.19%**	(+)12.64%	(-) 28.41%	**(+) 0.47%**
Q99	**(-) 4.27%**	(+)19.58%	(+)19.58%	(-) 28.41%	(+) 7.62%

Under the CCC climate conditions, precipitation showed no evident trends. Yet, the significant increase in temperature was capable to produce significant decreasing trends in low flows in Scenario 1a. The addition of land use change under Scenario 3a, built on the effect of the temperature by making the decreasing trends in low flow slightly more significant with slightly lower rejection probabilities. However, only a slight offset to the decreasing peak flows was observed, which was not sufficient enough to produce any increasing trend in peak flows with the addition of land use change in Scenario 3a.

The significant increasing trend in precipitation under the Hadley climate conditions was the dominant influence on streamflow distribution and thus led to significantly increasing peaks. The positive increasing trend in temperature was not capable to sufficiently enhance evaporation to counteract the effect of the significant increase in precipitation. The additions of land use slightly reduced the observed increasing trends but not sufficiently enough to offset the significant increases. In

Scenario 2, even though there are no observed significant trends, the direction of the change in low flows is in contrary of our expectations. Table 4-4 shows a slight increasing trend in low flows whereas we expect urbanization to cause diminished low flows. This is probably due to the slightly increasing trend in the simulated historical precipitation time series in Scenario 2. Although the trend was proven insignificant at a 5% level of significance (Table 3-14), it probably was still capable to offset any decreasing effect on low flows due to the effect of urbanization. This builds on our previous findings that precipitation is stronger than an increase in imperviousness by 10% in creating a trend in streamflows.

4.6 Comparing the outcomes of the regression and continuous streamflow models

One of the advantages of the continuous streamflow model approach over the regression model approach discussed in Chapter 3, is that the former produces a complete daily simulated streamflow time series whereas the latter predicts a single value per year. The outcome of each of the future simulated runs is a simulated daily streamflow time series which enables us to study the whole distribution of streamflows. Thus, Chapter 4 studies the effect of land use and climate change on the entire distribution of streamflows including the 7-day low flows. Although we don't anticipate learning any new information from the 7-day low flow that was not presented by looking at the Q1, Q5, Q10, Q50, Q90, Q95, and Q99, it is presented here for consistency with the work presented in Chapter 3 where it was only possible to adequately predict the 7-day low flow.

4.6.1 Simulated 7-day low flows under each of the three proposed future scenarios

In order to determine the 7-day low flow time series for each of the three proposed future scenarios, the minimum 7-day simulated streamflow is calculated on an annual basis. Then error bars will be considered to address the level of uncertainty in our future predictions of the 7-day low flows. These results can be compared to the results presented in Chapter 3, (Figures 3-17 through 3-21).

Comparing the historical observed 7-day low flows with their corresponding 7-day windows of simulated 7-day streamflows produced the error distribution shown in Figure B-4. Errors, E , are defined as simulated flow, Q_p , minus observed flow, Q_{obs} , so a negative quantity suggests an under-estimation and a positive quantity suggests an over-estimation (Equation 4-6a). The errors showed some local biases of having a tendency to over-predict 7-day low flows for the smallest low flow values and to under-predict at for medium and higher low flow values. Errors were plotted for the individual watersheds and the same error structure emerged. The fact that errors contain local biases is certainly a shortcoming of the continuous streamflow model. This was observed in the calibration process and is shown in Figure 4-4, where base flows are generally under predicted by the calibrated continuous streamflow model.

$$E = \hat{Q}_p - Q_{obs} \tag{4-6a}$$

The distribution of errors was then studied to better understand the error structure and to later address the level of uncertainty in the future predictions. Thus we needed to fit a distribution to the errors obtained from the historical runs to later impose on the future simulated values to address the level of uncertainty in the continuous streamflow model predictions. It is physically rational to expect minimum 7-day low flows to become

values very close to zero in dry years and to be much larger in magnitude in wet years. Thus, improperly imposing an error structure can lead to irrational flow values in the case that error bounds extend into the negative range. For this reason, relative errors were utilized instead to eliminate the possibility of irrationality. Relative errors, *RE*, are defined here as the error from equation 4-6a divided by the observed 7-day low flow value, Q_{obs} (See Equation 4-6b). Figure 4-13 below shows the distribution of the relative errors. Note, the relative error values can't be lower than the value negative one. This can be simply explained by considering an extreme scenario where the continuous streamflow model predicts a 7-day drought with a flow value of zero. Substituting a simulated 7-day low flow value, Q_p , of zero into Equation (4-6b), would produce a relative error value of negative one. This will eliminate the possibility of irrationality when imposing error bounds on the future simulations.

$$RE = (\hat{Q}_p - Q_{obs}) / Q_{obs} \quad \text{(4-6b)}$$

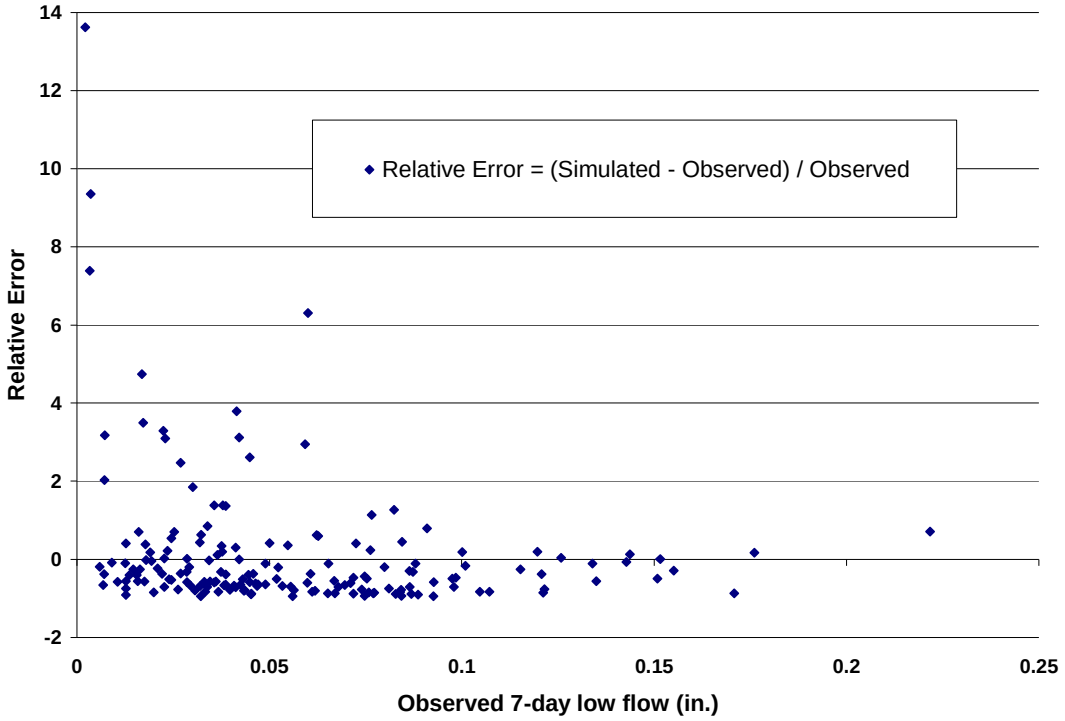

Figure 4-13. Relative errors based on the 47 simulation runs for the historical data using the hydrologic continuous streamflow model.

Figure 4-14 below shows a frequency histogram of the relative errors. The histogram has positive skew which agrees with our observation in Figure 4-13, which showed more negative values than positive ones. A 2-parameter gamma distribution of transformed data was fitted to the frequency histogram. Transforming the data by adding a value of one to the relative error time series would enforce relative error values to be larger than zero. The two gamma parameters were determined based on the method of moments. The scale parameter, *b*, and the shape parameter, *c*, are defined in equations 4-7a and 4-7b below. The calculation of the sample mean ($\overline{X}$ = 0.9942), and the sample variance (S^2 = 1.0375) is detailed in Table A-35.

$$b = S^2 / \overline{X} \qquad (4\text{-}7a)$$

$$c = \left(\overline{X} \Big/ S \right)^2 \tag{4-7b}$$

Substituting the values of $\overline{X}$ and S^2 into equations 4-7a and 4-7b produces a scale parameter, *b*, equal to 1.0436 and a shape parameter, *c*, equal to 0.9526. Using these two values produce the best fit gamma distribution to the relative errors (Figure 4-14). Placing a 90% two-tail confidence interval on the simulated 7-day low flow values, $\hat{Q}_7(t)$, would result in an error bar with high, $Q_7^+(t)$, and low bounds, $Q_7^-(t)$, that are defined in equation 4-8a and 4-8b, respectively.

$$Q_7^+(t) = (2.933715) \cdot \hat{Q}_7(t) \tag{4-8a}$$

$$Q_7^-(t) = (0.056589) \cdot \hat{Q}_7(t) \tag{4-8b}$$

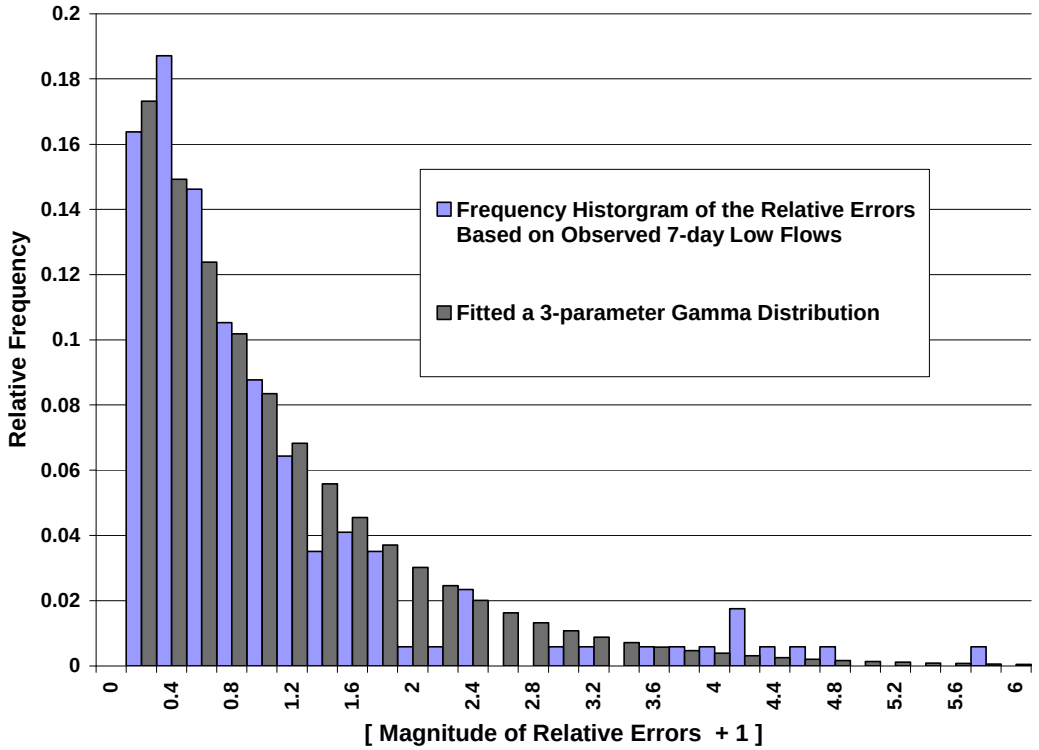

Figure 4-14. Frequency histogram of the relative errors in using the continuous streamflow model approach to predict the minimum 7-day low flow for the historical values. A 2-parameter gamma distribution of transformed data is compared to actual frequency histogram.

4.6.2 Simulated 7-day low flows using the continuous streamflow model

Figures 4-15 through 4-19 convey in a sense the same information that was learned when low flows: Q1, Q5 and Q10, were analyzed under each of the three proposed future scenarios: land use change only, climate change only under the CCC and Hadley climate conditions, and the joint effects of both land use and climate change under the CCC and Hadley climate conditions. They are listed below for the purpose of completeness and to be consistent with the format of results presented in Chapter 3.

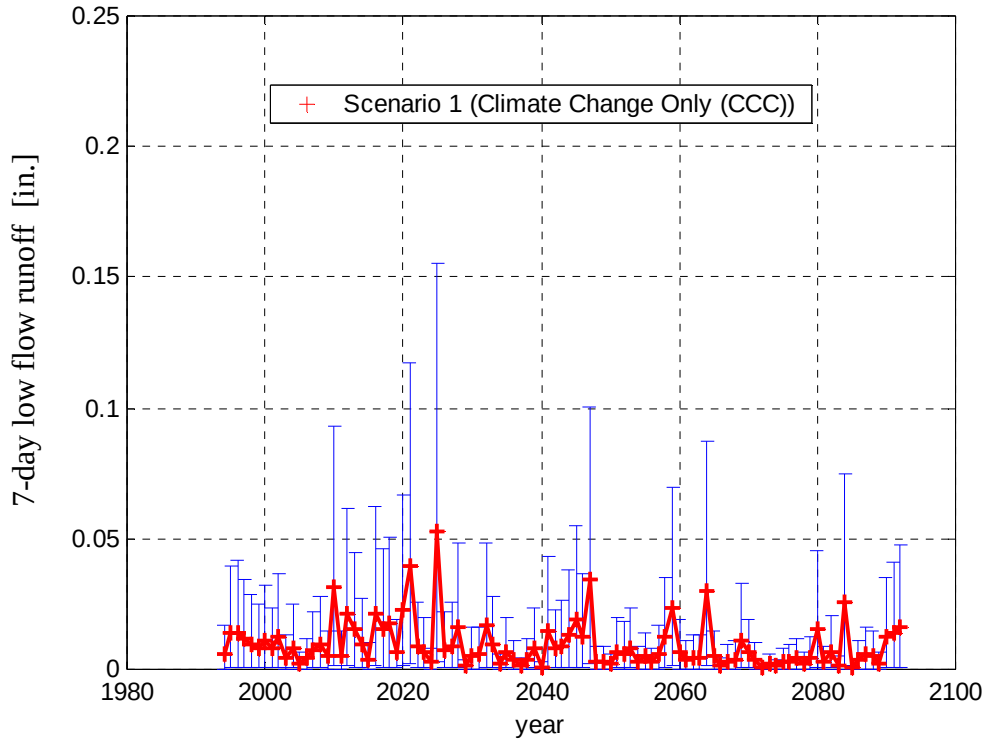

Figure 4-15. Future 7-day low flows based on the continuous streamflow model when imposing climate change only under the CCC climate conditions (Scenario 1a). Heavy line shows mean behavior. Error bars show 90% confidence intervals.

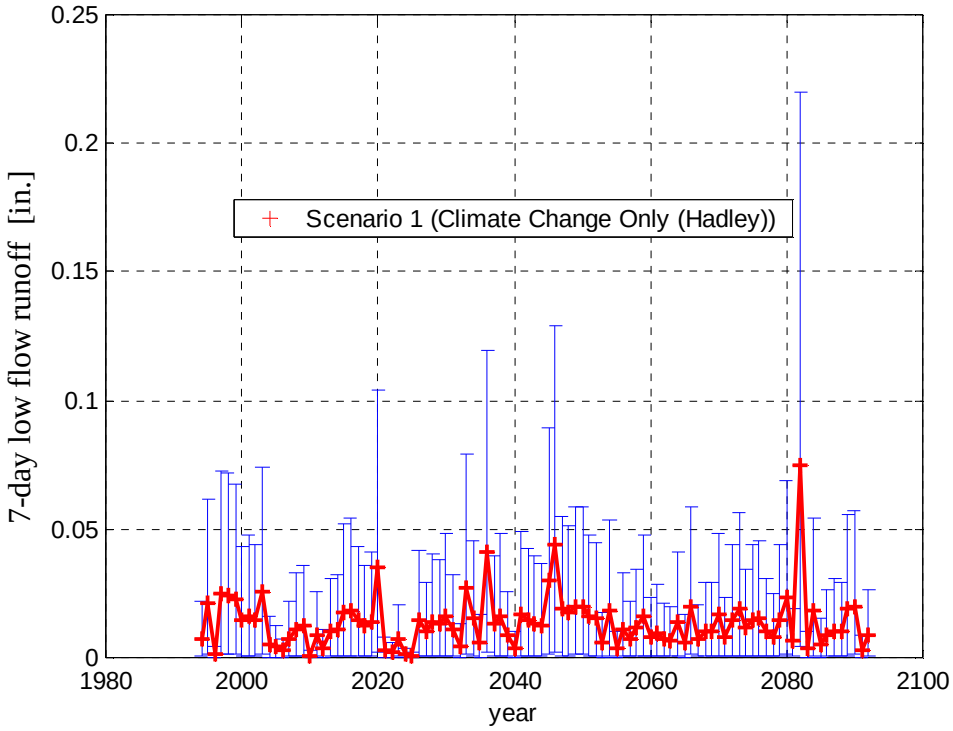

Figure 4-16. Future 7-day low flows based on the continuous streamflow model when imposing climate change only under the Hadley climate conditions (Scenario 1b). Heavy line shows mean behavior. Error bars show 90% confidence intervals.

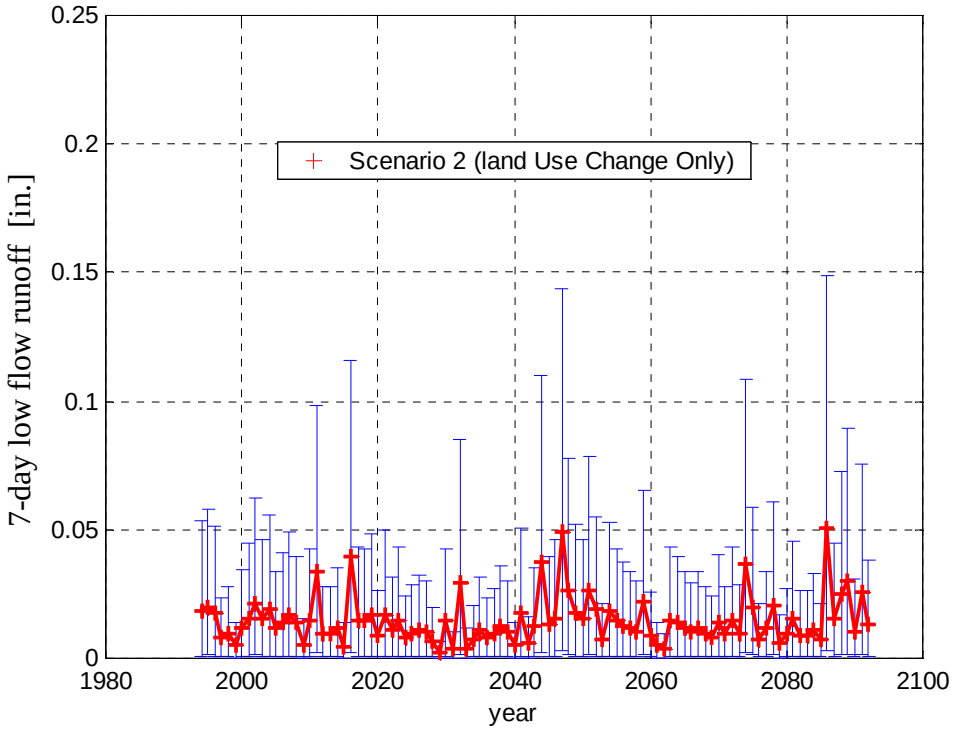

Figure 4-17. Future 7-day low flows based on the continuous streamflow model when imposing land use change only (Scenario 2). Heavy line shows mean behavior. Error bars show 90% confidence intervals.

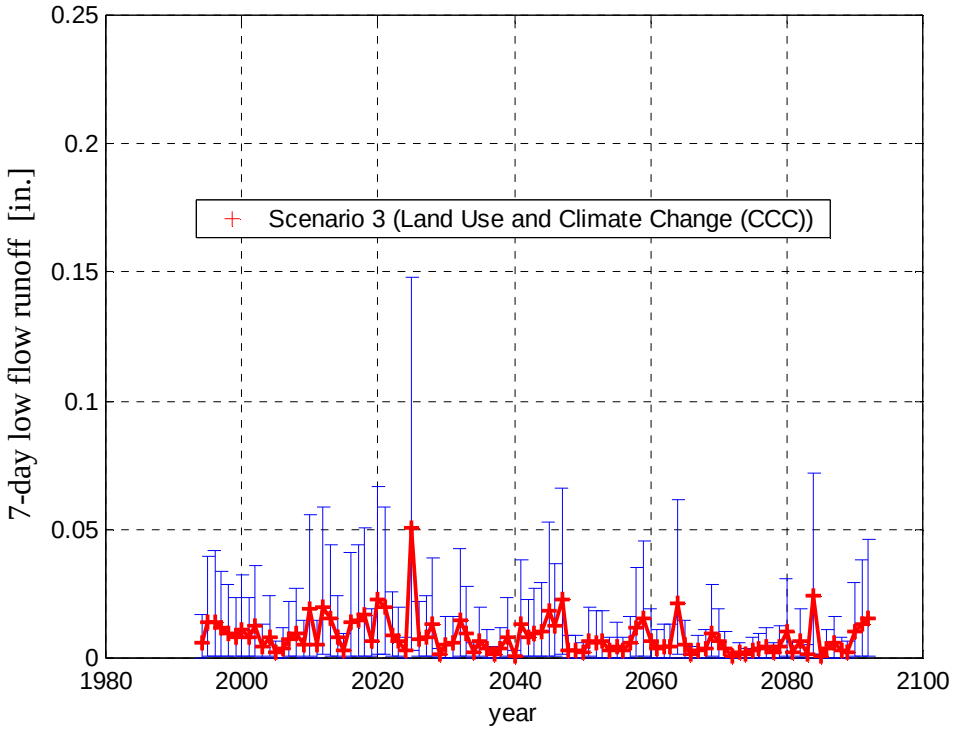

Figure 4-18. Future 7-day low flows based on the continuous streamflow model when imposing climate and land use change under the CCC climate conditions (Scenario 3a). Heavy line shows mean behavior. Error bars show 90% confidence intervals.

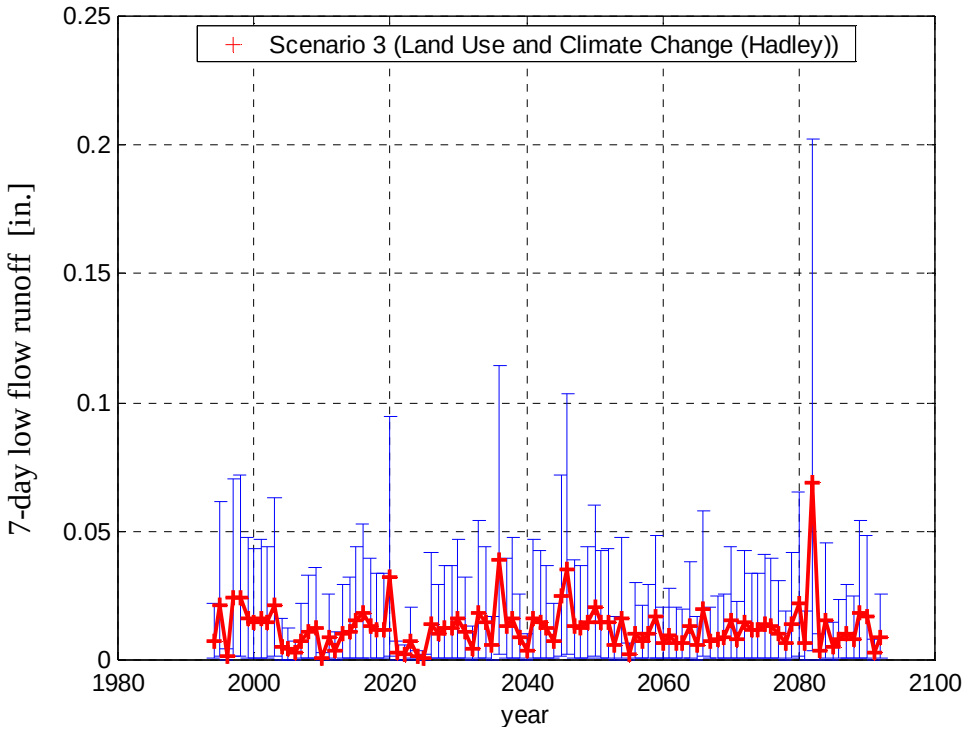

Figure 4-19. Future 7-day low flows based on the continuous streamflow model when imposing climate and land use change under the Hadley climate conditions (Scenario 3b). Heavy line shows mean behavior. Error bars show 90% confidence intervals.

4.7 Summary of continuous streamflow model approach

One of the strengths of this work is the successful elimination of some subjectivity in the calibration of the continuous streamflow model. The merger of the continuous streamflow model with a numerical optimization algorithm, NUMOPT, allowed for a stand-alone program to perform the calibration process. In addition to the employment of a systematic calibration routine, it also allowed the achievement of the optimum calibration condition based on a fixed criterion objective or objectives. Another strength of this work is the ability to use imperviousness as a dynamic input variable into the continuous streamflow model. Past research has generally assumed imperviousness to be a static condition of the watershed. This shortcoming is overcome in the context of our work.

The continuous streamflow model used in this chapter is driven by climate and land use data as well as some hydrologic input variables that are watershed-dependent to study the effects of land use and climate change on the distribution of streamflows. Six watersheds in the Maryland Piedmont region and of different sizes and urbanization experiences were utilized to carry out the analysis. The introduction or urbanization only with a 10% increase in imperviousness over the duration of a 99-year span in the NWB watershed, showed little increasing effects in peak and median flows and no apparent changes in low flows. When climate change was introduced under both the CCC and Hadley climate models, precipitation became the main driver in causing future trends in the distribution of streamflows. With Hadley predicting wetter conditions, increasing trends were observed in the whole distribution: Peak flows as well as median and low flows increased over the span of the future simulation. The simultaneous increase in temperatures tended to enhance the evaporation rates and thus reduce low flows during the summer

season. However, since the climate change is imposed by the simultaneous simulation of temperature and precipitation time series, precipitation was dominant in controlling the outcome of Scenarios 1 and 3.

The addition of the effect of urbanization to the conditions in Scenario 1 showed a very clear reduction in low flows and increase in peak flows. This agrees with the physical interpretation of the effect of urbanization on the distribution of flows in a watershed. The more impervious area, the less water that will infiltrate into the ground and appear later as base flows. Imperviousness allows water to travel faster to streams which leads to larger peak flow. However the hydrologic effect of land use change on the distribution of streamflows was not apparent under Scenario 2 due to the variability introduced by the simulated historical climate drivers.

CHAPTER FIVE

SUMMARY, CONCLUSIONS, AND RECOMMENDATIONS

5.1 Overview

The main objective was to study the joint effect of both climate and land use change on streamflow and specifically how low flows and peak flows respond to these changes. Two approaches were used to fulfill the objectives: a regression approach and a continuous streamflow model approach. A regional regression equation was developed to predict the 7-day low flow in the Maryland Piedmont region under three imposed future scenarios: climate change only, land use change only, and climate and land use change jointly. Similarly, a continuous streamflow model was calibrated and then modified to function as a predictive model to illustrate how streamflows change under each of the three imposed future scenarios. The findings of each of the two approaches are discussed. Then the limitations of the approach and possible future extensions will be presented.

5.2 Summary of modeling results

The effect of climate and land use change on streamflows was studied under three proposed future scenarios in which each of climate and land use varied individually then jointly. Two approaches were used to achieve the objectives of this research. Regression equations and a continuous streamflow model were calibrated to best describe the historical conditions. Each of the two methods was then modified to be used in a predictive sense to produce future streamflow values or time series under each of the

three proposed scenarios: climate change only with current land use conditions, land use change only with current climate conditions, and climate and land use change jointly.

5.2.1 Regression approach

A regional regression equation, Eq. 3-10, was calibrated based on historical 270-day antecedent precipitation, 60-day antecedent temperature, and annual imperviousness time series for six watersheds in the Maryland Piedmont region. The equation predicts the 7-day low flow based on the 270-day antecedent precipitation depth in inches, the average of the 60-day antecedent temperature in degrees Fahrenheit, the annual imperviousness value in percent, and the area of the watershed in square miles. The equation was then used in a predictive sense to implement each of three proposed future scenarios on the NWB watershed. However, since the equation form lacks the capability of identifying the day of the year in which the 7-day low event is expected to occur, the probability distribution of the timing of historical low flows was determined and approximated by a normal distribution. Then a Monte Carlo analysis was performed based on the fitted normal distribution to identify the day of the year to apply the equation to and ultimately predict the low flow estimates for the proposed future scenarios.

The Cox-Stuart trend test was applied to the 270-antecedent precipitation and the 60-day antecedent temperature future time series under both the CCC and Hadley predictions. The test concluded at a 5 percent level of significance that both CCC and Hadley predict significant increasing trends in the simulated 60-day antecedent temperature time series whereas only Hadley at the same level of significance predicts a significant increasing trend in the simulated 270-day antecedent precipitation time series.

The Cox-Stuart trend test was then applied to the mean 7-day low flow time series over each of the future scenarios. The test indicated a significant increasing trend in future low flows under the Hadley climate predictions. On the other hand, a significant decreasing trend in future low flows was simulated using the CCC climate predictions under the conditions of jointly varying climate and land use. Comparing the CCC and Hadley predictions of low flows under constant land use, shows that the climatic inputs of temperature and precipitation play opposing effects on low flows. These findings are explained by two arguments. First, the CCC model predicted a drier and hotter future climate than the Hadley model. Second, low flows have stronger dependency on precipitation than on urbanization or temperature. This is in agreement with the magnitude and signs of the exponents of the calibrated model from Equation 3-10, where precipitation has an exponent that is approximately two times larger in magnitude than the exponents of the temperature predictor and the imperviousness predictor.

5.2.2 Continuous streamflow model approach

In Chapter 4, the historical daily precipitation and average temperature time series were used as inputs to a continuous streamflow model, which is a conceptually-based, hydrologic model developed by McCuen (1986), and modified in this work to accept a daily temperature time series. The continuous streamflow model was then embedded in a numerical optimization program, NUMOPT (McCuen, 1993). This optimization program handled the calibration process of 47 historical runs, and in essence eliminated some of the subjectivity in calibration. The optimization was based on maximizing a weighted average of two criteria: minimizing the summation of squared errors and maximizing a core component of the modified correlation coefficient.

The continuous streamflow model initially required as input ten input variables that capture the hydrology characteristics of the watershed. These ten input variables were reduced to two input variables, PINF and SROP, which were anticipated to be correlated with the imperviousness time series. They were selected based on their physical relation to the land use condition of the watershed. Building regression equations that relate PINF and SROP to the imperviousness of a watershed, allowed the imposition of the land use change effect on the continuous streamflow model by varying these input variables as a function of imperviousness. However, the calibration of the 47-historical runs showed no significant relationships between PINF or SROP and imperviousness. The exercise was continued although it ought to be noted that the results were presented to illustrate the methodology of our approach.

The continuous streamflow model was modified to accept annual land use data in the form of imperviousness time series as an input, so land use is no longer considered as a static characteristic of the watershed. The land use change scenarios allowed a linear increase in imperviousness of 10% over the 99-year simulation. Varying climate conditions were imposed by driving the continuous streamflow model with daily precipitation and temperature time series obtained through the CCC and Hadley predictions.

5.3 Conclusions

The lessons learned from this research effort were only drawn from the results of the regression approach because the continuous streamflow model did not show a statistically significant relationship between imperviousness and model input variables. Climate and land use change both have proven to be able to shift the magnitudes both of

low and peak flows. Land use change scenarios showed that increasing the imperviousness of a watershed can lead to diminished low flows but observed trends were proven statistically insignificant at a 5% level of confidence. With imposing a 10% increase in imperviousness, climate change was still the dominant driver of low flows under future scenarios. In Scenarios 1a and 2, neither the apparent significant increase in temperature under the CCC climate predictions nor the imposed increase in imperviousness by 10%, respectively, was individually capable in leading to a significant decreasing trend in low flows. However, the combination of the two effects was capable to induce a significant decreasing trend in streamflow at a 5% level of significance. On the other hand, in the case of the Hadley climate predictions, precipitation exhibited a significant increasing trend which was capable of dominating the direction of low flow trends. The wetter climate led to an increasing trend in streamflow under the effect of climate solely while land use was held constant at current levels. The addition of land use change was capable of counteracting the significant increasing trend in streamflow previously observed by the climate change only condition, leading to no significant trend in streamflow when both the Hadley climate and urbanization were acting together.

Thus under the scenario of jointly varying climate and land use change, a trend in precipitation can dominate the influence on low flows: higher precipitation leads to higher low flows and vice versa. However, in the event when precipitation is not predicted to undergo any significant change (CCC predictions), the increase in temperature and land use led to a combined effect of lowering low flows.

In predicting low flows, the regression model approach and the continuous streamflow model approach agreed under certain scenarios and disagreed in others. Table

5-1 below summarizes findings under each of the proposed scenarios and both climate predictions.

Table 5-1. Comparison between the outcomes of the regression model and the continuous streamflow model on low flows based on the Cox-Stuart test for trend at a 5 percent level of significance under the three proposed scenarios.

	Scenario 1a Climate change only (CCC)	Scenario 1b Climate change only (Hadley)	Scenario 2 Land use change only	Scenario 3a Climate & land use change (CCC)	Scenario 3b Climate & land use change (Hadley)
Regression Model	No significant Trend	**Significant Increase**	No significant Trend	**Significant Decrease**	No significant Trend
Continuous Streamflow Model	**Significant Decrease**	No significant Trend	No significant Trend	**Significant Decrease**	No significant Trend
Agreement	NO	NO	YES	YES	YES

In Scenarios 1a and 1b, the regression model and the continuous streamflow model predict differently. Hence, the main difference was that one showed a significant trend based on a 5% level of significance and the other model failed to produce a significant trend at the same level of significance. Thus the outcomes under Scenarios 1a and 1b are not opposed, but they disagree about the presence of a significant trend. Their difference is due to the uncertainty in the simulated climate time series under both the CCC and Hadley. Additionally, when land use change alone is imposed in Scenarios 2 or coupled with the climate change in Scenarios 3a and 3b, both the regression model and the continuous streamflow model produce consistent results.

5.4 Limitations/assumptions/extensions

In a modeling exercise of this kind, it becomes very important to explicitly note the limitations and assumptions associated with the findings and results. There are also several

extensions to this modeling exercise that would be useful to conduct, but were not performed here for lack of data, time, or the scientific means to carry them out.

First and foremost, this exercise is premised on a chain of models. Climate models provided the input time series of precipitation and temperature required by the regional regression model and the continuous streamflow model. The continuous streamflow model is really a set of simplified empirical models of surface runoff, subsurface runoff, evaporation, and groundwater runoff. The relationships between known land use and the appropriate model input variables in the continuous streamflow model were modeled here only crudely using simple regression results between PINF and SROP, and imperviousness. In reality, all of these models contain many uncertainties and potential errors. Such uncertainty propagates from one model to the next and should be recognized to be present in the final results documented here. It is appropriate to consider these results as a best estimate of scenarios considered, but caution should be exercised given the propagated uncertainty.

The use of both the CCC and Hadley future climates illustrates the uncertainty in climate modeling. These climates, when used as input to the regression equation and the continuous streamflow model, produced different results to the actual observed precipitation and temperature. The Hadley climate indicated a significant increasing trend in precipitation and temperature. The CCC, on the other hand, showed a slightly larger departure in predicted temperatures, with a more significant increasing trend, from the historical records than did the Hadley climate. These variations led to differing conclusions under Scenarios 1 and 3 as presented in Table 5-1. These discrepancies may be attributed to uncertainties in the chain of models used to derive these results.

The climate time series data used here, whether from actual observations or simulated weather data were point data and do not reflect any spatial variability that is present. Future studies could easily employ time series of adjacent grid cells in the climate models to quantify uncertainty envelopes associated with spatial variability in temperature and precipitation. In the context of the watersheds considered in this analysis, we expect this uncertainty to be relatively small, owing to the relatively small scale of the watersheds being considered. Considerations of spatial variability would be more important across a larger region or within larger scale watersheds.

Possible extensions to this study can be implemented in several dimensions. More data and larger regions can provide a better representation to how streamflows react to climate and land use changes on a regional scale. Investigating other regression model forms and more meaningful predictor variables may lead to more reliable predictions of streamflow under future scenarios. Another expansion of this work is to produce regional regression models for other levels of the flow distribution and to investigate how the length of antecedent precipitation and temperature periods shift as we predict different quantiles.

Moreover, the continuous streamflow model used in Chapter Four is a lumped model form that assigns single input values to describe the characteristics over the entire watershed area. Thus using distributed models may provide a more realistic representation of the expected variation in the input variables in a watershed. Incorporating a distributed model form into the GIS interface, can grant the ability to consider each grid unit as a distinct hydrologic unit, in which all units that constitute the watershed are hydrologically connected. Additionally, more sophisticated continuous streamflow models may provide better predictions of streamflows, and low flows in particular. The future of climate and

land use change modeling will need to take advantage of higher resolution data and simulations, faster computers, and more sophisticated ways to quantify the uncertainty inherent in all models used in the progression from increased CO_2 concentrations to streamflow impacts.

APPENDIX A

SUPPLEMENTAL LIST OF TABLES

Table A-1. Summary of the highest correlation coefficient between the historical low flow events in the NWB watershed and various ranges of average antecedent temperature records.

Antecedent Tmin of x-days	*Min Q-1 day*	*Min Q-2 day*	*Min Q-3 day*	*Min Q-7 day*
1	-0.3188	-0.5020	-0.6043	-0.4414
7	-0.3507	-0.5541	-0.5242	-0.5096
14	-0.4069	-0.6064	-0.5686	-0.5601
30	-0.4758	-0.6192	-0.6045	-0.5581
60	-0.5668	-0.6806	-0.7002	-0.6121
90	-0.5636	-0.5592	-0.6278	-0.5258
120	-0.4212	-0.2897	-0.4003	-0.3289
150	-0.2410	-0.0195	-0.1359	-0.1233
180	-0.1148	0.1384	0.0455	0.0236
210	-0.0285	0.2334	0.1474	0.1227
230	0.0438	0.2904	0.2145	0.1893
270	0.0772	0.3033	0.2422	0.2196
Tmax	*min1day*	*min2day*	*min3day*	*min7day*
1	-0.3990	-0.5643	-0.6515	-0.5588
7	-0.4727	-0.6258	-0.6163	-0.5793
14	-0.5034	-0.6511	-0.6214	-0.6209
30	-0.5335	-0.6446	-0.6367	-0.5915
60	-0.6013	-0.6680	-0.7001	-0.6147
90	-0.6396	-0.6070	-0.6760	-0.5729
120	-0.5340	-0.4086	-0.5041	-0.3999
150	-0.2957	-0.0248	-0.1640	-0.1509
180	-0.1545	0.1554	0.0454	0.0053
210	-0.0613	0.2562	0.1546	0.1110
230	0.0358	0.3453	0.2539	0.1993
270	0.0872	0.3819	0.3065	0.2510
Tavg	*min1day*	*min2day*	*min3day*	*min7day*
1	-0.3680	-0.5489	-0.6501	-0.5111
7	-0.4219	-0.6038	-0.5870	-0.5547
14	-0.4690	-0.6451	-0.6111	-0.6045
30	-0.5215	-0.6496	-0.6365	-0.5908
60	-0.6107	-0.6987	-0.7236	-0.6332
90	-0.6394	-0.6168	-0.6861	-0.5727
120	-0.5059	-0.3673	-0.4763	-0.3774
150	-0.2814	-0.0231	-0.1571	-0.1419
180	-0.1402	0.1527	0.0474	0.0152
210	-0.0470	0.2539	0.1565	0.1207
230	0.0417	0.3304	0.2433	0.2019
270	0.0878	0.3604	0.2882	0.2473

Table A-2. Correlations between annual minimum low flows and various durations of antecedent precipitation.

	min. 1-day runoff	min. 2-day runoff	min. 3-day runoff	min. 7-day runoff
prec-30	0.2011	0.2420	0.1500	0.1708
prec-60	0.4751	0.2797	0.4094	0.2343
prec-90	0.6175	0.3869	0.4925	0.5502
prec-120	0.6658	0.5718	0.5410	0.6513
prec-150	0.6887	0.5879	0.5795	0.6373
prec-180	0.6864	0.5784	0.5417	0.6461
prec-210	0.6691	0.6419	0.6048	0.6738
prec-240	0.7073	0.6918	0.6341	0.7268
prec-270	0.7161	0.6844	0.6685	0.7698
prec-300	0.7173	0.6835	0.6543	0.7769
prec-330	0.7195	0.6598	0.6454	0.7536
prec-360	0.6918	0.6160	0.6057	0.7565

Table A-3. A summary of the correlation coefficient (R), bias, and the calibrated coefficients for the power model form on the NWB time series of the 1, 2, 3, and 7-day low flows against the time series of antecedent precipitation of 8, 9, 10, and 11 months using the three proposed model forms.

Minimum 1-day lowflow		Predicted Runoff prec-240	Predicted Runoff prec-270	Predicted Runoff prec-300	Predicted Runoff prec-330
Equation 3-1	R	0.8118	0.8106	0.7978	0.7829
	bias (cfs)	8.32E-07	2.79E-08	8.82E-07	1.53E-05
	C1	-0.8087	-0.6795	-0.8260	-1.0977
	C2	0.2764	0.2487	0.2264	0.2057
	C3	-0.2453	-0.2577	-0.2362	-0.2084
Equation 3-2	R	0.8120	0.8238	0.8082	0.7969
	bias (cfs)	1.1481	1.0816	1.0729	0.6142
	C1	0.0279	0.0235	0.0178	0.0160
	C2	1.9640	2.0414	2.0025	1.9725
	C3	-0.6899	-0.8208	-0.7136	-0.7022
Equation 3-3	R	0.8305	0.8385	0.8195	0.8066
	bias (cfs)	-0.0322	-0.0423	0.0013	-0.0398
	C1	3.5716	4.5984	3.8912	3.7225
	C2	-10.5098	-12.8255	-11.2875	-11.6374
	C3	0.2745	0.2495	0.2248	0.2052
	C4	0.0444	0.0947	0.0737	0.1119
Minimum 2-day lowflow		Predicted Runoff prec-240	Predicted Runoff prec-270	Predicted Runoff prec-300	Predicted Runoff prec-330
Equation 3-1	R	0.7958	0.7955	0.7770	0.7413
	bias (cfs)	-1.80E-06	-6.79E-06	0.0015	1.71E-07
	C1	-0.8514	-0.6373	-1.0723	-1.0202
	C2	0.5607	0.5043	0.4593	0.4034
	C3	-0.5489	-0.5670	-0.5141	-0.4689
Equation 3-2	R	0.7985	0.8068	0.7884	0.7507
	bias (cfs)	3.3823	3.6352	3.0984	2.3583
	C1	0.0933	0.0866	0.0541	0.0667
	C2	1.8988	1.9225	1.9502	1.8372
	C3	-0.7953	-0.8830	-0.7915	-0.7830
Equation 3-3	R	0.8205	0.8303	0.8048	0.7798
	bias (cfs)	-0.4640	-0.0726	0.0042	-0.0053
	C1	9.0201	11.5992	9.8652	11.6831
	C2	-23.9077	-29.8702	-26.3046	-31.0171
	C3	0.5596	0.5083	0.4576	0.4077
	C4	0.1102	0.2533	0.2076	0.3813

Minimum 3-day lowflow		Predicted Runoff prec-240	Predicted Runoff prec-270	Predicted Runoff prec-300	Predicted Runoff prec-330
Equation 3-1	R	0.7597	0.7797	0.7548	0.7298
	bias (cfs)	-0.0013	-1.15E-04	-3.25E-05	0.0033
	C1	0.2976	-0.5750	-0.6797	-1.0940
	C2	0.8407	0.7674	0.6929	0.6153
	C3	-0.9245	-0.8837	-0.8260	-0.7457
Equation 3-2	R	0.7587	0.7915	0.7642	0.7413
	bias (cfs)	7.8062	10.0185	11.6679	3.8601
	C1	0.2999	0.2557	0.2300	0.1104
	C2	1.7354	1.7607	1.6803	1.8143
	C3	-0.8691	-0.9203	-0.8089	-0.7787
Equation 3-3	R	0.7910	0.8158	0.7874	0.7683
	bias (cfs)	-0.0105	-0.6740	-0.3438	-0.8214
	C1	17.9055	18.0434	17.8287	17.3104
	C2	-42.3268	-44.9687	-44.4424	-44.5748
	C3	0.8361	0.7681	0.6890	0.6166
	C4	0.2389	0.3459	0.3926	0.4752
Minimum 7-day lowflow		Predicted Runoff prec-240	Predicted Runoff prec-270	Predicted Runoff prec-300	Predicted Runoff prec-330
Equation 3-1	R	0.8167	0.8449	0.8352	0.8075
	bias (cfs)	-7.9443	-11.9579	-14.6766	-14.4398
	C1	-7.9443	-11.9579	-14.6766	-14.4398
	C2	2.3286	2.1708	2.0227	1.8071
	C3	-2.0922	-1.9512	-1.7511	-1.6251
Equation 3-2	R	0.8241	0.8761	0.8515	0.8316
	bias (cfs)	27.2552	7.0431	16.1817	10.2067
	C1	0.4358	0.0935	0.0692	0.0690
	C2	1.8699	2.2839	2.1914	2.1834
	C3	-0.8329	-0.8883	-0.6878	-0.7589
Equation 3-3	R	0.8391	0.8721	0.8546	0.8328
	bias (cfs)	-1.0871	-0.0372	-0.3931	2.4787
	C1	33.3794	34.8338	22.3226	28.7608
	C2	-98.9288	-111.4282	-89.4168	-102.3400
	C3	2.3012	2.1482	2.0078	1.7803
	C4	0.6477	1.1033	0.7390	1.1939

Table A-4. Summary of the predicted annual 7-day low flow for the NWB watershed under each of the three proposed model forms.

1	2	3	4	5	6	Eq. 3-1	Eq. 3-2	Eq. 3-3
year	day of year	Observed Q7 (cfs)	P_{270} (in)	T_{60} [C]	I(t) (%)	Q7 (cfs)	Q7 (cfs)	Q7 (cfs)
1951	225	85.6	31.79	23.75683	6.2529	37.6985	43.3483	37.7315
1952	308	59.4	36.87	15.76958	6.4067	61.9833	66.6699	61.4024
1953	319	76	37.53	14.48998	6.7288	65.1211	68.6963	65.0776
1954	1	77	35.02	6.29326	6.8262	75.8093	77.0053	76.8478
1955	214	9.6	22.25	24.56284	6.975	17.3411	18.5914	18.081
1956	243	19.6	21.88	23.898	7.1056	17.7065	17.8627	17.2601
1957	225	7.1	24	26.02459	7.1699	17.5178	21.0048	18.4864
1958	288	42	36.96	19.51275	7.2719	53.7136	57.088	53.2146
1959	184	19.2	21.29	22.14936	7.4547	19.3697	16.6927	21.2752
1960	246	37.1	36.45	24.24408	7.6015	43.3039	50.0291	43.367
1961	268	26.7	31.13	24.35792	7.7782	32.9412	35.155	33.442
1962	253	13.9	24.27	22.65027	8.0485	23.0183	20.7101	22.141
1963	218	8.8	17.93	23.97996	8.8637	7.4613	9.9766	7.7103
1964	249	6	20.91	23.77049	9.1305	12.9668	13.5727	12.5459
1965	225	12.7	23.67	23.39253	9.8473	17.6757	16.8116	17.5236
1966	248	0	13.56	25.2459	10.2787	-5.2627	4.8757	-5.107
1967	274	26.3	24.25	20.35974	10.7628	23.0476	17.3701	21.9376
1968	274	10.2	18.2	20.75137	11.0088	10.6965	9.2376	9.647
1969	181	12.9	17.25	19.96357	11.6472	9.4206	8.0173	10.6911
1970	282	20.5	27.05	21.20219	11.9909	24.72	20.0012	24.5975
1971	193	47	34.61	20.57832	12.2632	39.4973	33.5278	40.376
1972	284	55.6	46.33	19.8725	12.7703	61.7785	61.1614	61.6311
1973	290	46	42.21	19.84517	12.9485	53.9067	49.7182	54.0969
1974	198	24.6	31.92	20.67395	13.2804	32.7279	26.6266	33.2289
1975	236	47.8	39.87	23.18761	13.4884	42.3975	40.6636	42.3876
1976	252	21.5	28.9	21.53461	13.5983	24.9983	20.9203	23.9445
1977	262	11	20.79	22.3133	14.0237	7.8117	10.0551	7.1888
1978	270	32	36.69	21.95811	14.3704	37.4369	33.154	37.3289
1979	216	56.8	43.02	20.89253	14.456	51.0607	47.0324	50.7802
1980	255	18.1	30.89	23.72951	14.7444	22.7396	22.0278	22.8649
1981	280	16.2	24.47	20.57832	14.9396	16.4804	13.9406	16.0172
1982	238	14.9	23.73	22.29508	15.2764	11.3325	12.5228	10.5958
1998	272	4	29.61	23.48361	20.3554	12.0146	16.0252	12.8405
1999	208	0	21.38	24.64481	20.4182	-5.5482	7.8867	-3.8009
2000	255	26	29.63	22.47723	20.5233	13.6907	16.1828	13.4685

Table A-5. Intercorrelation matrix for the power model form for the annual 7-day low flow (NWB).

	precip.(in)	*temp.(C)*	*Imperv.(%)*	Simulated Q7	Observed Q7
precip.(in)	1				
temp.(C)	-0.397117	1			
Imperv. (%)	0.0404291	0.200107	1		
Simulated Q7	0.8439817	-0.67119	-0.36841	1	
Observed Q7	0.7698421	-0.63317	-0.31677	0.8928261	1

Table A-6. Summary of the residuals and the calculations associated with the three model forms calibrated on the NWB watershed 7-day low flow time series.

min 7-day Runoff (cfs)	MODEL 1 Predicted Runoff (cfs)	MODEL 2 Predicted Runoff (cfs)	MODEL 3 Predicted Runoff (cfs)	MODEL 1 e (cfs)	MODEL 2 e (cfs)	MODEL 3 e (cfs)	MODEL 1 e^2 (cfs)	MODEL 2 e^2 (cfs)	MODEL 3 e^2 (cfs)
85.6	37.70	43.35	37.73	47.90	42.25	47.87	2294.55	1785.21	2291.39
59.4	61.98	66.67	61.40	-2.58	-7.27	-2.00	6.67	52.85	4.01
76	65.12	68.70	65.08	10.88	7.30	10.92	118.35	53.34	119.30
77	75.81	77.01	76.85	1.19	-0.01	0.15	1.42	0.00	0.02
9.6	17.34	18.59	18.08	-7.74	-8.99	-8.48	59.92	80.85	71.93
19.6	17.71	17.86	17.26	1.89	1.74	2.34	3.59	3.02	5.48
7.1	17.52	21.00	18.49	-10.42	-13.90	-11.39	108.53	193.34	129.65
42	53.71	57.09	53.21	-11.71	-15.09	-11.21	137.21	227.65	125.77
19.2	19.37	16.69	21.28	-0.17	2.51	-2.08	0.03	6.29	4.31
37.1	43.30	50.03	43.37	-6.20	-12.93	-6.27	38.49	167.16	39.28
26.7	32.94	35.16	33.44	-6.24	-8.46	-6.74	38.95	71.49	45.45
13.9	23.02	20.71	22.14	-9.12	-6.81	-8.24	83.14	46.38	67.91
8.8	7.46	9.98	7.71	1.34	-1.18	1.09	1.79	1.38	1.19
6	12.97	13.57	12.55	-6.97	-7.57	-6.55	48.54	57.35	42.85
12.7	17.68	16.81	17.52	-4.98	-4.11	-4.82	24.76	16.91	23.27
0	-5.26	4.88	-5.11	5.26	-4.88	5.11	27.70	23.77	26.08
26.3	23.05	17.37	21.94	3.25	8.93	4.36	10.58	79.74	19.03
10.2	10.70	9.24	9.65	-0.50	0.96	0.55	0.25	0.93	0.31
12.9	9.42	8.02	10.69	3.48	4.88	2.21	12.11	23.84	4.88
20.5	24.72	20.00	24.60	-4.22	0.50	-4.10	17.81	0.25	16.79
47	39.50	33.53	40.38	7.50	13.47	6.62	56.29	181.50	43.88
55.6	61.78	61.16	61.63	-6.18	-5.56	-6.03	38.17	30.93	36.37
46	53.91	49.72	54.10	-7.91	-3.72	-8.10	62.52	13.83	65.56
24.6	32.73	26.63	33.23	-8.13	-2.03	-8.63	66.06	4.11	74.46
47.8	42.40	40.66	42.39	5.40	7.14	5.41	29.19	50.93	29.29
21.5	25.00	20.92	23.94	-3.50	0.58	-2.44	12.24	0.34	5.98
11	7.81	10.06	7.19	3.19	0.94	3.81	10.17	0.89	14.53
32	37.44	33.15	37.33	-5.44	-1.15	-5.33	29.56	1.33	28.40
56.8	51.06	47.03	50.78	5.74	9.77	6.02	32.94	95.41	36.24
18.1	22.74	22.03	22.86	-4.64	-3.93	-4.76	21.53	15.43	22.70
16.2	16.48	13.94	16.02	-0.28	2.26	0.18	0.08	5.10	0.03
14.9	11.33	12.52	10.60	3.57	2.38	4.30	12.73	5.65	18.53
4	12.01	16.03	12.84	-8.01	-12.03	-8.84	64.23	144.61	78.15
0	-5.55	7.89	-3.80	5.55	-7.89	3.80	30.78	62.20	14.45
26	13.69	16.18	13.47	12.31	9.82	12.53	151.52	96.38	157.04
Total Bias (cfs)				3.52	-12.06	1.28	3652.38	3600.36	3664.49
Average Bias (cfs)				0.10	-0.34	0.04			
Standard Error of Estimate, Se (cfs)							10.520	10.445	10.538
Correlation Coefficient, R							0.8908	0.8928	0.8904

Table A-7. Summary of the NWB time series used to calibrate for the regional regression model.

Year	Obs. Q7 (cfs)	P_{270} (In.)	T_{60} (^{o}F.)	I(t) (%)	Area (mi^2)
1946	52.6	27.63	56.7705	5.7775	21.1
1947	50.3	26.07	68.3115	5.86592	21.1
1948	71.4	33.72	71.8115	5.94543	21.1
1949	88	37.39	68.8443	6.01161	21.1
1950	86	34.27	69.0164	6.1092	21.1
1951	85.6	31.79	75.6639	6.2529	21.1
1952	59.4	36.87	58.5	6.4067	21.1
1953	76	37.18	57.2377	6.7288	21.1
1954	81	22.24	53.6639	6.8262	21.1
1955	9.6	23.59	77.418	6.975	21.1
1956	19.6	22.02	75.041	7.1056	21.1
1957	7.1	23.29	78.3607	7.1699	21.1
1958	42	36.43	66.2541	7.2719	21.1
1959	19.2	21.29	72.3197	7.4547	21.1
1960	37.1	35.00	75.6885	7.6015	21.1
1961	26.7	30.63	74.6803	7.7782	21.1
1962	13.9	20.53	72.6311	8.0485	21.1
1963	8.8	22.83	75.2705	8.8637	21.1
1964	6	21.91	74.8279	9.1305	21.1
1965	12.7	24.82	75.7623	9.8473	21.1
1966	0	20.74	75.9918	10.2787	21.1
1967	26.3	27.54	67.7295	10.7628	21.1
1968	10.2	22.98	69.0902	11.0088	21.1
1969	12.9	20.10	69.2295	11.6472	21.1
1970	20.5	26.53	69.1311	11.9909	21.1
1971	47	30.57	70.0492	12.2632	21.1
1972	55.6	40.94	66.2459	12.7703	21.1
1973	46	32.84	66.1885	12.9485	21.1
1974	24.6	29.88	69.7869	13.2804	21.1
1975	47.8	36.64	73.8279	13.4884	21.1
1976	21.5	28.98	70.6311	13.5983	21.1
1977	11	20.43	71.8361	14.0237	21.1
1978	32	36.64	70.541	14.3704	21.1
1979	56.8	42.99	69.918	14.456	21.1
1980	18.1	30.85	74.1393	14.7444	21.1
1981	16.2	24.47	65.6803	14.9396	21.1
1982	14.9	23.11	71.5246	15.2764	21.1
1998	4	30.61	73.0656	20.3554	21.1
1999	0	21.36	76.8934	20.4182	21.1
2000	26	29.32	71.7541	20.5233	21.1

Table A-8. Summary of the Seneca time series used to calibrate for the regional regression model.

Year	Obs. Q7 (cfs)	P_{270} (In.)	T_{60} (^{o}F.)	I(t) (%)	Area (mi^2)
1951	182	27.16	71.4262	12.6141	101
1952	329	37.33	58.2377	12.6197	101
1953	193	31.62	68.7705	12.6226	101
1954	77.6	21.78	69.3115	12.6277	101
1955	42.8	18.22	74.6557	12.6337	101
1956	195	19.94	66.8934	12.6478	101
1957	54.1	19.52	73.8443	12.6608	101
1958	239	29.01	38.459	12.6721	101
1959	99	23.25	73.2787	12.685	101
1960	197	33.11	73.6393	12.7001	101
1961	166	29.70	69.4672	12.7247	101
1962	108	24.55	72.1311	12.7583	101
1963	63.9	22.16	72.5492	12.7804	101
1964	62.4	19.35	73.8689	12.8237	101
1965	105	26.59	74.2705	12.8712	101
1966	16	23.22	74.1557	12.9123	101
1967	203	26.78	72.6066	12.9352	101
1968	117	25.55	69.3033	12.9728	101
1969	121	21.00	69.6066	13.0036	101
1970	111	30.52	70.7541	13.0401	101
1971	325	33.98	71.2951	13.0772	101
1972	330	38.45	65.9098	13.1571	101
1973	291	34.47	65.7459	13.2525	101
1974	189	27.57	65.8033	13.3313	101
1975	247	32.01	74.4672	13.3481	101
1976	208	34.88	70.7295	13.3842	101
1977	92	24.73	73.3852	13.4819	101
1978	228	32.31	71.6311	13.6163	101
1979	478	42.28	70.4508	13.6692	101
1980	206	26.20	68.2459	13.7358	101
1981	145	25.64	73.5246	13.8138	101
1982	203	27.94	70.6066	13.882	101
1983	195	33.34	77.2541	13.985	101
1984	229	28.63	70.4508	14.0759	101
1985	127	23.67	72.1557	14.1808	101
1986	102	18.66	70.2377	14.3181	101
1987	161	28.01	76.6721	14.4994	101
1988	274	29.69	78	14.609	101
1989	236	30.55	73.5492	14.7096	101
1990	217	32.11	68.4262	14.7485	101
1991	151	22.17	76.0328	14.7798	101
1992	207	27.17	73.459	14.8297	101
1993	209	34.56	74.7705	14.8893	101

1994	313	37.99	61.1311	14.9492	101
1995	112	26.17	73.8197	15.0269	101
1996	602	35.48	33.3934	15.0631	101
1997	163	26.87	73.8689	15.1061	101
1998	136	38.70	71.6066	15.1189	101
1999	105	24.06	74.2295	15.1762	101
2000	328	37.76	69.9754	15.1762	101

Table A-9. Summary of the Watts time series used to calibrate for the regional regression model.

Year	Obs. Q7 (cfs)	P_{270} (In.)	T_{60} (^{o}F.)	I(t) (%)	Area (mi^2)
1958	7.7	36.96	66.9344	16.0998	3.7
1959	2.6	25.20	75.8443	16.1105	3.7
1960	9.8	34.91	75.7377	17.9299	3.7
1961	5.2	30.28	74.6803	18.2339	3.7
1962	2.2	22.99	72.6393	18.4761	3.7
1963	3.2	21.96	75.2869	18.848	3.7
1964	3	20.85	71.5164	19.1898	3.7
1965	2.9	25.04	75.4016	19.828	3.7
1966	0.7	18.03	77.459	20.7749	3.7
1967	5.2	23.39	73.1393	21.26	3.7
1968	3.2	22.14	74.8115	22.8336	3.7
1969	2.9	18.47	72.7459	23.3489	3.7
1970	4.2	33.07	69.1311	23.744	3.7
1971	8.2	34.47	73.0984	23.9036	3.7
1972	9.7	46.70	70.4918	24.1036	3.7
1973	8.6	41.38	65.8033	24.1701	3.7
1974	4.1	36.88	69.6967	24.2115	3.7
1975	6.7	37.79	73.8525	24.2115	3.7
1976	4.2	28.79	70.959	24.2115	3.7
1977	1.8	20.22	68.9262	24.2263	3.7
1978	6	30.18	59.1557	24.4108	3.7
1979	14.3	39.14	65.1475	24.4175	3.7
1980	3.4	30.92	68.1475	27.9553	3.7
1981	1.9	24.27	68.4344	28.178	3.7
1982	3.3	23.11	71.6557	28.2044	3.7
1983	2.4	31.37	75.4426	28.3603	3.7
1984	4.5	31.98	72.9098	28.4556	3.7
1985	2.3	24.29	70.8525	28.4759	3.7
1986	1.6	21.62	66.6967	28.8515	3.7

Table A-10. Summary of the Little Falls time series used to calibrate for the regional regression model.

Year	Obs. Q7 (cfs)	P_{270} (In.)	T_{60} (^{o}F.)	I(t) (%)	Area (mi^2)
1951	0.8	31.73	73.5902	35.1855	4.1
1952	1.9	39.45	63.959	35.3043	4.1
1953	1	39.14	72.1721	35.518	4.1
1954	0.1	25.84	76.6475	35.7761	4.1
1955	0.8	25.87	77.459	35.9979	4.1
1956	0.8	30.52	65.8443	36.1976	4.1
1957	0.2	23.94	77.2459	36.4062	4.1
1958	0.4	43.55	74.4754	36.4115	4.1
1962	1.4	25.24	64.9672	36.6033	4.1
1963	1.4	28.28	74.8361	36.6033	4.1
1964	1.5	25.51	76.8279	36.6033	4.1
1965	1.4	22.74	47.2295	36.6033	4.1
1966	1.4	21.72	79.7459	36.6033	4.1
1967	3.2	31.12	70.877	36.5979	4.1
1968	2.8	27.63	79.2459	36.5979	4.1
1969	3	24.07	74.5656	36.5979	4.1
1970	4.2	28.96	78.1885	36.5979	4.1
1971	6.6	37.46	69.9016	36.5979	4.1
1972	3	42.64	68.2459	36.5979	4.1
1973	4.8	30.28	59.6967	36.5979	4.1
1974	4	27.70	70.2869	36.6137	4.1
1975	5	33.18	78.4918	36.6137	4.1
1976	7.2	24.18	78.082	36.6137	4.1
1977	6.2	21.09	76.7459	36.6414	4.1
1978	6.8	26.04	65.4672	36.6414	4.1

Table A-11. Summary of the Hawlings time series used to calibrate for the regional regression model.

Year	Obs. Q7 (cfs)	P_{270} (In.)	T_{60} (^{o}F.)	I(t) (%)	Area (mi^2)
1979	98	39.64	68.5738	8.46016	27
1980	32.6	23.37	67.0328	8.48445	27
1981	25.9	28.21	67.3443	8.49363	27
1982	25.9	29.84	69.4672	8.53343	27
1983	32.9	36.62	76.7131	8.56555	27
1984	49.3	32.14	72.0082	8.59997	27
1985	22.3	24.98	71.2295	8.66554	27
1986	15.2	22.61	66.6967	8.74907	27
1987	23.4	28.46	80.5902	8.92852	27
1988	30.6	34.00	78.9918	8.99874	27
1989	67.3	44.27	74.1803	9.05901	27
1990	45.5	33.31	68.3115	9.11846	27
1991	17.4	25.94	76.9426	9.16206	27
1992	39.8	27.24	70.5246	9.19743	27
1993	28.1	29.58	75.582	9.21277	27
1994	63.4	35.31	63.8852	9.26522	27
1995	12.5	24.71	76.3525	9.31849	27
1996	124	38.09	72.9836	9.35354	27
1997	24	23.21	67.7131	9.38796	27
1998	27.4	30.47	72.7295	9.41484	27
1999	2.4	21.01	77.6639	9.44573	27
2000	56.1	29.27	59.2295	9.44573	27

Table A-12. Summary of the Rock Creek time series used to calibrate for the regional regression model.

Year	Obs. Q7 (cfs)	P_{270} (In.)	T_{60} (^{o}F.)	I(t) (%)	Area (mi^2)
1967	12.8	23.39	73.2131	11.0433	9.73
1968	3.8	23.40	74.8115	11.3581	9.73
1969	4.2	18.51	72.7459	11.5475	9.73
1970	10.8	33.86	68.8689	11.9007	9.73
1971	16.3	31.71	71.7541	12.3511	9.73
1972	19.7	46.51	70.2951	12.6423	9.73
1973	22.1	41.65	74.2459	12.9165	9.73
1974	9.8	31.92	69.6721	13.0488	9.73
1975	22.6	37.79	73.8525	13.0488	9.73
1976	12.8	28.79	70.959	13.0572	9.73

Table A-13. Summary of the one-dimensional response surface (Se/Sy) for the regional regression model (Equation 3-9).

	0.90*C(I)	0.95*C(I)	1.00*C(I)	1.05*C(I)	1.10*C(I)
C1 (Intercept)	0.332327	0.315794	0.310102	0.315836	0.332406
C2 (P)	0.664202	0.462444	0.310102	0.572324	1.19778
C3 (T)	0.689988	0.41517	0.310102	0.3826	0.510848
C4 (I)	0.312891	0.310791	0.310102	0.310761	0.312694
C5 (A)	0.575963	0.414035	0.310102	0.472261	0.876149

Table A-14. Summary of the one-dimensional response surface (relative bias) for the regional regression model (Equation 3-9).

	0.90*C(I)	0.95*C(I)	1.00*C(I)	1.05*C(I)	1.10*C(I)
C1 (Intercept)	-0.09201	-0.04157	0.008873	0.059317	0.10976
C2 (P)	-0.47928	-0.27533	0.008873	0.405061	0.957552
C3 (T)	0.540353	0.246546	0.008873	-0.18341	-0.33898
C4 (I)	0.043246	0.025914	0.008873	-0.00788	-0.02436
C5 (A)	-0.37701	-0.20797	0.008873	0.287341	0.645344

Table A-15. Determining the correlation coefficient (R) between imperviousness and low flow of the NWB watershed after removing the effects of precipitation and temperature.

	Obs. Q7 (cfs)	Prec. (In.)	Temp. (Feh.)	Pred. Q7(cfs)	Error (cfs)	Imperv. (%)
1	52.6	27.63	56.77	41.52	11.085	5.78
2	50.3	26.07	68.31	28.74	21.558	5.87
3	71.4	33.72	71.81	43.92	27.476	5.95
4	88	37.39	68.84	56.77	31.234	6.01
5	86	34.27	69.02	47.87	38.132	6.11
6	85.6	31.79	75.66	36.49	49.108	6.25
7	59.4	36.87	58.50	69.24	-9.839	6.41
8	76	37.18	57.24	72.52	3.483	6.73
9	81	22.24	53.66	29.61	51.394	6.83
10	9.6	23.59	77.42	19.95	-10.354	6.98
11	19.6	22.02	75.04	18.26	1.342	7.11
12	7.1	23.29	78.36	19.15	-12.047	7.17
13	42	36.43	66.25	56.95	-14.951	7.27
14	19.2	21.29	72.32	18.01	1.187	7.45
15	37.1	35.00	75.69	43.86	-6.762	7.60
16	26.7	30.63	74.68	34.60	-7.903	7.78
17	13.9	20.53	72.63	16.70	-2.801	8.05
18	8.8	22.83	75.27	19.48	-10.685	8.86
19	6	21.91	74.83	18.15	-12.155	9.13
20	12.7	24.82	75.76	22.66	-9.965	9.85

21	0	20.74	75.99	16.00	-15.996	10.28
22	26.3	27.54	67.73	32.31	-6.010	10.76
23	10.2	22.98	69.09	22.22	-12.016	11.01
24	12.9	20.10	69.23	17.14	-4.239	11.65
25	20.5	26.53	69.13	29.24	-8.736	11.99
26	47	30.57	70.05	37.67	9.331	12.26
27	55.6	40.94	66.25	71.24	-15.643	12.77
28	46	32.84	66.19	46.74	-0.743	12.95
29	24.6	29.88	69.79	36.24	-11.644	13.28
30	47.8	36.64	73.83	49.57	-1.766	13.49
31	21.5	28.98	70.63	33.62	-12.116	13.60
32	11	20.43	71.84	16.80	-5.800	14.02
33	32	36.64	70.54	52.79	-20.793	14.37
34	56.8	42.99	69.92	72.61	-15.807	14.46
35	18.1	30.85	74.14	35.44	-17.336	14.74
36	16.2	24.47	65.68	26.88	-10.679	14.94
37	14.9	23.11	71.52	21.41	-6.506	15.28

Goodness-of-Fit Statistics for: $Q_7 = b_0 * P_{270}^{b1} * T_{60}^{b2}$

18.9517	=	Standard Error of Estimate, Se
26.1328	=	Standard Deviation of Y, Sy
0.7252	=	Se/Sy
0.6920	=	Correlation Coefficient
0.4788	=	Explained Variance
0.4855	=	Bias
0.0137	=	Relative Bias
-0.5541	=	The correlation coefficient between Residuals and Imperviousness time series
19.2361	=	b_0
1.9171	=	b_1
-1.3848	=	b_2

Table A-16. Determining the correlation coefficient between imperviousness and low flow of Watts Branch watershed after removing the effects of precipitation and temperature.

	Obs.Q7 (cfs)	Prec. (In.)	Temp. (Feh.)	Pred. Q7(cfs)	Error (cfs)	Imperv. (%)
1	7.7	36.96	66.93	7.59	0.105	16.10
2	2.6	25.2	75.84	3.12	-0.523	16.11
3	9.8	34.91	75.74	5.87	3.926	17.93
4	5.2	30.28	74.68	4.54	0.663	18.23
5	2.2	22.99	72.64	2.75	-0.553	18.48
6	3.2	21.96	75.29	2.41	0.785	18.85
7	3	20.85	71.52	2.32	0.678	19.19
8	2.9	25.04	75.40	3.11	-0.207	19.83
9	0.7	18.03	77.46	1.59	-0.895	20.77
10	5.2	23.39	73.14	2.82	2.377	21.26
11	3.2	22.14	74.81	2.47	0.728	22.83
12	2.9	18.47	72.75	1.80	1.100	23.35
13	4.2	33.07	69.13	5.90	-1.695	23.74
14	8.2	34.47	73.10	5.98	2.222	23.90
15	9.7	46.7	70.49	11.23	-1.525	24.10
16	8.6	41.38	65.80	9.64	-1.041	24.17
17	4.1	36.88	69.70	7.21	-3.109	24.21
18	6.7	37.79	73.85	7.05	-0.355	24.21
19	4.2	28.79	70.96	4.37	-0.172	24.21
20	1.8	20.22	68.93	2.29	-0.486	24.23
21	6	30.18	59.16	5.94	0.057	24.41
22	14.3	39.14	65.15	8.76	5.539	24.42
23	3.4	30.92	68.15	5.27	-1.866	27.96
24	1.9	24.27	68.43	3.28	-1.381	28.18
25	3.3	23.11	71.66	2.83	0.474	28.20
26	2.4	31.37	75.44	4.80	-2.400	28.36
27	4.5	31.98	72.91	5.19	-0.688	28.46
28	2.3	24.29	70.85	3.15	-0.854	28.48
29	1.6	21.62	66.70	2.71	-1.105	28.85

Goodness-of-Fit Statistics for: $Q_7 = b_0 * P_{270}^{b1} * T_{60}^{b2}$

1.8760	=	Standard Error of Estimate, Se
3.0926	=	Standard Deviation of Y, Sy
0.6066	=	Se/Sy
0.7834	=	Correlation Coefficient
0.6137	=	Explained Variance
0.0069	=	Bias
0.0015	=	Relative Bias
-0.3317	=	The correlation coefficient between Residuals and Imperviousness time series
1.0363	=	b_0
1.9330	=	b_1
-1.1861	=	b_2

Table A-17. Summary of the goodness-of-fit statistics and the calibrated coefficients for the regional power model form (Equation 3-6) for all the data while the exponent associated to the imperviousness predictor is fixed at a value of - 0.80.

G-o-f Statistics	Low flow (all)	NWB	Seneca	Little Falls	Hawlings	Rock Creek	Watts	Watts+NWB
Obs. Q_7 (cfs)	68.655	34.430	190.952	2.817	39.587	13.606	4.693	21.879
Pred. Q_7(cfs)	68.408	33.610	189.816	2.796	39.273	13.490	4.683	21.452
Se (cfs)	31.090	15.239	56.881	2.404	18.538	4.558	1.845	11.436
Sy (cfs)	97.858	26.207	107.995	2.229	28.544	6.713	3.093	24.591
Se/Sy	0.318	0.581	0.527	1.079	0.649	0.679	0.597	0.465
R	0.944	0.811	0.845	-0.017	0.763	0.751	0.798	0.880
R^2	0.891	0.658	0.714	0.000	0.582	0.564	0.636	0.775
Bias (cfs)	-1.454	0.786	-3.029	-0.031	0.222	0.140	-0.032	0.536
Avg Bias (cfs)	-1.454	0.786	-3.029	-0.031	0.222	0.140	-0.032	11.896
Sd. Dev. Bias	30.698	14.620	55.027	2.248	17.162	3.719	1.743	13.537
relative Bias	-0.021	0.023	-0.016	-0.011	0.006	0.010	-0.007	0.544
c1 (Intercept)	0.181	2.654	55.326	2.928	41.031	0.006	1.675	1.018
c2 (prec. In.)	2.086	2.032	2.174	-0.159	2.707	1.526	2.050	1.935
c3 (temp. F)	-1.010	-0.597	-0.957	0.785	-1.778	1.038	-0.808	-0.821
c4 (imp. %)	-0.800	-0.800	-0.800	-0.800	-0.800	-0.800	-0.800	-0.800
c5 (A. mi^2)	1.354							0.734

Table A-18. Summary of the goodness-of-fit statistics and the calibrated coefficients for the regional power model form (Equation 3-6) for all the data while the exponent associated to the imperviousness predictor is fixed at a value of - 0.85.

G-o-f Statistics	Low flow (all)	NWB	Seneca	Little Falls	Hawlings	Rock Creek	Watts	Watts+NWB
Obs. Q7 (cfs)	68.655	34.430	190.952	2.817	39.587	13.606	4.693	21.879
Pred. Q7(cfs)	68.408	33.610	189.816	2.796	39.273	13.490	4.683	21.452
Se (cfs)	31.195	15.191	57.083	2.405	18.660	4.591	1.855	11.423
Sy (cfs)	97.858	26.207	107.995	2.229	28.544	6.713	3.093	24.591
Se/Sy	0.319	0.580	0.529	1.079	0.654	0.684	0.600	0.465
R	0.944	0.812	0.844	-0.033	0.760	0.749	0.796	0.880
R^2	0.891	0.659	0.712	0.001	0.577	0.560	0.633	0.775
Bias (cfs)	-1.280	0.700	-3.187	-0.031	0.051	0.128	-0.045	0.416
Avg Bias (cfs)	-1.280	0.700	-3.187	-0.031	0.051	0.128	-0.045	0.416
Sd. Dev. Bias	30.810	14.578	55.214	2.249	17.275	3.746	1.752	11.074
relative Bias	-0.019	0.020	-0.017	-0.011	0.001	0.009	-0.010	0.019
c1 (Intercept)	0.224	2.950	64.255	3.603	28.005	0.009	1.289	0.678
c2 (prec. In.)	2.063	2.009	2.179	-0.105	2.744	1.538	2.071	1.955
c3 (temp. F)	-1.019	-0.578	-0.966	0.736	-1.695	0.958	-0.728	-0.704
c4 (imp. %)	-0.850	-0.850	-0.850	-0.850	-0.850	-0.850	-0.850	-0.850
c5 (A. mi^2)	1.361							0.718

Table A-19. Summary of the goodness-of-fit statistics and the calibrated coefficients for the regional power model form (Equation 3-6) for all the data while the exponent associated to the imperviousness predictor is fixed at a value of - 0.90.

G-o-f Statistics	Low flow (all)	NWB	Seneca	Little Falls	Hawlings	Rock Creek	Watts	Watts+NWB
Obs. Q7 (cfs)	68.655	34.430	190.952	2.817	39.587	13.606	4.693	21.879
Pred. Q7(cfs)	68.408	33.610	189.816	2.796	39.273	13.490	4.683	21.452
Se (cfs)	31.322	15.161	57.741	2.404	18.660	4.432	1.871	11.425
Sy (cfs)	97.858	26.207	107.995	2.229	28.544	6.713	3.093	24.591
Se/Sy	0.320	0.578	0.535	1.079	0.654	0.660	0.605	0.465
R	0.943	0.812	0.841	-0.033	0.760	0.763	0.793	0.880
R^2	0.890	0.659	0.708	0.001	0.577	0.582	0.628	0.774
Bias (cfs)	-1.136	0.538	-4.026	-0.030	0.063	0.207	-0.044	0.087
Avg Bias (cfs)	-1.136	0.538	-4.026	-0.030	0.063	0.207	-0.044	0.087
Sd. Dev. Bias	30.941	14.556	55.798	2.249	17.275	3.613	1.767	11.083
relative Bias	-0.017	0.016	-0.021	-0.011	0.002	0.015	-0.009	0.004
c1 (Intercept)	0.287	3.906	44.693	5.095	35.005	0.000	0.668	0.602
c2 (prec. In.)	2.046	1.992	2.264	-0.123	2.738	1.502	2.068	1.983
c3 (temp. F)	-1.037	-0.606	-0.919	0.711	-1.716	1.763	-0.534	-0.697
c4 (imp. %)	-0.900	-0.900	-0.900	-0.900	-0.900	-0.900	-0.900	-0.900
c5 (A. mi^2)	1.364							0.748

Table A-20. Summary of the subset time series from the NWB and Watts watersheds; subsets were formed based on the closeness of P_{270} and T_{60} data.

Subsets of NWB time series

	Q7 (cfs)	P_{270} (in.)	T_{60} (^{o}F.)	Imp. (%)
SET 1	32	36.64	70.541	14.3704
	42	36.43	66.2541	7.2719
	46	32.84	66.1885	12.9485
	71.4	33.72	71.8115	5.94543
	86	34.27	69.0164	6.1092
	88	37.39	68.8443	6.01161
	Q7	P_{270}	T_{60}	Imp.
SET 2	4	30.61	73.0656	20.3554
	85.6	31.79	75.6639	6.2529
	26.7	30.63	74.6803	7.7782
	18.1	30.85	74.1393	14.7444
	Q7	P_{270}	T_{60}	Imp.
SET 3	21.5	28.98	70.6311	13.5983
	24.6	29.88	69.7869	13.2804
	47	30.57	70.0492	12.2632
	26	29.32	71.7541	20.5233
	Q7	P_{270}	T_{60}	Imp.
SET 4	50.3	26.07	68.3115	5.86592
	26.3	27.54	67.7295	10.7628
	20.5	26.53	69.1311	11.9909
	16.2	24.47	65.6803	14.9396
	Q7	P_{270}	T_{60}	Imp.
SET 5	0	20.74	75.9918	10.2787
	0	21.36	76.8934	20.4182
	6	21.91	74.8279	9.1305
	7.1	23.29	78.3607	7.1699
	8.8	22.83	75.2705	8.8637
	9.6	23.59	77.418	6.975
	19.6	22.02	75.041	7.1056
	Q7	P_{270}	T_{60}	Imp.
SET 6	19.2	21.29	72.3197	7.4547
	10.2	22.98	69.0902	11.0088
	11	20.43	71.8361	14.0237
	12.9	20.1	69.2295	11.6472
	13.9	20.53	72.6311	8.0485
	14.9	23.11	71.5246	15.2764

Subsets of Watts time series

	Q7 (cfs)	P_{270} (in.)	T_{60} (^{o}F.)	Imp. (%)
SET 1	8.6	41.38	65.8033	24.1701
	14.3	39.14	65.1475	24.4175
	7.7	36.96	66.9344	16.0998
	4.1	36.88	69.6967	24.2115
	Q7	P_{270}	T_{60}	Imp.
SET 2	2.4	31.37	75.4426	28.3603
	5.2	30.28	74.6803	18.2339
	4.2	28.79	70.959	24.2115
	4.5	31.98	72.9098	28.4556
	Q7	P_{270}	T_{60}	Imp.
SET 3	1.9	24.27	68.4344	28.178
	2.2	22.99	72.6393	18.4761
	2.3	24.29	70.8525	28.4759
	5.2	23.39	73.1393	21.26
	3.3	23.11	71.6557	28.2044
	Q7	P_{270}	T_{60}	Imp.
SET 4	2.9	18.47	72.7459	23.3489
	3.2	21.96	75.2869	18.848
	3.2	22.14	74.8115	22.8336
	3	20.85	71.5164	19.1898
	0.7	18.03	77.459	20.7749

Table A-21. Summary of residuals of the calibrated power models for the 6 subsets (NWB).

All data				SET 1			
	Predicted Q7 (cfs)	Observed Q7 (cfs)	Residuals (cfs)		Predicted Q7 (cfs)	Observed Q7 (cfs)	Residuals (cfs)
	51.52	52.6	-1.08		34.88	32	2.88
	40.72	50.3	-9.58		61.55	42	19.55
	65.26	71.4	-6.14		35.29	46	-10.71
	81.31	88	-6.69		80.45	71.4	9.05
	67.27	86	-18.73		75.21	86	-10.79
	53.81	85.6	-31.79		77.06	88	-10.94
	81.92	59.4	22.52	SET 2	Pred. Q7	Obs. Q7	Residuals
	80.67	76	4.67		0.64	4	-3.36
	29.69	81	-51.31		84.24	85.6	-1.36
	26.56	9.6	16.96		31.61	26.7	4.91
	23.18	19.6	3.58		2.41	18.1	-15.69
	25.08	7.1	17.98	SET 3	Pred. Q7	Obs. Q7	Residuals
	66.41	42	24.41		17.59	21.5	-3.91
	21.19	19.2	1.99		33.10	24.6	8.50
	54.59	37.1	17.49		42.78	47	-4.22
	41.31	26.7	14.61		24.72	26	-1.28
	18.35	13.9	4.45	SET 4	Pred. Q7	Obs. Q7	Residuals
	20.35	8.8	11.55		50.23	50.3	-0.07
	18.31	6	12.31		25.78	26.3	-0.52
	21.77	12.7	9.07		21.96	20.5	1.46
	14.62	0	14.62		15.19	16.2	-1.01
	26.34	26.3	0.04	SET 5	Pred. Q7	Obs. Q7	Residuals
	17.79	10.2	7.59		4.45	0	4.45
	12.93	12.9	0.03		0.29	0	0.29
	21.91	20.5	1.41		5.07	6	-0.93
	28.25	47	-18.75		12.04	7.1	4.94
	50.30	55.6	-5.30		4.82	8.8	-3.98
	32.04	46	-13.96		11.92	9.6	2.32
	25.17	24.6	0.57		13.26	19.6	-6.34
	36.08	47.8	-11.72	SET 6	Pred. Q7	Obs. Q7	Residuals
	23.02	21.5	1.52		16.59	19.2	-2.61
	11.05	11	0.05		13.29	10.2	3.09
	34.96	32	2.96		12.05	11	1.05
	48.05	56.8	-8.75		12.17	12.9	-0.73
	23.57	18.1	5.47		15.86	13.9	1.96
	15.74	16.2	-0.46		12.22	14.9	-2.68
	13.11	14.9	-1.79				
	17.47	4	13.47				
	8.27	0	8.27				
	16.08	26	-9.92				

Table A-22. Summary of residuals of the calibrated power models for the 4 subsets (Watts).

All data	Predicted Q7 (cfs)	Observed Q7 (cfs)	Residuals (cfs)
	8.33	14.3	-5.97
	6.95	9.8	-2.85
	11.18	9.7	1.48
	9.28	8.6	0.68
	5.95	8.2	-2.25
	9.15	7.7	1.45
	7.04	6.7	0.34
	5.37	6	-0.63
	5.25	5.2	0.05
	2.93	5.2	-2.27
	4.67	4.5	0.17
	5.76	4.2	1.56
	4.23	4.2	0.03
	7.03	4.1	2.93
	4.66	3.4	1.26
	2.49	3.3	-0.81
	2.70	3.2	-0.50
	2.48	3.2	-0.72
	2.52	3	-0.48
	3.41	2.9	0.51
	1.75	2.9	-1.15
	3.85	2.6	1.25
	4.38	2.4	1.98
	2.76	2.3	0.46
	3.08	2.2	0.88
	2.85	1.9	0.95
	2.14	1.8	0.34
	2.28	1.6	0.68
	1.69	0.7	0.99

	Predicted Q7 (cfs)	Observed Q7 (cfs)	Residuals (cfs)
	11.54	8.6	2.94
	9.67	14.3	-4.63
	7.25	7.7	-0.45
	6.30	4.1	2.20
SET 2	Pred. Q7	Obs. Q7	Residuals
	3.55	2.4	1.15
	5.25	5.2	0.05
	3.67	4.2	-0.53
	3.88	4.5	-0.62
SET 3	Pred. Q7	Obs. Q7	Residuals
	2.26	1.9	0.36
	3.43	2.2	1.23
	2.63	2.3	0.33
	3.37	5.2	-1.83
	3.38	3.3	0.08
SET 4	Pred. Q7	Obs. Q7	Residuals
	2.14	2.9	-0.76
	2.95	3.2	-0.25
	3.60	3.2	0.40
	2.88	3	-0.12
	1.52	0.7	0.82

Table A-23. Summary of the goodness-of-fit statistics and calibrated coefficients for the power models associated the subsets of the NWB time series.

	All data	SET 1	SET 2	SET 3	SET 4	SET 5	SET 6
Se (cfs)	15.168	20.291	Infinity	Infinity	Infinity	5.959	3.809
Sy (cfs)	26.207	24.038	35.907	11.636	15.223	6.673	3.222
Se/Sy	0.579	0.844	---	---	---	0.893	1.182
R	0.811	0.705	0.733	0.646	0.748	0.665	0.554
R^2	0.658	0.497	0.537	0.418	0.560	0.443	0.307
E (cfs)	0.541	-0.159	-3.877	-0.228	-0.035	0.105	0.016
Rel. Bias	0.016	-0.003	-0.115	-0.008	-0.001	0.014	0.001
C2 (P_{270})	1.991	0.138	2.450	16.319	1.069	-4.692	0.492
C3 (T_{60})	-0.571	1.113	0.400	-12.755	0.400	4.641	1.798
C4 (Imp.)	-0.906	-0.937	-4.050	0.854	-1.190	-3.880	-0.455
C1 (inter)	3.421	2.257	5.217	1.002	2.335	105.456	0.004

Table A-24. Summary of the goodness-of-fit statistics and calibrated coefficients for the power models associated the subsets of the Watts time series.

	All data	SET 1	SET 2	SET 3	SET 4
Se (cfs)	1.833	Infinity	Infinity	2.261	1.222
Sy (cfs)	3.093	4.224	1.193	1.348	1.070
Se/Sy	0.593	---	---	1.677	1.142
R	0.800	0.441	0.550	0.458	0.660
R^2	0.640	0.194	0.303	0.210	0.435
E (cfs)	0.013	0.014	0.010	0.033	0.018
Rel. Bias	0.003	0.002	0.002	0.011	0.007
C2 (P_{270})	1.991	3.720	2.481	-4.092	3.382
C3 (T_{60})	-0.819	-3.078	-1.292	4.401	-2.628
C4 (Imp.)	-0.553	-0.018	-1.055	0.156	0.805
C1 (inter)	1.005	4.679	6.252	0.005	0.689

Table A-25. Summary of the goodness-of-fit statistics and calibrated coefficients for the power models calibrated based on the imperviousness as the sole predictor for each of the subsets of the NWB time series.

	All data	SET 1	SET 2	SET 3	SET 4	SET 5	SET 6
Se (cfs)	24.273	14.823	17.623	13.204	1.575	5.496	2.997
Sy (cfs)	26.200	24.038	35.907	11.636	15.223	6.636	3.222
Se/Sy	0.926	0.617	0.491	1.135	0.103	0.828	0.930
Bias (cfs)	-10.310	-1.389	-2.041	-1.269	0.017	-2.121	-0.221
Mean Rel. Error	6.952	0.185	0.386	0.252	0.036	2.459	0.151
Std. Of Rel. Error	30.881	0.159	0.158	0.129	0.027	5.419	0.106
Intercept coefficient	683.29	349.47	3473.10	116.48	437.39	127733	34.69
Slope coefficient	-1.542	-0.866	-2.148	-0.527	-1.214	-4.851	-0.399
t	-0.402	-0.837	-0.932	-0.352	-0.995	-0.816	-0.509
MULTIPLE R	-0.402	-0.837	-0.932	-0.352	-0.995	-0.816	-0.509
MULTIPLE R^2	0.162	0.701	0.869	0.124	0.989	0.665	0.259
t*R	0.162	0.701	0.869	0.124	0.989	0.665	0.259

Table A-26. Summary of the correlation coefficients (R) among minimum temperature time series at the four grid points nearest to the studied six watersheds.

Historical Climate Predictions				CCC Climate Predictions				Hadley Climate Predictions			
Grid	#1	#2	#3	Grid	#1	#2	#3	Grid	#1	#2	#3
#2	0.055			#2	0.038			#2	0.029		
#3	0.047	0.044		#3	0.041	0.047		#3	0.028	0.020	
#4	0.039	0.023	0.050	#4	0.033	0.036	0.026	#4	0.027	0.031	0.014

Table A-27. Summary of the correlation coefficients (R) among maximum temperature time series at the four grid points nearest to the studied six watersheds.

Historical Climate Predictions				CCC Climate Predictions				Hadley Climate Predictions			
Grid	#1	#2	#3	Grid	#1	#2	#3	Grid	#1	#2	#3
#2	0.775			#2	0.769			#2	0.783		
#3	0.774	0.772		#3	0.775	0.771		#3	0.784	0.785	
#4	0.805	0.806	0.806	#4	0.811	0.808	0.808	#4	0.816	0.815	0.819

Table A-28. Summary of the correlation coefficients (R) among precipitation time series at the four grid points nearest to the studied six watersheds.

Historical Climate Predictions				CCC Climate Predictions				Hadley Climate Predictions			
Grid	#1	#2	#3	Grid	#1	#2	#3	Grid	#1	#2	#3
#2	0.831			#2	0.824			#2	0.833		
#3	0.819	0.819		#3	0.816	0.816		#3	0.824	0.822	
#4	0.814	0.815	0.807	#4	0.815	0.813	0.804	#4	0.819	0.819	0.813

Table A-29. Summary of the numbers of rainy days in 99 years (36159 days) at the four grid points nearest to the studied six watersheds.

Grid #	Historical	Hadley	CCC
1	12536	13184	12743
2	12773	13377	12545
3	11590	12438	11599
4	10929	11335	10753

Table A-30. Summary of the numbers of rainy days in 99 years (compared to station 1) at the four grid points nearest to the studied six watersheds.

Grid #	Historical	Hadley	CCC
1	12536	13184	12743
2	4633	5014	4586
3	4148	4680	4215
4	3880	4275	3900

Table A-31. Statistics of the weighted average precipitation time series (99 years) for the NWB and Hawlings watersheds based on the four grid points.

Historical (prec)	Station 1	Station 2	Station 3	Station 4	Hawlings	NWB
Mean (in.)	0.11	0.12	0.11	0.12	0.11	0.11
Median (in.)	0	0	0	0	0.06	0.04
Mode (in.)	0	0	0	0	0	0
Standard Deviation	0.28	0.29	0.28	0.30	0.16	0.19
Kurtosis	49.15	67.75	28.48	24.00	24.25	14.89
Skewness	4.98	5.29	4.37	4.21	3.29	3.19
Minimum (in.)	0	0	0	0	0	0
Maximum (in.)	7.68	9.08	4.82	3.98	3.36	2.41
Annual Precipitation(in.)	41.83	42.50	40.58	42.73	41.88	41.88
Count	36159	36159	36159	36159	36159	36159
Numb. Of Rainy Days	12536	12773	11590	10929	28527	28527

Table A-32. Frequencies of the timing in the year of the observed 7-day low events for the data of all 6 watersheds combined.

Lower X	*Upper X*	*Freq.*	*%*
0	31	3	0.01
32	59	2	0.01
60	90	0	0.00
91	120	0	0.00
121	151	0	0.00
152	181	0	0.00
182	212	22	0.10
213	243	54	0.23
244	273	81	0.35
274	304	55	0.24
305	334	11	0.05
335	365	3	0.01
	TOTAL=	231	1

Table A-33. Cumulative probability function for the Cox-Stuart trend test.

X	Cumul. Binomial	X	Cumul. Binomial
1	0.00000000000009	26	0.71591379357542
2	0.00000000000218	27	0.80419854472626
3	0.00000000003491	28	0.87356513491620
4	0.00000000041127	29	0.92379611401926
5	0.00000000379858	30	0.95728343342130
6	0.00000002863883	31	0.97780791950643
7	0.00000018122892	32	0.98935294292931
8	0.00000098232689	33	0.99530037923806
9	0.00000463177320	34	0.99809917279513
10	0.00001922955847	35	0.99929865574815
11	0.00007098534260	36	0.99976512134100
12	0.00023487865900	37	0.99992901465740
13	0.00070134425185	38	0.99998077044153
14	0.00190082720487	39	0.99999536822680
15	0.00469962076194	40	0.99999901767311
16	0.01064705707069	41	0.99999981877108
17	0.02219208049357	42	0.99999997136117
18	0.04271656657870	43	0.99999999620142
19	0.07620388598074	44	0.99999999958873
20	0.12643486508380	45	0.99999999996510
21	0.19580145527375	46	0.99999999999782
22	0.28408620642458	47	0.99999999999991
23	0.38772482734078	48	1.00000000000000
24	0.50000000000000	49	1.00000000000000
25	0.61227517265922		

Table A-34. Summary of the variable values obtained in calibration for the continuous streamflow model and the goodness-of-fit statistics for each of the 47 historical calibration runs.

	Period	PINF	SROP	GWS (in.)	SUBFLO (in.)	IMP. (%)	Se/Sy	Rm	R
Hawlings	79-82	0.743	0.622	15.300	3.815	8.493	0.838	0.387	0.569
	83-86	0.776	0.477	12.919	0.100	8.645	0.826	0.524	0.634
	87-90	0.848	0.400	10.696	1.635	9.026	0.863	0.471	0.592
	91-94	0.758	0.523	10.136	4.750	9.209	0.816	0.385	0.593
	95-97	0.783	0.374	0.587	3.702	9.353	0.827	0.341	0.566
	98-00	0.684	0.570	15.650	5.257	9.435	0.871	0.587	0.621

	Period	PINF	SROP	GWS	SUBFLO	IMP.	Se/Sy	Rm	R
Little Falls	51-54	0.739	0.107	3.756	5.254	35.446	0.630	0.783	0.802
	55-58	0.767	0.010	0.513	0.103	36.253	0.701	0.662	0.735
	62-65	0.776	0.383	0.512	4.015	36.603	0.712	0.754	0.754
	66-69	0.768	0.237	0.525	7.154	36.599	0.711	0.748	0.748
	70-72	0.800	0.593	0.525	3.948	36.598	1.001	0.500	0.500
	73-75	0.692	0.250	3.239	3.081	36.608	0.710	0.727	0.744
	76-78	0.748	0.370	8.250	10.210	36.632	0.776	0.699	0.699
	Period	PINF	SROP	GWS	SUBFLO	IMP.	Se/Sy	Rm	R
NWB	46-49	0.789	0.344	18.550	3.760	5.900	0.934	0.465	0.521
	50-53	0.747	0.179	15.038	2.214	6.374	0.734	0.619	0.702
	54-57	0.815	0.010	16.875	3.800	7.019	0.708	0.678	0.732
	58-61	0.804	0.416	15.650	3.121	7.527	0.862	0.639	0.639
	62-65	0.799	0.011	19.101	2.694	8.973	0.874	0.633	0.633
	66-69	0.836	0.203	0.501	3.451	10.924	0.744	0.727	0.727
	70-73	0.756	0.144	16.475	2.610	12.493	0.421	0.911	0.911
	74-76	0.813	0.010	16.144	2.140	13.456	0.533	0.682	0.848
	77-79	0.623	0.221	0.506	0.716	14.283	0.693	0.638	0.741
	80-82	0.740	0.372	9.600	3.238	14.987	0.886	0.619	0.619
	98-00	0.618	0.298	0.530	0.100	20.432	0.819	0.675	0.675
	Period	PINF	SROP	GWS	SUBFLO	IMP.	Se/Sy	Rm	R
Rock Creek	67-70	0.800	0.130	18.013	5.529	11.462	0.900	0.579	0.592
	71-73	0.765	0.034	13.694	4.707	12.637	0.389	0.845	0.920
	74-76	0.832	0.010	12.922	6.116	13.052	0.551	0.591	0.849
	Period	PINF	SROP	GWS	SUBFLO	IMP.	Se/Sy	Rm	R
Seneca	51-54	0.891	0.794	14.519	4.744	12.621	0.984	0.515	0.553
	55-58	0.766	0.371	10.550	0.311	12.654	0.841	0.542	0.612
	59-62	0.824	0.416	6.643	1.341	12.717	0.920	0.595	0.595
	63-66	0.976	0.858	9.405	2.559	12.847	1.193	0.389	0.528
	67-70	0.892	0.443	12.050	3.274	12.988	0.772	0.707	0.707
	71-74	0.803	0.305	10.637	1.782	13.205	0.525	0.862	0.862
	75-78	0.663	0.475	8.050	0.118	13.458	0.780	0.437	0.638
	79-82	0.798	0.072	11.100	8.384	13.775	0.719	0.470	0.697
	83-86	0.746	0.410	10.701	3.889	14.140	0.748	0.680	0.714
	87-90	0.776	0.409	11.250	2.620	14.642	0.726	0.545	0.694
	91-94	0.783	0.340	5.462	9.705	14.862	0.757	0.405	0.657
	95-97	0.679	0.511	0.503	2.512	15.065	0.808	0.459	0.616
	98-00	0.724	0.572	10.682	2.897	15.157	0.820	0.706	0.706
	Period	PINF	SROP	GWS	SUBFLO	IMP.	Se/Sy	Rm	R
Watts Branch	60-63	0.824	0.035	32.850	1.705	18.372	0.900	0.601	0.601
	64-67	0.811	0.010	19.443	7.703	20.263	0.712	0.709	0.738
	68-71	0.794	0.044	13.253	4.789	23.458	0.858	0.386	0.542
	72-75	0.748	0.345	25.725	3.960	24.174	0.834	0.495	0.600
	76-79	0.692	0.127	0.512	3.861	24.317	0.767	0.511	0.656
	80-83	0.750	0.076	22.553	5.001	28.175	0.744	0.651	0.705
	84-86	0.644	0.316	7.558	4.560	28.594	0.588	0.834	0.834

Table A-35. Summary of the calculations of the mean and variance of the relative errors based on the historical runs of the continuous streamflow model calibrations.

x	*Frequency*	*p(x)*	*x*p(x)*	*(x-x')*	*(x-x')^2*	*p(x)*(x-x')^2*
-0.2	0	0.0000	0.0000	-1.1942	1.4260	0.0000
0	0	0.0000	0.0000	-0.9942	0.9883	0.0000
0.2	28	0.1637	0.0327	-0.7942	0.6307	0.1033
0.4	32	0.1871	0.0749	-0.5942	0.3530	0.0661
0.6	25	0.1462	0.0877	-0.3942	0.1554	0.0227
0.8	18	0.1053	0.0842	-0.1942	0.0377	0.0040
1	15	0.0877	0.0877	0.0058	0.0000	0.0000
1.2	11	0.0643	0.0772	0.2058	0.0424	0.0027
1.4	6	0.0351	0.0491	0.4058	0.1647	0.0058
1.6	7	0.0409	0.0655	0.6058	0.3671	0.0150
1.8	6	0.0351	0.0632	0.8058	0.6494	0.0228
2	1	0.0058	0.0117	1.0058	1.0117	0.0059
2.2	1	0.0058	0.0129	1.2058	1.4541	0.0085
2.4	4	0.0234	0.0561	1.4058	1.9764	0.0462
2.6	0	0.0000	0.0000	1.6058	2.5787	0.0000
2.8	0	0.0000	0.0000	1.8058	3.2611	0.0000
3	1	0.0058	0.0175	2.0058	4.0234	0.0235
3.2	1	0.0058	0.0187	2.2058	4.8658	0.0285
3.4	0	0.0000	0.0000	2.4058	5.7881	0.0000
3.6	1	0.0058	0.0211	2.6058	6.7904	0.0397
3.8	1	0.0058	0.0222	2.8058	7.8728	0.0460
4	1	0.0058	0.0234	3.0058	9.0351	0.0528
4.2	3	0.0175	0.0737	3.2058	10.2775	0.1803
4.4	1	0.0058	0.0257	3.4058	11.5998	0.0678
4.6	1	0.0058	0.0269	3.6058	13.0021	0.0760
4.8	1	0.0058	0.0281	3.8058	14.4845	0.0847
5	0	0.0000	0.0000	4.0058	16.0468	0.0000
5.2	0	0.0000	0.0000	4.2058	17.6892	0.0000
5.4	0	0.0000	0.0000	4.4058	19.4115	0.0000
5.6	0	0.0000	0.0000	4.6058	21.2138	0.0000
5.8	1	0.0058	0.0339	4.8058	23.0962	0.1351
6	0	0.0000	0.0000	5.0058	25.0585	0.0000
0	5	0.0292	0.0000	-0.9942	0.9883	0.0000
Totals =	171	1.0000	0.9942	59.9930	226.3405	1.0375

APPENDIX B

SUPPLEMENTAL LIST OF FIGURES

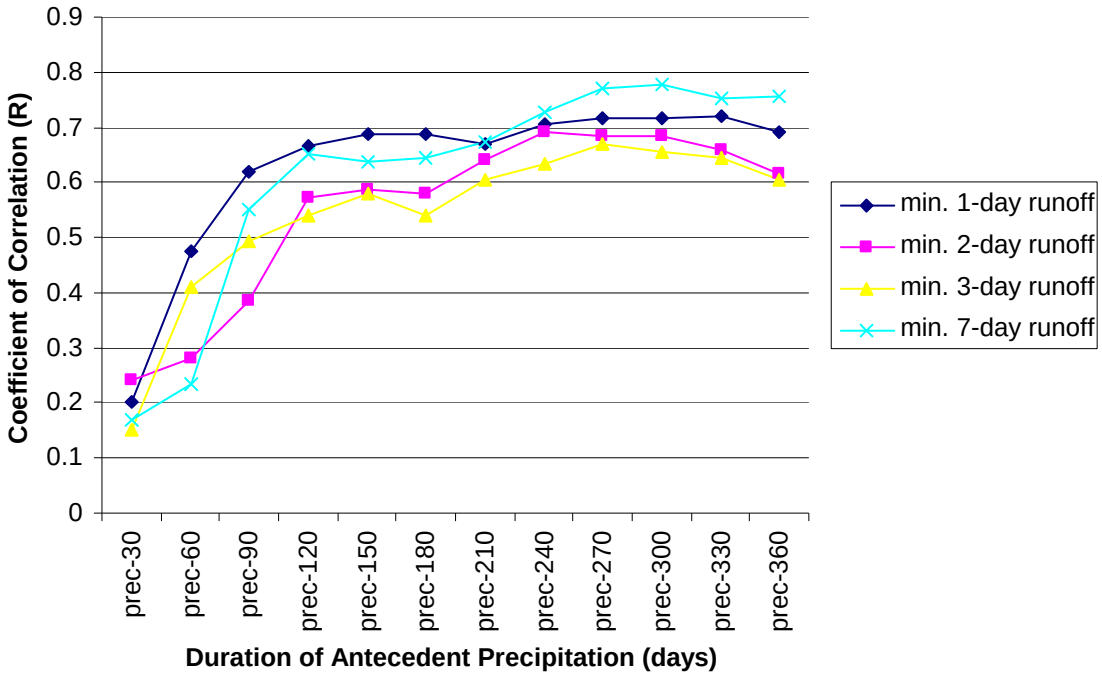

Figure B-1. Determining the optimum correlation between the 1, 2, 3, and 7-day low flows and the various durations of antecedent precipitation.

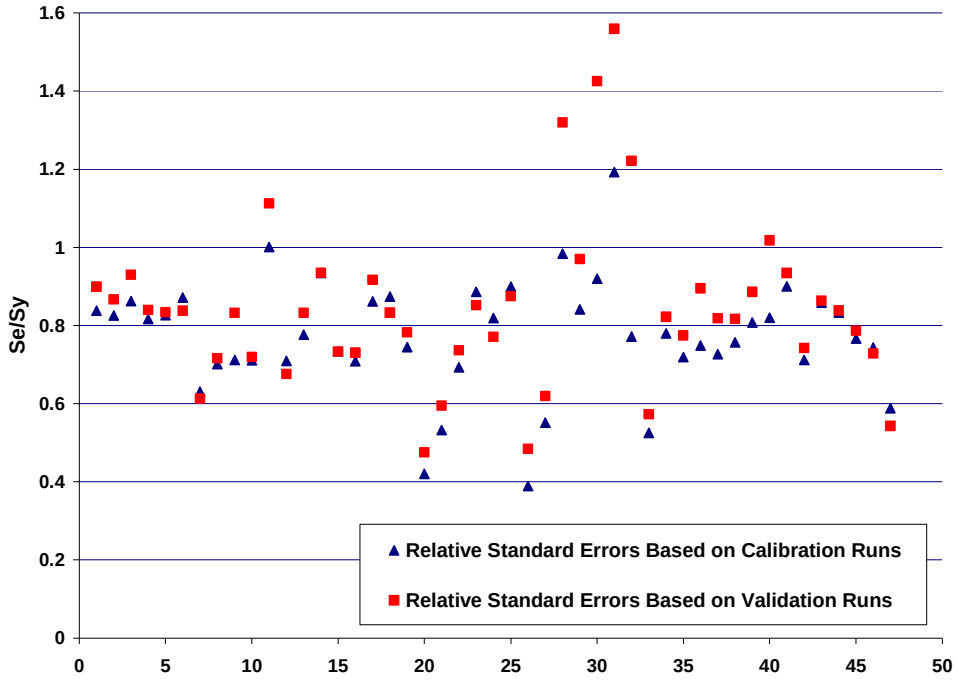

Figure B-2. Comparison of relative standard errors between the calibration and validation runs for the regional regression model.

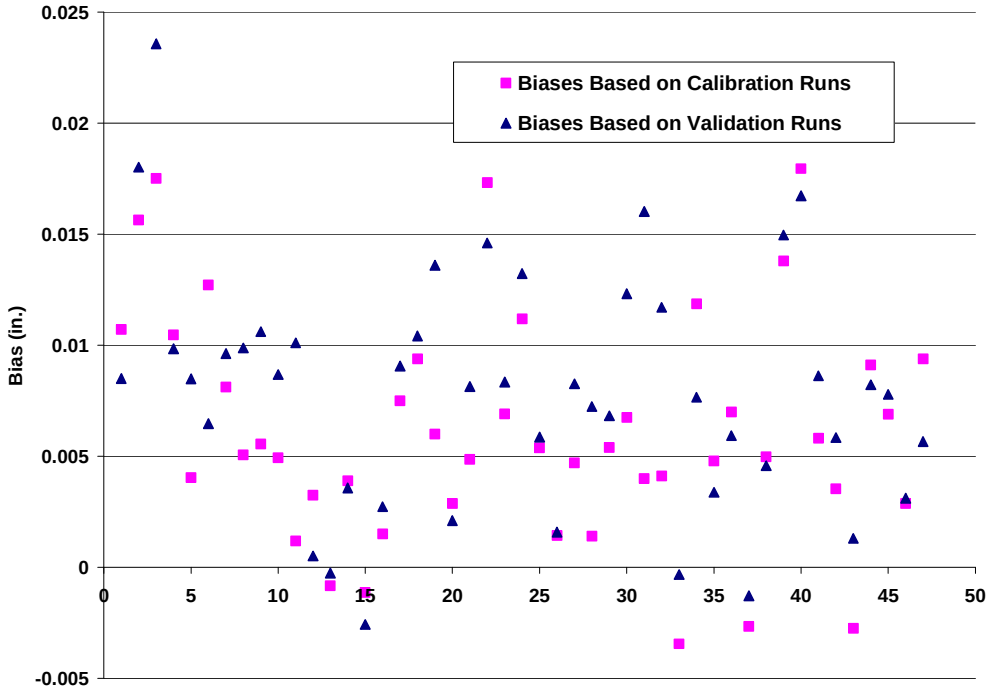

Figure B-3. Comparison of biases between the calibration and validation runs for the regional regression model.

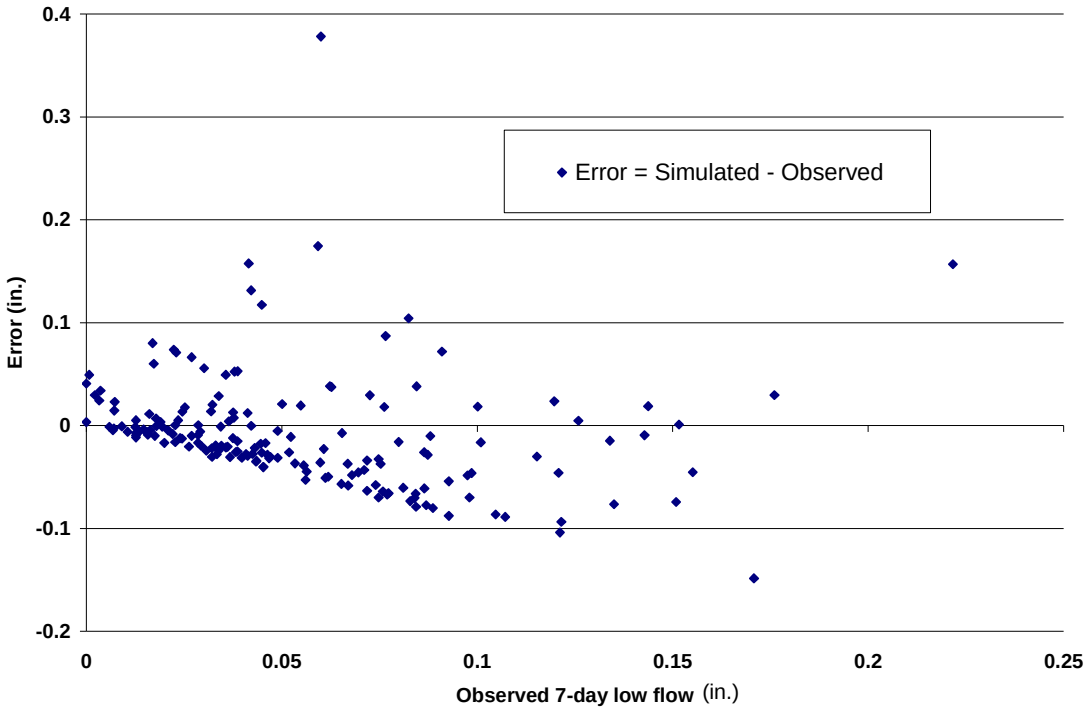

Figure B-4. Errors based on the 47 simulation runs for the historical data using the continuous streamflow model approach.

APPENDIX C

CALCULATIONS OF THE MULTIPLE-PART CORRELATION HYPOTHESIS TESTS ON RELATIONSHIPS BETWEEN LOW FLOW AND EACH OF IMPERVIOUSNESS AND TEMPERATURE BASED ON THE NORTHWEST BRANCH (NWB) AND WATTS BRANCH TIME SERIES

This appendix shows the calculations involved in determining the multiple-part correlation tests on both Imperviousness (*I(t)*) and antecedent temperature (T_{60}) to verify their significance to the accuracy of the regression model form to predict the minimum 7-day low flow (Q_7). These tests are based on the Northwest Branch (NWB) and Watts Branch time series data. The hypothesis test is as follows:

The null hypothesis:

H_0: ρ = 0 ; there is no significant relationship between *I(t)* (or T_{60}) and Q_7

The alternative hypothesis:

H_A: ρ $\neq 0$; there exists a significant relationship between *I(t)* (or T_{60}) and Q_7

In the case of testing the significance between imperviousness and base flow, the procedure is as follow:

1- Regress the model: $Q_7 = b_0 + b_1 \cdot P_{270} + b_2 \cdot T_{60}$

2- Calculate the residuals on the regression model.

3- Determine the correlation coefficient (R_m) between the residuals and the imperviousness time series.

4- Calculate the *t*-statistics and the critical *t*, where

$$t_{statistics} = \frac{R_m}{\left[\frac{1 - R_m}{n - 4}\right]^{0.5}}$$, where *n* is the sample size.

5- Compare the t-statistics to the critical *t* values to find the rejection regions

Steps 1 through 3: Calculating the correlation coefficient between the 7-day low flow and the residuals time series

The same steps are repeated for the relationship between antecedent temperature and base flow for both the NWB and Watts Branch. The regressed equations to address the relationship between Q_7 and $I(t)$ in both the NWB and Watts Branch data are presented in Equations C-1a and C-1b, respectively. Equations C-2a and C-2b represent the initial step to investigate the relationship between Q_7 and T_{60}. The goodness-of-fit statistics associated with the four regression equations are summarized below in Table C-1. These equations were calibrated using a numerical optimization program, NUMOPT. Tables C-2 and C-3 below summarize the residuals based on the regressed equations in Step 1 for both the NWB and Watts Branch.

$$Q_7 = 90.830 + 2.278 \cdot P_{270} - 1.728 \cdot T_{60} \quad \text{(C-1a)}$$

$$Q_7 = -0.579 + 0.319 \cdot P_{270} - 0.055 \cdot T_{60} \quad \text{(C-1b)}$$

$$Q_7 = -9.116 + 2.731 \cdot P_{270} - 3.449 \cdot I(t) \quad \text{(C-2a)}$$

$$Q_7 = -1.632 + 0.333 \cdot P_{270} - 0.141 \cdot I(t) \quad \text{(C-2b)}$$

Table C-1. Summary of goodness-of-fit statistics associated with the calibrated regression models for the NWB and Watts Branch as described in Step 1.

Goodness-of-fit Statistics	Equation (C-1a)	Equation (C-1b)	Equation (C-2a)	Equation (C-2b)
Multiple R^2	0.587	0.640	0.632	0.667
Multiple R	0.766	0.800	0.795	0.817
Se/Sy	0.661	0.623	0.624	0.599

Table C-2. Summary of residuals and the goodness-of-fit statistics associated with the calibrated regression models for the NWB as described in Step 2.

OBS. NO.	Q_{7pred} (cfs)	Q_{7Obs} (cfs)	RESIDUAL (cfs)	I(t) (%)
1	55.689	52.6	-3.089	5.778
2	32.197	50.3	18.103	5.866
3	43.576	71.4	27.824	5.945
4	57.062	88	30.938	6.012
5	49.657	86	36.343	6.109
6	32.524	85.6	53.076	6.253
7	73.748	59.4	-14.348	6.407
8	76.635	76	-0.635	6.729
9	48.778	81	32.222	6.826
10	10.815	9.6	-1.215	6.975
11	11.346	19.6	8.254	7.106
12	8.503	7.1	-1.403	7.170
13	59.350	42	-17.350	7.272
14	14.384	19.2	4.816	7.455
15	39.793	37.1	-2.693	7.602
16	31.581	26.7	-4.881	7.778
17	12.115	13.9	1.785	8.049
18	12.794	8.8	-3.994	8.864
19	11.463	6	-5.463	9.131
20	16.478	12.7	-3.778	9.847
21	6.787	0	-6.787	10.279
22	36.551	26.3	-10.251	10.763
23	23.813	10.2	-13.613	11.009
24	17.012	12.9	-4.112	11.647
25	31.829	20.5	-11.329	11.991
26	39.445	47	7.555	12.263
27	69.637	55.6	-14.037	12.770
28	51.286	46	-5.286	12.949
29	38.327	24.6	-13.727	13.280
30	46.743	47.8	1.057	13.488
31	34.818	21.5	-13.318	13.598
32	13.261	11	-2.261	14.024
33	52.422	32	-20.422	14.370
34	67.963	56.8	-11.163	14.456
35	33.017	18.1	-14.917	14.744
36	33.098	16.2	-16.898	14.940
37	19.904	14.9	-5.004	15.276

OBS. NO.	Q_{7pred} (cfs)	Q_{7Obs} (cfs)	RESIDUAL (cfs)	T_{60} (^{o}F.)
1	46.419	52.6	6.181	56.771
2	41.854	50.3	8.446	68.312
3	62.473	71.4	8.927	71.812
4	72.268	88	15.732	68.844
5	63.410	86	22.590	69.016
6	56.141	85.6	29.459	75.664
7	69.485	59.4	-10.085	58.500
8	69.221	76	6.779	57.238
9	28.081	81	52.919	53.664
10	31.255	9.6	-21.655	77.418
11	26.516	19.6	-6.916	75.041
12	29.763	7.1	-22.663	78.361
13	65.299	42	-23.299	66.254
14	23.318	19.2	-4.118	72.320
15	60.257	37.1	-23.157	75.689
16	47.712	26.7	-21.012	74.680
17	19.195	13.9	-5.295	72.631
18	22.665	8.8	-13.865	75.271
19	19.232	6	-13.232	74.828
20	24.707	12.7	-12.007	75.762
21	12.076	0	-12.076	75.992
22	28.978	26.3	-2.678	67.730
23	15.675	10.2	-5.475	69.090
24	5.608	12.9	7.292	69.230
25	21.984	20.5	-1.484	69.131
26	32.078	47	14.922	70.049
27	58.652	55.6	-3.052	66.246
28	35.914	46	10.086	66.189
29	26.685	24.6	-2.085	69.787
30	44.431	47.8	3.369	73.828
31	23.131	21.5	-1.631	70.631
32	-1.688	11	12.688	71.836
33	41.389	32	-9.389	70.541
34	58.436	56.8	-1.636	69.918
35	24.285	18.1	-6.185	74.139
36	6.187	16.2	10.013	65.680
37	1.311	14.9	13.589	71.525

Table C3. Summary of residuals and the goodness-of-fit statistics associated with the calibrated regression models for Watts as described in Step 2.

OBS. NO.	Q_{7pred} (cfs)	Q_{7Obs} (cfs)	RESIDUAL (cfs)	I(t) (%)
1	7.513	7.7	0.187	16.100
2	3.267	2.6	-0.667	16.111
3	6.372	9.8	3.428	17.930
4	4.953	5.2	0.247	18.234
5	2.739	2.2	-0.539	18.476
6	2.264	3.2	0.936	18.848
7	2.119	3	0.881	19.190
8	3.241	2.9	-0.341	19.828
9	0.890	0.7	-0.190	20.775
10	2.839	5.2	2.361	21.260
11	2.348	3.2	0.852	22.834
12	1.291	2.9	1.609	23.349
13	6.150	4.2	-1.950	23.744
14	6.377	8.2	1.823	23.904
15	10.424	9.7	-0.724	24.104
16	8.986	8.6	-0.386	24.170
17	7.334	4.1	-3.234	24.212
18	7.395	6.7	-0.695	24.212
19	4.683	4.2	-0.483	24.212
20	2.061	1.8	-0.261	24.226
21	5.779	6	0.221	24.411
22	8.307	14.3	5.993	24.418
23	5.518	3.4	-2.118	27.955
24	3.380	1.9	-1.480	28.178
25	2.832	3.3	0.468	28.204
26	5.258	2.4	-2.858	28.360
27	5.593	4.5	-1.093	28.456
28	3.253	2.3	-0.953	28.476
29	2.631	1.6	-1.031	28.852

OBS. NO.	Q_{7pred} (cfs)	Q_{7Obs} (cfs)	RESIDUAL (cfs)	T_{60} (^{o}F.)
1	8.390	7.7	-0.690	66.934
2	4.475	2.6	-1.875	75.844
3	7.449	9.8	2.351	75.738
4	5.865	5.2	-0.665	74.680
5	3.405	2.2	-1.205	72.639
6	3.009	3.2	0.191	75.287
7	2.592	3	0.408	71.516
8	3.896	2.9	-0.996	75.402
9	1.429	0.7	-0.729	77.459
10	3.144	5.2	2.056	73.139
11	2.506	3.2	0.694	74.812
12	1.211	2.9	1.689	72.746
13	6.014	4.2	-1.814	69.131
14	6.457	8.2	1.743	73.098
15	10.499	9.7	-0.799	70.492
16	8.719	8.6	-0.119	65.803
17	7.216	4.1	-3.116	69.697
18	7.519	6.7	-0.819	73.853
19	4.524	4.2	-0.324	70.959
20	1.670	1.8	0.130	68.926
21	4.958	6	1.042	59.156
22	7.939	14.3	6.361	65.148
23	4.703	3.4	-1.303	68.148
24	2.458	1.9	-0.558	68.434
25	2.069	3.3	1.231	71.656
26	4.795	2.4	-2.395	75.443
27	4.985	4.5	-0.485	72.910
28	2.423	2.3	-0.123	70.853
29	1.481	1.6	0.119	66.697

Step 4: Calculating the t-statistics values

NWB (Imperviousness Vs. Low flow)

$R_m = -0.586$

$t_{stat} = (0.586) / ((1-0.586)/(40-4))^{0.5} = 5.4645$

NWB (Temperature Vs. Low flow)

$R_m = -0.498$

$t_{stat} = (0.498) / ((1-0.498)/(40-4))^{0.5} = 4.2172$

Watts Branch (Imperviousness Vs. Low flow)

$R_m = -0.337$

$t_{stat} = (0.337) / ((1-0.337)/(29-4))^{0.5} = 2.0694$

Watts Branch (Temperature Vs. Low flow)

$R_m = -0.216$

$t_{stat} = (0.216) / ((1-0.216)/(29-4))^{0.5} = 1.2197$

Step 5: Calculating the t-critical values

NWB:

Sample size = 40

Degrees of freedom = 40 – 4 = 36

Alpha	10	5	2	1	0.5	0.1
t-critical	1.689	2.028	2.435	2.720	2.991	3.583

Watts:

Sample size = 29

Degrees of freedom = 29 – 4 = 25

Alpha	10	5	2	1	0.5	0.1
t-critical	1.708	2.060	2.485	2.787	3.078	3.725

Decisions on t-tests and implications:

Comparing the $t_{statistics}$ values in Step 4 and the $t_{criticl}$ values in Step 5, we can make the following conclusions:

1- Selecting a 0.1% level of significance, imperviousness shows a significant relationship with the 7-day low flow for the NWB watershed after eliminating the effects of other two variables - antecedent precipitation and antecedent temperature.

2- Selecting a 0.1% level of significance, antecedent temperature shows a significant relationship with the 7-day low flow for the NWB watershed after eliminating the effects of other two variables - antecedent precipitation and imperviousness.

3- Selecting a 10% level of significance, imperviousness shows a significant relationship with the 7-day low flow for the Watts Branch watershed after eliminating the effects of other two variables - antecedent precipitation and antecedent temperature.

4- Selecting a 10% level of significance, antecedent temperature still does not show a significant relationship with the 7-day low flow for the Watts Branch watershed after eliminating the effects of other two variables - antecedent precipitation and imperviousness.

APPENDIX D

KOLMOGOROV-SMIRNOV ONE-SAMPLE TEST ON THE DISTRIBUTION OF TIMING OF THE YEAR OF 7 DAY LOW FLOW OCCURRENCE FOR THE REGRESSION MODEL APPROACH

Based on the 231 low flow events from all six watersheds, the Kolmogorov-Smirnov one-sample test was performed to test for normality of the distribution of the timing of the 7-day low flow occurrence. The mean of the normal distribution was calculated by simply finding the mean of the 231 values. The standard deviation, however, was calculated based on the optimum minimum maximum-difference value between the cumulative normal distribution formed by the data and the Weibull ranking cumulative probability of the data. (See Table D-1 and Figure D-1).

Table D-1: Determination of the optimum standard deviation of the normal curve by finding the minimum max-difference value. (Optimum values are shown in bold).

Std. Dev.	max diff
35	0.078121698
35.1	0.078065674
35.2	0.078009969
35.3	0.077954579
35.4	0.077899501
35.5	0.077844733
35.6	0.077790273
35.7	0.077736117
35.8	**0.077682264**
35.9	0.077744037
36	0.078020905

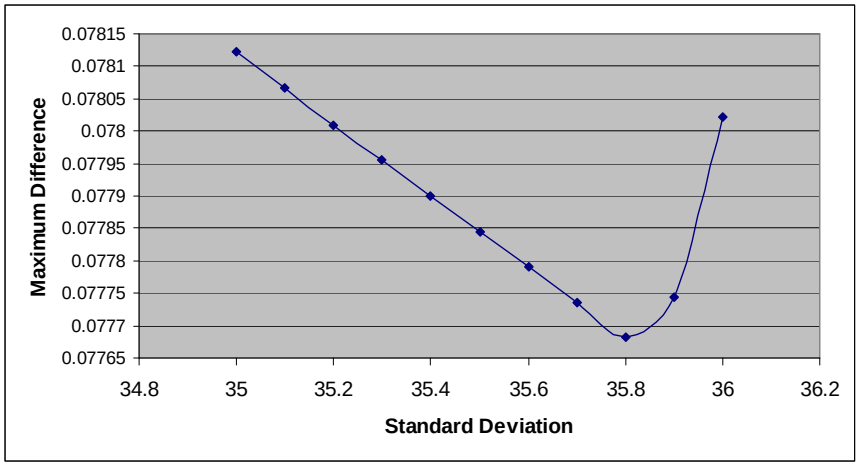

Figure D-1: Determination of the optimum standard deviation of the normal curve by finding the minimum max-difference value.

Having calculated the mean and standard deviation value to be 251.3 (September 8) and 35.8 days, respectively, they were used then in producing the normal distribution curve. A plot of the cumulative normal is shown in Figure D-2 below. Figure D-3 shows the level of variation between the cumulative normal curve and the cumulative ranking curve formed by the data. Thus, since the maximum difference value is 0.077682 and based on the alpha values listed below in Table D-2, the data meets normality at a significance level of 12.46%.

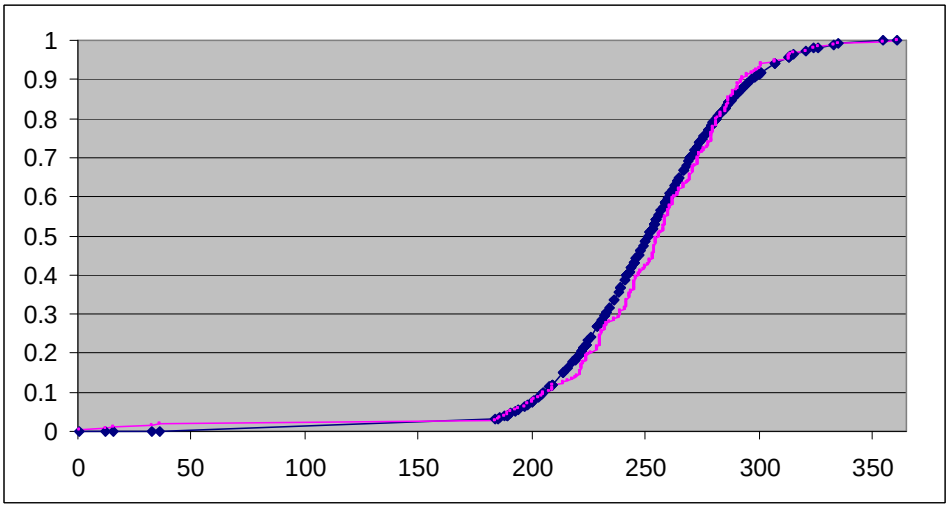

Figure D-2. Cumulative normal curve for the day of year of occurrence of 7-day low flow events.

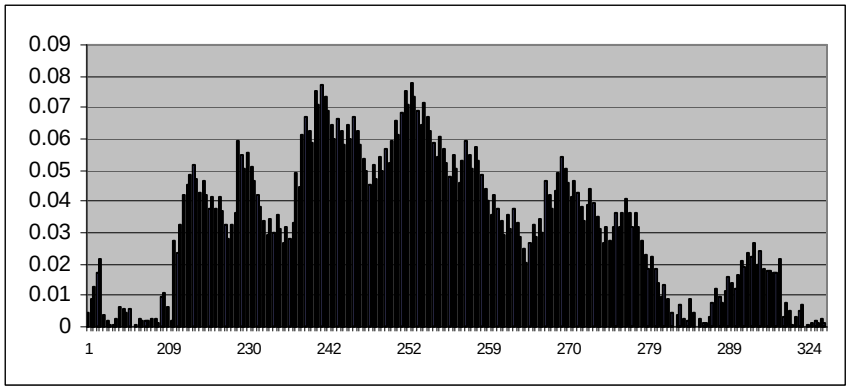

Figure D-3. Determination maximum-difference value of the Kolmogorov-Smirnov one-sample test.

Table D-2. The level of significance values used for the Kolmogorov-Smirnov one-sample test.

alpha = 20	0.070401
alpha = 15	0.075006
alpha = 10	0.080270
alpha = 5	0.089481
alpha = 1	0.107246

BIBLIOGRAPHY

Arnell, N.W., 1989. Changing frequency of extreme hydrological events in northern and western Europe. FRIENDS in Hydrology, IAHS Publication No. 187, pp. 237-249.

Ayyub, B.M., and R.H. McCuen, 2003. Probability, statistics, and reliability for engineers and scientists. Chapman & Hall/ CRC, D.C., U.S.A.

Barringer, T.H., R.G. Reiser, and C.V. Price, 1994. Potential effects of development on flow characteristics of two New Jersey streams. Water Resources Bulletin, 30, 283-295.

Beran, M.A., and A. Gustard, 1977. A study into the low-flow characteristics of British rivers. Journal of Hydrology. 35, 147-157.

Bicknell, B.R., J.C. Imhoff, J.L. Kittle, Jr., A.S. Donigian, Jr., and R.C. Johanson, 1997. Hydrologic simulations program-Fortran: user's manual version II. U.S. Environmental Protection Agency, National Exposure Research Laboratory, Athens, Georgia, EPA/600/R-97/080, 755.

Boer, G.J., N.A. McFarlane, and M. Lazare, 1992. Greenhouse gas-induced climate change simulated with the CCC second-generation general circulation model. American Meteorological Society, 5, 1045-1077.

Crawford, N.H., and R.K. Linsley, 1966. Digital Simulation in Hydrology: Stanford Watershed Model IV. Stanford University, Department of Civil Engineering Technical Report 39.

Donigan, A.S., and W.C. Huber, 1991. Modeling of nonpoint source water quality in urban and non-urban areas. EPA/600/391/039, U.S. EPA, Environmental Research Laboratory, Athlens, Georgia.

Duell, L. F.W., Jr., 1992. Use of regression models to estimate effects of climate change on seasonal streamflow in the American and Carson river basins, California-Nevada. In: Managing Water Resources During Global Change, R. Herrmann (Editor). 28th American Water Resources Association Conference, Reno, Nevada, 1992, Proceedings, 731-740.

Duell, L. F.W., Jr., 1994. The sensitivity of northern Sierra Nevada streamflow to climate change. Water Resources Bulletin, 30(5), 841-859.

Fang, M., and K.K. Tung, 1999. Time-dependant non-linear Hadley circulation. American Meteorological Society, 56, 1797-1807.

Ferguson, B.K., and P.W. Sucking, 1990. Changing rainfall-runoff relationships in the urbanizing Peachtree creek watershed, Atlanta, Georgia. Water Resources Bulletin. 26 (2), 313-322.

Flaschka, I., C.W. Stockton, and W.R. Boggess, 1987. Climatic variation and surface water resources in the great basin region. Water Resources Bulletin, 23(1), 47-57.

Flato, G.M. , G.J. Boer, W.G. Lee, N.A. McFarlane, D. Ramsden, M.C. Reader, and A.J. Weaver, 2000. The Canadian center for climate modelling and Analysis global coupled model and its climate. Climate Dynamics, 16, 451-467.

Gleick, P.H., 1987. Regional Hydrologic consequences of increases in atmospheric CO_2 and other trace gases. Climatic Change, 10, 137-161.

Hamon, R.W., 1963. Computation of direct runoff amounts from storm rainfall. Willingford, Oxon., U.K., International Association of Scientific Hydrology Publication 63.

Huber, W.C., and R.E. Dickinson, 1988. Storm water management model, version 4: user's manual. . U.S. Environmental Protection Agency, National Exposure Research Laboratory, Athens, Georgia, EPA/600/3-88-001a, 569.

Intergovernment Panel on Climate Change (I.P.C.C.), 2001. Climate change 2001: the scientific basis. http://www.grida.no/climate/ipcc_tar/wg1/index.htm (Accessed Apr. 2004).

Gustard, A., A. Bullock, and A.M. Dixon, 1992. Low flow estimation in the United Kingdom. Institute of Hydrology, Report No. 108, 88.

Kasparek, L., and K. Krejcova, 1994. BILAN water balance mode.. User's guide and background information. T. G. Masaryk Water Research Institute, Prague.

Kittel, T.G.F., N.A. Rosenbloom, C. Kaufman, J.A. Royle, C. Daly, H.H. Fisher, W.P. Gibson, S. Aulenbach, D.N. Yates, R. McKeown, D.S. Schimel, and VEMAP2 Participants. 2000. VEMAP Phase 2 Historical and Future Scenario Climate Database for the Conterminous US. Available online from the ORNL Distributed Active Archive Center, Oak Ridge National Laboratory, Oak Ridge, Tennessee. http://www.daac.ornl.gov (Accessed Jan. 2003).

Kittel, T.G.F., N.A. Rosenbloom, J.A. Royle, C. Daly, W.P. Gibson, H.H. Fisher, P. Thornton, D. Yates, S. Aulenbach, C. Kaufman, R. McKeown, D. Bachelet, D.S. Schimel, and VEMAP2 Participants. 2003. The VEMAP Phase 2 bioclimatic database. I: A gridded historical (20th century) climate dataset for modeling ecosystem dynamics across the conterminous United States. Climate Research, under review.

Klein, R.D., 1979. Urbanization and stream quality impairment. Water Resources Bulletin, 15, 948-963.

Liebscher, H.J., 1983. The use of long-term river level and discharge records in the study of climatic variations in the Federal Republic of Germany. Proceedings of the Symposium on Variations in the Global Water Budget, Reidel, Oxford, 173-184.

Ludwig, A.H., and G.D. Tasker, 1993. Regionalization of low-flow characteristics of Arkansas streams. US Geological Survey, Water-Resources Investigation Report, 93-4013.

McCabe, G.J., Jr., and M.A. Ayers, 1989. Hydrologic effects of climate change in the Delaware river basin. Water Resources Bulletin, 25(6), 1231-1241.

McCuen, R.H., and W.M. Snyder, 1975. A proposed index for comparing hydrographs. Water Resources Research, 11(6), 1021-1024.

McCuen, R.H., 1986. Hydrologic analysis and design. Prentice-Hall, New Jersey, U.S.A.

McCuen, R.H., 1993. Microcomputer applications in statistical hydrology. Prentice-Hall, New Jersey, U.S.A.

McCuen, R.H., 2003. Modeling hydrologic change: statistical methods. Lewis Publishers, D.C., U.S.A.

McDonald, M.G., and A.W. Harbaugh, 1988. A modular three-dimensional finite-difference groundwater flow model. US Geological Survey, Ohio, TWRI Book 6(A1), 586.

McMahon, T.A., and A.D. Arenas, 1982. Methods of computation of low streamflow. Paris, UNESCO Studies and Reports in Hydrology, 36, 107.

Moglen, G.E., and R.E. Beighley, 2002. Spatially explicit modeling of land use change. Journal of the American Water Res. Assoc., 38(1), 241-253.

National Climatic Data Center (NCDC), 2003. NNDC climate data online. http://cdo.ncdc.noaa.gov/plclimprod/plsql/poemain.poe (Accessed Jan. 2003).

National Center for Atmospheric Research (NCAR), 2003. The Vegetation/Ecosystem Modeling and Analysis Project (VEMAP). http://dataserver.ucar.edu/vemap/main.html (Accessed Jan. 2003).

Paul, M., J. Meyer, and L. Judy, 2001. Streams in the urban landscape. Annu. Rev. Ecol. Syst., 32, 333-365.

Pirt, J., and M. Simpson, 1983. The estimate of river flows. Severn Trent Water Authority, UK, 41.

Puacko, A., 1993. Variations in Northern Sierra Nevada streamflow: implication of climate change. Water Resources Bulletin, 29(2), 283-290.

Querner, E.P., 1997. Description and application of the combined surface and groundwater flow model MOGROW. J. Hydro.
Querner, E.P., L.M. Talkaksen, L. Kasparek, and H.A.J. Lanen, 1997. Impact of land use, climate change and groundwater abstractions on streamflow droughts using physically-based models. In: FRIEND'97 – Regional Hydrology: Concepts and Models for Sustainable Water Resource Management, LAHS Publication No. 246, 171-179.

Revelle, R.R., and P.E. Waggoner, 1983. Effects of carbon dioxide induced climate change on water supplies in the western United States. In: Changing Climate. Report of the Crabon Dioxide Assessment Committee, National Academy Press, D.C., 419-432.

Riggs, H.C., 1972. Low flow investigations. Techniques of Water Resources Investigations of the USGS, Book 4, Hydrological Analysis and Interpretation, D.C., 18.

Roesner, L.A., J.A. Aldrich, and R.E. Dickinson, 1988. Storm water management model user's manual. Version 4: Addendum I, EXTRAN, EPA/600/3-88/001b (NTIS PB88236658/AS). Environmental Protection Agency, Athens, Georgia.

Schaake, J.C., and L. Chunzhun, 1989. Development and application of simple water balance models to understand the relationship between climate and water resources. New directions for surface water modeling. Proceedings of a Baltimore Symposium, IAHS Publication No. 181, 343-352.

Simmons, D.L., and R.J. Reynolds, 1982. Effects of urbanization on base flow of selected south-shore streams. Long Islend New York. Water Resources Bulletin. 18, 797-805.

Smakhtin, V.U., 2001. Low flow hydrology: a review. Journal of Hydrology 240, 147-186.

Tallaksen, L.M., and B. Erichsen, 1994. Modelling low flow response to evapotranspiration. In: FRIEND: Flow Regimes from International Experminatal and Network Data (ed. By P. Seuna, A. Gustard, N.W. Arnell, and G.A. Cole) (Proc. Braunschweig Conf., Oct. 1993), 95-102. IAHS Publ. no. 221.

Tasker, G. D., 1972. Estimating low-flow characteristics of streams in southeastern Massachusetts from maps of ground-water availability. U.S. Geol. Survey Prof. paper 800-D, D217-D220.

Tasker, G. D., 1978. A Comparison of methods for estimating low flow characteristics of streams. Journal of Water Resources Bulletin, 23(6), 1077-1083.

Vogel, R.M., and N.M. Fennessey, 1994. Flow duration curves. I. A new interpretation and confidence intervals. Journal of Water Resources Plan. Manag., ASCE, 120 (4), 485-504.

Warner, R.F., 1984. Man's impact on Australian drainage systems. Aust. Geographer 16, 133-141.

Wilby, R., B. Greenfield, and C. Glenny, 1994. A coupled synoptic-hydrological model for climate change impact assessment. Journal of Hydrology. 153, 265-290.